

AWARD NUMBER: W81XWH-19-1-0621
BM180109

TITLE: Unraveling the Role of DDX41 in Hematopoiesis and MDS

PRINCIPAL INVESTIGATOR: Teresa Bowman

CONTRACTING ORGANIZATION: Albert Einstein College of Medicine

REPORT DATE: October 2021

TYPE OF REPORT: ANNUAL

PREPARED FOR: U.S. Army Medical Research and Development Command
Fort Detrick, Maryland 21702-5012

DISTRIBUTION STATEMENT: Approved for Public Release;
Distribution Unlimited

The views, opinions and/or findings contained in this report are those of the author(s) and should not be construed as an official Department of the Army position, policy or decision unless so designated by other documentation.

REPORT DOCUMENTATION PAGE

Form Approved
OMB No. 0704-0188

Public reporting burden for this collection of information is estimated to average 1 hour per response, including the time for reviewing instructions, searching existing data sources, gathering and maintaining the data needed, and completing and reviewing this collection of information. Send comments regarding this burden estimate or any other aspect of this collection of information, including suggestions for reducing this burden to Department of Defense, Washington Headquarters Services, Directorate for Information Operations and Reports (0704-0188), 1215 Jefferson Davis Highway, Suite 1204, Arlington, VA 22202-4302. Respondents should be aware that notwithstanding any other provision of law, no person shall be subject to any penalty for failing to comply with a collection of information if it does not display a currently valid OMB control number. **PLEASE DO NOT RETURN YOUR FORM TO THE ABOVE ADDRESS.**

1. REPORT DATE October 2021		2. REPORT TYPE ANNUAL		3. DATES COVERED 09/01/2020-08/31/2021	
4. TITLE AND SUBTITLE Unraveling the Role of DDX41 in Hematopoiesis and MDS				5a. CONTRACT NUMBER W81XWH-19-1-0621	
				5b. GRANT NUMBER BM180109	
				5c. PROGRAM ELEMENT NUMBER	
6. AUTHOR(S) Teresa Bowman E-Mail: Teresa.bowman@einsteinmed.org				5d. PROJECT NUMBER	
				5e. TASK NUMBER	
				5f. WORK UNIT NUMBER	
7. PERFORMING ORGANIZATION NAME(S) AND ADDRESS(ES) Albert Einstein College of Medicine				8. PERFORMING ORGANIZATION REPORT NUMBER	
9. SPONSORING / MONITORING AGENCY NAME(S) AND ADDRESS(ES) U.S. Army Medical Research and Development Command Fort Detrick, Maryland 21702-5012				10. SPONSOR/MONITOR'S ACRONYM(S) DOD/BMFRP	
				11. SPONSOR/MONITOR'S REPORT NUMBER(S)	
12. DISTRIBUTION / AVAILABILITY STATEMENT Approved for Public Release; Distribution Unlimited					
13. SUPPLEMENTARY NOTES					
14. ABSTRACT Myelodysplastic syndromes (MDS) are bone marrow failure disorders arising from defects in blood-forming stem cells resulting in stem cell expansion and decreased production of mature blood cells. MDS in adults is largely thought to be acquired, but the recent identification of a familial form of adult-onset MDS linked to germline mutations in the <i>DEAD-box Helicase 41</i> gene (<i>DDX41</i>) challenges this dogma. Although this form of MDS is rare, lessons learned from familial forms of human diseases often provide information that is more broadly applicable to acquired forms of a disease that arise from sporadic and/or complex genetic changes. Germline mutations in <i>DDX41</i> disrupt its function such that insufficiency of normal levels of DDX41 is thought to contribute to MDS formation. DDX41 plays several roles in cellular homeostasis, thus it is unclear which aspects are aberrant when DDX41 is mutated and how dysfunction of these processes contribute to MDS. To address this question, we have established a zebrafish model of <i>ddx41</i> deficiency, which is one of the first animal models for studying the <i>in vivo</i> requirements of Ddx41 in hematopoiesis. Human and zebrafish DDX41 are highly conserved, thus we anticipate that our studies in zebrafish will be informative for understanding the function of human DDX41 in hematopoiesis. Zebrafish is an easily manipulated vertebrate model system that has been used extensively to study the basis of both benign and malignant hematopoiesis including MDS. We aim to utilize the advantages of the zebrafish to uncover how Ddx41 regulates hematopoiesis and identify novel therapeutic targets for the treatment of MDS.					
15. SUBJECT TERMS Myelodysplastic syndrome, DDX41, hematopoiesis, inflammation, DNA damage					
16. SECURITY CLASSIFICATION OF:			17. LIMITATION OF ABSTRACT	18. NUMBER OF PAGES	19a. NAME OF RESPONSIBLE PERSON
a. REPORT	b. ABSTRACT	c. THIS PAGE			19b. TELEPHONE NUMBER (include area code)
Unclassified	Unclassified	Unclassified	Unclassified	65	USAMRMC

TABLE OF CONTENTS

	<u>Page</u>
1. Introduction	4
2. Keywords	4
3. Accomplishments	4-6
4. Impact	6-7
5. Changes/Problems	7
6. Products	7
7. Participants & Other Collaborating Organizations	7-8
8. Special Reporting Requirements	8
9. Appendices	9-65

1. Introduction

Myelodysplastic syndromes (MDS) are a spectrum of disorders arising from hematopoietic stem and progenitor cell (HSPC) dysfunction resulting in ineffective hematopoiesis and cytopenias. MDS in adults is largely thought to be an acquired disorder, but the recent identification of an inherited form of adult-onset MDS linked to germline mutations in the *DEAD-box Helicase 41* gene (*DDX41*) challenges this dogma. Germline mutations in *DDX41* primarily occur in the N-terminal domain leading to an early stop codon, suggesting that diminished function of *DDX41* contributes to MDS initiation. *DDX41* is a nucleic acid-activated ATPase linked to immunity, splicing, and R-loop regulation. All three of these processes have been implicated in MDS, thus the underlying mechanism for how *DDX41* mutations contribute to hematologic malfunctioning is unclear. Our central *premise* is that the varied functions of *DDX41* are connected and necessary for hematopoietic homeostasis. To discover how *DDX41* insufficiency could lead to MDS, we established a zebrafish model of *ddx41* deficiency, which is one of the first animal models for studying the *in vivo* requirements of *Ddx41* in hematopoiesis. Human and zebrafish *DDX41* are highly conserved sharing >85% amino acid identity, thus we anticipate that our studies in zebrafish will be informative for understanding the function of human *DDX41* in hematopoiesis. Zebrafish is a genetically malleable vertebrate model system that has been used extensively to study the basis of both benign and malignant hematopoiesis including MDS. Zebrafish mutants for *ddx41* display HSPC expansion as well as neutropenia and anemia, phenotypes reminiscent of human MDS. We aim to utilize the advantages of the zebrafish to uncover how *Ddx41* regulates hematopoiesis and identify novel therapeutic targets for the treatment of MDS.

2. Keywords

Myelodysplastic syndrome, *DDX41*, hematopoiesis, inflammation, DNA damage

3. Accomplishments

Major goals:

Goals as outlined in the approved Statement of Work:

	Timeline Months	Site 1
Task: Seek regulatory approval for the use of animals	1-3	Local IACUC and DoD ACURO
Aim 1: To determine R-loop involvement in <i>Ddx41</i> regulation of hematopoiesis formation		
1.1 To determine if <i>DDX41</i> regulates R-loop levels.	1-6	Bowman lab
1.2 To determine if R-loops contribute to hematopoietic defects in <i>ddx41</i> mutants.	1-18	Bowman lab
1.3 To determine how R-loops regulate hematopoietic gene expression.	1-24	Bowman lab
Milestone Achieved: Delineate how <i>DDX41</i> -mediated R-loop regulation contributes to blood defects.	24	
Aim 2: To Determine R-loop-triggered DNA damage responses during development.		
2.1 To determine if inflammatory signaling is perturbed in <i>ddx41</i> mutants.	1-12	Bowman lab
2.2 To determine if STING-mediated inflammatory signaling plays a role in hematopoietic defects in <i>ddx41</i> mutants.	6-24	Bowman lab
2.3 To determine if elevated levels of R-loops alter inflammatory signaling in <i>ddx41</i> mutants.	12-18	Bowman lab
Milestone Achieved: Define how <i>DDX41</i> insufficiency alters the inflammatory milieu and the impact of this on hematopoiesis	24	

Progress towards year 2 goals:

Task: Seek regulatory approval for the use of animals: The project was approved by both the IACUC at Albert Einstein College of Medicine (12/18/19) and the DOD ACURO (2/24/20).

Aim 1.2: To determine if R-loops contribute to hematopoietic defects in *ddx41* mutants. Using the *M27RNASEH1-GFP* transgene, we explored the impact of excess R-loops on hematopoietic phenotypes in *ddx41* mutants. In our preliminary studies, we demonstrated that *ddx41* mutants have excessive HSPCs, but diminished

erythrocytes, macrophages and neutrophils compared to control siblings. As quantified by assessment of both absolute number of *runx1:mcherry*⁺ HSPCs per embryo and *runx1 in situ* hybridization staining at 40 hpf, HSPC levels were significantly reduced in *ddx41* mutants after transient global RNASEH1-GFP expression. To elucidate if the impact of excess R-loops on HSPC expansion was cell-intrinsic, we injected *ddx41* mutants with either *ubi:gfp* (control) or *fli1:M27RNASEH1-GFP* which would deplete R-loops only in *fli1*⁺ endothelial cells including those that give rise to HSPCs. As quantified by assessment of *runx1:mcherry*⁺ HSPCs per embryo at 40 hpf, HSPC levels were significantly reduced in *ddx41* mutants injected with *fli1:M27RNASEH1-GFP* compared to control. These data show that aberrant R-loop accumulation can intrinsically promote HSPC expansion *in vivo*. These findings are included in our published study (Weinreb *et al.* Developmental Cell, 2021).

Paradoxically, when we transiently overexpressed *RNASEH1-GFP*, rather than suppressing the erythrocyte defect in *ddx41* mutants it exacerbated the anemia as measured by a decrease in the amount of hemoglobinized erythrocytes. Through these studies, we uncovered that *ddx41* mutants display a strong DNA damage response that induces a cell cycle arrest in erythrocyte precursors and suppresses maturation. These findings are now published (Weinreb *et al.* Haematologica, 2021).

Aim 1.3: To determine how R-loops regulate hematopoietic gene expression. R-loops are known to regulate gene expression via modulation of transcriptional elongation and epigenetic modifiers. Based on this, we hypothesized that DDX41-mediated R-loop regulation controls expression of critical genes for hematopoiesis, and that disruption of this regulation contributes to hematopoietic dysfunction in *ddx41* mutants. As our initial results regarding R-loop regulation of hematopoiesis were in erythrocytes, we first explored R-loop regulation of erythroid gene expression. This hypothesis was supported by a recent study that mapped the genomic locations of R-loops in human K562 erythroleukemia cells and identified an R-loop near the promoter of the *GATA1* gene. To identify R-loop-regulated gene expression in *ddx41* mutant erythrocytes, we performed RNA-seq on cells isolated from *ddx41* mutants and siblings either with or without R-loop depletion via RNASEH1-GFP overexpression. From our initial analysis, we observed few changes in transcript expression levels, but significant alterations in splicing. There were more than 600 RNASEH1-sensitive alternative splicing events in *ddx41* mutant cells.

Aim 2.1: To determine if inflammatory signaling is perturbed in *ddx41* mutants. Growing evidence suggests that perturbed inflammatory signaling is a common feature of MDS that contributes to disease pathophysiology. In addition to a role in RNA:DNA hybrid resolution, DDX41 is implicated in inflammatory signaling. DDX41 acts as an intracellular DNA sensor that activates the STING (Stimulator of Interferon Genes) pathway in both mammals and zebrafish. When activated, STING triggers a signaling cascade leading to activation of TBK1 (Tank Binding Kinase 1), the transcription factors NFκB (Nuclear Factor κ-B) and IRF3 (Interferon Response Factor 3), and production of Type I Interferon. Activation of the STING pathway in mice can induce HSPC cell cycle entry and mobilization, and thus could be involved in HSPC expansion. STING is activated by a number of cytosolic sensors in addition to DDX41. A recent study found that RNA:DNA hybrids can activate cGAS (cyclic GMP-AMP synthase), another cytosolic nucleic-acid sensor that triggers STING activation. To assess pathway activation in *ddx41* mutants and sibling controls, we measured phosphorylation of TBK1-Ser172 and NFκB transcriptional activity. We found elevated phospho-TBK1 and NFκB transcriptional reporter activity in *ddx41* mutants compared to siblings. Pathway activation was diminished upon cGAS/STING knockdown and R-loop depletion. Studies examining interferon-responsive gene expression using the *interferon-phi:mcherry* transgenic zebrafish are still underway, but using RT-qPCR we did demonstrate a decrease in Type I IFN responsive genes in *ddx41* mutants upon R-loop depletion. To assess the cell types with elevated inflammation, we examined *nfkB:gfp* levels in HSPCs and found that levels are higher in *ddx41* mutant HSPCs compared to sibling controls. *The data strongly indicate that excessive R-loops resulting from ddx41 loss trigger a cGAS/STING-mediated inflammatory response.* These findings are included in our published study (Weinreb *et al.* Developmental Cell, 2021).

Aim 2.2: To determine if STING-mediated inflammatory signaling plays a role in hematopoietic defects in *ddx41* mutants. We tested the role of the cGAS/STING signaling components on the HSPC expansion in *ddx41* mutants. Lowering cGAS or STING activation using numerous genetic approaches significantly reduced HSPC numbers in *ddx41* mutants, as measured by quantification of *cd41:gfp*⁺ HSPC numbers per embryo using flow cytometry and *runx1 in situ* hybridization. *These results indicate that the cGAS-STING inflammatory cascade mediates HSPC accumulation in ddx41 mutants.* These findings are included in our published study (Weinreb *et al.* Developmental Cell, 2021). Studies on the impact of inflammatory signaling in *ddx41* mutant erythrocyte, macrophage, and neutrophil defects is still underway.

Aim 2.3: To determine if elevated levels of R-loops alter inflammatory signaling in *ddx41* mutants. We deciphered that the elevated phospho-TBK1 levels were dampened following cGAS morpholino-mediated knockdown and following RNA:DNA hybrid depletion via RNASEH1-GFP overexpression. Additionally, we demonstrated a decrease in some interferon-stimulated genes (ISGs) following R-loop depletion strengthening the model that R-loops activate a cGAS/STING inflammatory cascade leading to aberrant HSPC expansion. These findings are included in our published study (Weinreb *et al.* Developmental Cell, 2021).

Professional development:

As part of my professional development, I attended several virtual conferences including the 2020 MDS Summit, 2020 American Society of Hematology Conference, 2021 Keystone Hematopoiesis Symposium, and 2021 International Society of Experimental Hematology Conference.

Dissemination of results:

We have presented some of the data from this project at National and International Conferences (ASH and ISEH) as well invited seminar series at US-based research institutes.

Plans for next reporting period within the No-Cost Extension:

Experimental

Aim 1.1: To determine if DDX41 regulates R-loop levels- We have completed all the proposed experiments for this goal.

Aim 1.2: To determine if R-loops contribute to hematopoietic defects in *ddx41* mutants- We have completed all the proposed experiments for this goal.

Aim 1.3: To determine how R-loops regulate hematopoietic gene expression- We performed RNA-sequencing analysis of *gata1:gfp*⁺ erythroid progenitors from *ddx41* mutants and siblings with or without RNASEH1-GFP overexpression to deplete R-loops. We will analyze the data to define how R-loops affect transcript levels and splice isoform selection in both mutants and siblings. We strive to identify signatures of R-loop regulated gene expression under normal (siblings) and defective (mutant) conditions. Additionally, as R-loops are known to impact chromatin, we will perform ATAC-sequencing in the same cell populations as the RNA-seq to decipher if R-loops alter chromatin accessibility in control or *ddx41* mutant erythroid progenitors. These data will provide insight into how homeostatic R-loops and excessive R-loops impact hematopoietic gene expression.

Aim 2.1: To determine if inflammatory signaling is perturbed in *ddx41* mutants- We have completed all the proposed experiments for this goal.

Aim 2.2: To determine if STING-mediated inflammatory signaling plays a role in hematopoietic defects in *ddx41* mutants- We will focus on deciphering if cGAS/STING activity contributes to the diminished levels of *ddx41* mutant erythrocytes and myeloid cells.

Aim 2.3: To determine if elevated levels of R-loops alter inflammatory signaling in *ddx41* mutants- Our data indicate that depletion of RNA:DNA hybrids in *ddx41* mutants lowers phospho-TBK1 levels. We will examine R-loop regulation of inflammatory gene expression. We will examine our RNA-seq and ATAC-seq data specifically for inflammatory genes as well as R-loop-regulated splicing alterations in *ddx41* mutant *gata1:gfp*⁺ erythroid progenitors.

Publications

1. Weinreb JT, Ghazale N, Pradhan K, Gupta V, Potts KS, Tricomi B, Daniels NJ, Padgett RA, De Oliveira S, Verma AK, and **Bowman TV**. Excessive R-loops Trigger an Inflammatory Cascade Leading to Aberrant HSPC Expansion. Developmental Cell, 2021; 56(5):627-640 e5. PMID: 33651979.
2. Weinreb JT, Gupta V, Sharvit E, Weil R, and **Bowman TV**. Ddx41 inhibition of DNA damage signaling permits erythroid progenitor expansion in zebrafish. Haematologica, 2021; doi:10.3324/haematol.2020.257246. PMID: 33763998.

4. Impact

Impact on the principal discipline: Mutations in *DDX41* in MDS were identified over 6 years ago, but how defects in this factor might contribute to hematopoietic dysfunction remains unknown. Our studies have revealed that *in vivo* DDX41 acts as a R-loop repressor and that loss of this function results in elevated R-loop levels, cGAS/STING pathway activation, and subsequent aberrant HSPC expansion. These mechanistic discoveries pave the way towards future biochemical studies on DDX41-RNA:DNA hybrid interactions, R-loop

activation of cGAS, and the function of the cGAS/STING signaling in hematopoietic homeostasis. Moreover, these findings strongly suggest that inhibitors of the cGAS/STING pathway could be novel therapeutics for the treatment of MDS. Indeed, several STING antagonist are currently in pre-clinical and clinical develop for other diseases which could allow for more streamlined testing of these molecules for MDS.

Impact on other disciplines: Nothing to Report

Impact on society beyond science and technology: Nothing to Report

5. Changes/Problems

Nothing to Report

6. Products

Journal publications:

Weinreb JT, Ghazale N, Pradhan K, Gupta V, Potts KS, Tricoli B, Daniels NJ, Padgett RA, De Oliveira S, Verma AK, and **Bowman TV**. Excessive R-loops Trigger an Inflammatory Cascade Leading to Aberrant HSPC Expansion. *Developmental Cell*, 2021; 56(5):627-640 e5. PMID: 33651979.

Weinreb JT, Gupta V, Sharvit E, Weil R, and **Bowman TV**. Ddx41 inhibition of DNA damage signaling permits erythroid progenitor expansion in zebrafish. *Haematologica*, 2021; doi:10.3324/haematol.2020.257246. PMID: 33763998.

Conference papers and presentations:

Nov 2020 Department of Genetics, Cell Biology, and Anatomy, University of Nebraska Medical Center, Omaha, NE (Virtual)

Dec 2020 ASH Myeloid Workshop, 2020 ASH Annual Meeting (Virtual)

Nov 2021 NIH Workshop: Biological Functions of DEAD/H-box Helicase in Health and Diseases

7. Participants

Name:	Teresa V. Bowman, PhD
Project Role:	Principal Investigator
Research Identifier (e.g. ORCID ID):	
Nearest person month worked:	3
Contribution to project:	Dr. Bowman oversaw all of the work performed for the project, mentored and managed all participants, helped with data analysis, and wrote/edited all manuscripts.
Funding Support:	
Name:	Kathryn Potts, PhD
Project Role:	Postdoctoral Researcher
Research Identifier (e.g. ORCID ID):	
Nearest person month worked:	12
Contribution to project:	Dr. Potts performed the experiments in the project along with Joshua Weinreb.
Funding Support:	
Name:	Joshua Weinreb
Project Role:	Graduate Student
Research Identifier (e.g. ORCID ID):	
Nearest person month worked:	12
Contribution to project:	Joshua Weinreb performed all the experiments in the project along with Dr. Potts.
Funding Support:	Mr. Weinreb is supported by an F30 NIH predoctoral fellowship (1F30HL142161)
Name:	Varun Gupta

Project Role:	Bioinformatician
Research Identifier (e.g. ORCID ID):	
Nearest person month worked:	0.6
Contribution to project:	Varun Gupta performed all the computational analysis of the RNA-sequencing data.
Funding Support:	

Changes in active other support to Principal Investigator:

New Active Grants:

Edward P. Evans Foundation MDS Discovery Research Grant: 2021-2024
 “Delineating mechanisms of DDX41 insufficiency in MDS”
 Principal Investigator: Teresa Bowman

NIH/NIDDK: 1R01DK131445: 2021-2024
 “Identification of novel regulators of HSC specification and maturation”
 Principal Investigator: Teresa Bowman

Completed Grants:

Other organizations: Nothing to Report

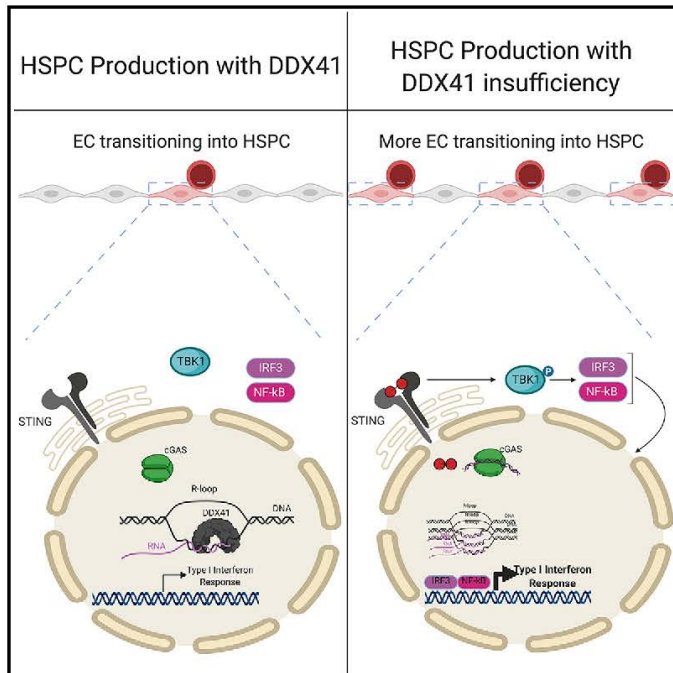
8. Special Reporting Requirements: Nothing to Report

9. Appendices:

Developmental Cell

Excessive R-loops trigger an inflammatory cascade leading to increased HSPC production

Graphical abstract



Authors

Joshua T. Weinreb, Noura Ghazale, Kith Pradhan, ..., Sofia De Oliveira, Amit Verma, Teresa V. Bowman

Correspondence

teresa.bowman@einsteinmed.org

In Brief

Weinreb et al. show a link between R-loops, inflammation, and the developing hematopoietic system. Ddx41 acts as a gatekeeper of HSPC production by suppressing R-loop accumulation and the cGAS-STING inflammatory pathway. Elevated R-loops and inflammatory signaling were also observed in human cells with decreased DDX41, suggesting possible conservation of mechanism.

Highlights

- Ddx41 regulates HSPC number *in vivo*
- Ddx41 constrains R-loop levels *in vivo*
- Elevated R-loop levels increase HSPC production via cGAS-STING inflammatory signaling
- DDX41 suppression of R-loop levels and inflammatory signaling is observed in human cells



Weinreb et al., 2021, *Developmental Cell* 56, 627–640
 March 8, 2021 © 2021 Elsevier Inc.
<https://doi.org/10.1016/j.devcel.2021.02.006>



Article

Excessive R-loops trigger an inflammatory cascade leading to increased HSPC production

Joshua T. Weinreb,^{1,2} Noura Ghazale,^{1,2} Kith Pradhan,^{1,3} Varun Gupta,⁴ Kathryn S. Potts,^{1,2} Brad Tricomi,^{2,4} Noah J. Daniels,⁵ Richard A. Padgett,⁵ Sofia De Oliveira,^{1,6} Amit Verma,^{1,2,7} and Teresa V. Bowman^{1,2,7,8,*}

¹Department of Developmental and Molecular Biology, Albert Einstein College of Medicine, Bronx, NY, USA

²Gottesman Institute for Stem Cell Biology and Regenerative Medicine, Albert Einstein College of Medicine, Bronx, NY, USA

³Department of Epidemiology and Population Health, Albert Einstein College of Medicine, Bronx, NY, USA

⁴Department of Cell Biology, Albert Einstein College of Medicine, Bronx, NY, USA

⁵Cardiovascular and Metabolic Sciences, Lerner Research Institute, Cleveland Clinic, Cleveland, OH, USA

⁶Department of Medicine (Hepatology) and Marion Bessin Liver Research Center, Albert Einstein College of Medicine and Montefiore Medical Center, Bronx, NY, USA

⁷Department of Medicine (Oncology), Albert Einstein College of Medicine and Montefiore Medical Center, Bronx, NY, USA

⁸Lead contact

*Correspondence: teresa.bowman@einsteinmed.org

<https://doi.org/10.1016/j.devcel.2021.02.006>

SUMMARY

Hematopoietic stem and progenitor cells (HSPCs) arise during embryonic development and are essential for sustaining the blood and immune systems throughout life. Tight regulation of HSPC numbers is critical for hematopoietic homeostasis. Here, we identified DEAD-box helicase 41 (Ddx41) as a gatekeeper of HSPC production. Using zebrafish *ddx41* mutants, we unveiled a critical role for this helicase in regulating HSPC production at the endothelial-to-hematopoietic transition. We determined that Ddx41 suppresses the accumulation of R-loops, nucleic acid structures consisting of RNA:DNA hybrids and ssDNAs whose equilibrium is essential for cellular fitness. Excess R-loop levels in *ddx41* mutants triggered the cGAS-STING inflammatory pathway leading to increased numbers of hemogenic endothelium and HSPCs. Elevated R-loop accumulation and inflammatory signaling were observed in human cells with decreased DDX41, suggesting possible conservation of mechanism. These findings delineate that precise regulation of R-loop levels during development is critical for limiting cGAS-STING activity and HSPC numbers.

INTRODUCTION

The hematopoietic system is maintained by multipotent hematopoietic stem and progenitor cells (HSPCs) that sustain the stem cell pool via self-renewal divisions and generate all mature blood cells through multilineage differentiation. Precise maintenance of the HSPC pool is critical for healthy hematopoiesis throughout life. A paucity of functional HSPCs can result in bone marrow failure, and aberrant expansion of HSPCs is a common feature in clonal hematologic malignancies (Kurze, 2018; Sperling et al., 2017). Functional hematopoietic transplantation studies indicate that the frequency of HSPCs across vertebrates is astoundingly conserved (Fraint et al., 2020; Hess et al., 2013; Szilvassy et al., 2003). Shifts in HSPC frequency during embryogenesis are linked to inherited bone marrow failure syndromes, underlying the importance of identifying factors that ensure robustness in HSPC development (Kurze, 2018).

Inflammatory signaling plays a physiological role in regulating HSPC biology from the earliest stages of stem cell formation in the embryo and throughout the aging process (Espin-Palazon et al., 2018; Pietras, 2017). During development, nuclear factor

kappa-light-chain enhancer of activated B cells (NFκB) and interferon (IFN) signaling are critical for the initial establishment of definitive HSPCs (He et al., 2015; Espin-Palazon et al., 2014; Li et al., 2014; Sawamiphak et al., 2014). Prior work suggested that sterile inflammation, a non-pathogen-mediated activation of immunomodulatory signaling, is at the heart of the inflammatory signals required for HSPC formation. Our knowledge of the non-infectious stimuli and the downstream signaling cascades relevant for the impact of sterile inflammation on HSPC production in embryogenesis is incomplete.

Many of the transcription factors widely studied in HSPC development, such as AML/RUNX1, TAL1/SCL, and TEL1/ETV6, were first uncovered due to their aberrant function in hematologic malignancies. In humans, *DEAD-box helicase 41* (*DDX41*) was recently shown to be mutated in both germline and acquired forms of myelodysplastic syndrome (MDS), a clonal HSPC disorder (Sperling et al., 2017; Polprasert et al., 2015). The clinical link is suggestive, but the precise role for DDX41 in HSPC biology has yet to be demonstrated. DDX41 has pleiotropic cellular functions associated with inflammation, splicing, and, more recently, R-loops (Wang et al., 2018;



Polprasert et al., 2015; Zhang et al., 2013; Parvatiyar et al., 2012; Zhang et al., 2011).

R-loops are three-stranded nucleic acid structures consisting of an RNA:DNA hybrid and ssDNA. They are natural consequences of transcription that play roles in numerous cellular functions, including immunoglobulin class-switch recombination, mitochondrial replication, and transcriptional and epigenetic regulation (Crossley et al., 2019). Recent work demonstrated that the genome-wide R-loop landscape is dynamic during differentiation of human pluripotent stem cells into numerous lineages suggesting that the regulation of R-loop levels could be important during developmental fate transitions (Yan et al., 2020). Additionally, mutations in R-loop-regulating factors are found in humans with autoimmune disorders, suggesting that R-loop imbalance could affect inflammatory signaling (Günther et al., 2015; Lim et al., 2015).

Here, we show that DDX41 sits at a crossroad of R-loop metabolism and inflammation to regulate HSPC homeostasis. To uncover if DDX41 plays a role in HSPC development, we established a zebrafish *ddx41* loss-of-function mutant to study the *in vivo* requirements of Ddx41. We demonstrated that Ddx41 regulates HSPC number by increasing hemogenic endothelium. Mechanistically, loss of *ddx41* leads to R-loop accumulation triggering NF κ B-mediated inflammation via activation of the cyclic GMP-AMP synthase (cGAS)-stimulator of interferon genes (STING) signaling pathway. This sterile inflammatory cascade in the mutants underlies their increased HSPC production. Elevated R-loop accumulation and inflammatory signaling were also observed in human cells with decreased DDX41, suggesting possible conservation of mechanism in humans. Together, our data establish that Ddx41 constrains HSPC production during development by maintaining R-loop homeostasis and preventing aberrant inflammatory signaling.

RESULTS

Ddx41 regulates HSPC number

As DDX41 mutations are linked to hematologic diseases driven by HSPC dysfunction, we hypothesized that this helicase might have a role in HSPC homeostasis. We explored this question with a zebrafish *ddx41* loss-of-function mutant (*ddx41*^{sa14887}) (Kettleborough et al., 2013). DDX41 is highly conserved between humans and zebrafish with an overall 89% identity and 94% similarity between the two proteins with almost identical DEAD box and helicase domains (Figure S1A), suggesting that the lessons learned about the *in vivo* role of zebrafish Ddx41 function in hematopoiesis will be relevant to human DDX41.

In zebrafish, definitive hematopoiesis begins ~24 h post fertilization (hpf), creating HSPCs that can self-renew and reconstitute all adult blood lineages (Nik et al., 2017). During development, HSPCs derive directly from the aortic hemogenic endothelium—which is located in the ventral floor of the dorsal aorta in a region known as the aorta gonad mesonephros (AGM)—via a process termed endothelial-to-hematopoietic transition (EHT) (Ottersbach, 2019; Bertrand et al., 2010; Boisset et al., 2010; Kissa and Herbomel, 2010). This process involves the transition of a subset of endothelial cells into HSPCs. We examined HSPC formation at the time of this transition via *in situ* hybridization for expression of *runx1*, a marker of hemogenic endothelium

and nascent HSPCs (Burns et al., 2002). At 40 hpf, levels of *runx1*⁺ cells were elevated in *ddx41* mutants compared with sibling controls (Figures 1A and 1B). We also demonstrated this increase by measuring the absolute number of HSPCs per embryo using flow cytometry quantification with the HSPC fluorescent reporters *runx1+23:mcherry* (hereafter referred to as *runx1:mcherry*) (Tampin et al., 2015) and *cd41:gfp* (Lin et al., 2005). In agreement with the *runx1 in situ* results, we observed a significant increase in the number of both *runx1:mcherry*⁺ and *cd41:gfp*⁺ HSPCs in *ddx41* mutants (Figures 1C–1F). Taken together, our results indicate that decreased *ddx41* levels lead to a significant increase in HSPCs.

We next wanted to elucidate if HSPC expansion in *ddx41* mutants is occurring via an increase in proliferation and/or production. To examine proliferation, we analyzed cell cycle status of *ddx41* mutant *cd41:gfp*⁺ HSPCs by flow cytometry quantification of DNA synthesis via 5-Ethynyl-2'-deoxyuridine (EdU) incorporation and DNA content via DAPI incorporation. At 40 hpf, *ddx41* mutant *cd41:gfp*⁺ HSPCs showed a reduction of cells in S phase and an accumulation in the G2/M phase compared with sibling controls (Figures S1C and S1D). These results suggest a decrease in proliferation rather than an increase, which indicates that HSPC expansion in *ddx41* mutants is not a result of increased cell division.

A second mechanism we tested was increased HSPC production. Hemogenic endothelial cells undergoing EHT express features of both endothelial cells and HSPCs (Bertrand et al., 2010). First, we examined the vasculature via *in situ* hybridization for *flt4* (vein) and *notch1b* (aorta) and observed no difference between siblings and *ddx41* mutants, suggesting that the artery-vein specification was unaffected (Figures S1E and S1F). Next, we performed flow cytometry to quantify endothelial cells (*kdr1:dsred*⁺), hemogenic endothelial cells (*cd41:gfp*⁺;*kdr1:dsred*⁺), and HSPCs (*cd41:gfp*⁺) in sibling controls versus *ddx41* mutants. At 40 hpf, we observed no significant difference in the number of *kdr1:dsred*⁺ endothelial cells, but a significant increase in the number of both *cd41:gfp*⁺ HSPCs and *cd41:gfp*⁺;*kdr1:dsred*⁺ double positive hemogenic endothelial cells in *ddx41* mutants (Figures 1G, 1H, S1G, and S1H). To visualize EHT changes, we performed whole mount time-lapse confocal imaging of *cd41:gfp*⁺;*kdr1:dsred*⁺ sibling controls and *ddx41* mutants between ~36–44 hpf (Videos S1 and S2). Consistent with the flow cytometry data, we observed that *ddx41* mutants had an increased number of *cd41:gfp*⁺;*kdr1:dsred*⁺ cells undergoing EHT morphological changes earlier in development than sibling controls. Taken together, our results indicate that the expansion of HSPCs in *ddx41* mutants is via an increased rate of EHT.

Ddx41 constraint of R-loop levels is critical for HSPC homeostasis

Cells possess numerous safeguards to tightly regulate R-loop levels, such as: formation inhibition by splicing factors, destruction by RNA:DNA hybrid ribonucleases, and removal by RNA:DNA hybrid helicases (Crossley et al., 2019). Based on the evidence that DDX41 binds to RNA:DNA hybrids and that its activity is stimulated by this interaction (Stavrou et al., 2018; Wang et al., 2018; Yoneyama-Hirozane et al., 2017), we hypothesized that Ddx41 might prevent R-loop accumulation *in vivo*. To address this question, we measured R-loop levels in *ddx41*

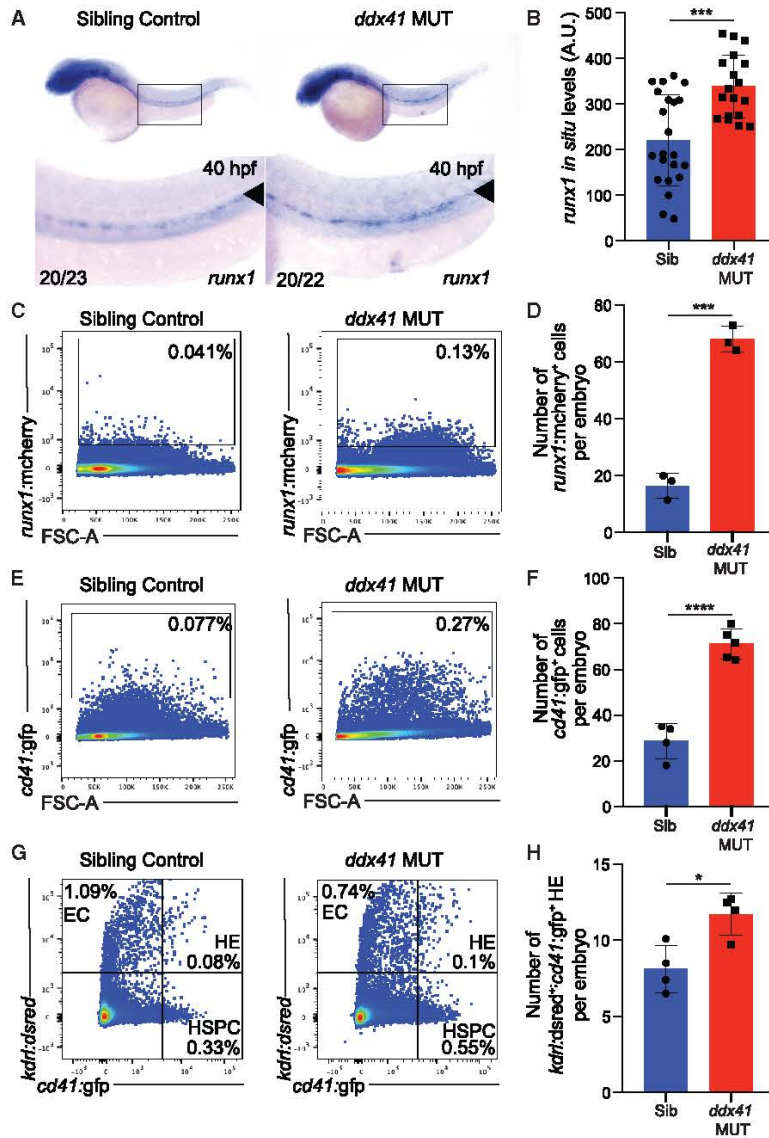


Figure 1. Ddx41 regulates HSPC number

(A) *In situ* hybridization of the HSPC marker *runx1* at 40 hpf in sibling controls (left) and *ddx41* mutants (right). Numbers on bottom left corner indicate the fraction of embryos with the same phenotype as the one depicted in the image. Inset underneath shows a higher magnification (8 \times) view of the boxed AGM region above. The aorta is marked with arrowheads.

(B) Quantification of *runx1* *in situ* hybridization levels from (A). Quantification was done using Fiji. a.u., arbitrary unit.

(C and E) Flow cytometry plots of *runx1*:mcherry⁺ (C) and *cd41*:gfp⁺ (E) HSPCs from sibling controls (left) and *ddx41* mutants (right) at 40 hpf.

(D and F) Graphs depicting the absolute number of *runx1*:mcherry⁺ (D) and *cd41*:gfp⁺ (F) per embryo at 40 hpf.

(G) Flow cytometry plots of *kdr1*:dsred⁺; *cd41*:gfp⁺, and *kdr1*:dsred⁺; *cd41*:gfp⁺ double positive cells from sibling controls (left) and *ddx41* mutants (right) at 40 hpf.

(H) Graphs depicting the absolute number of *kdr1*:dsred⁺; *cd41*:gfp⁺ double positive hemogenic endothelial cells per embryo at 40 hpf. Graphs display means \pm standard deviations (stds) with p values calculated with unpaired Student's t test. *p < 0.05, ***p < 0.001, ****p < 0.0001. N = 3–5 replicates per experiment.

at 6 hpf, separated transgenic and non-transgenic siblings according to GFP expression, and then assessed R-loop levels (Figure 2A). Our results showed that R-loop levels were increased nearly 2-fold in *ddx41* mutants compared with sibling cells and that the effect was suppressed by RNASEH1-GFP expression (Figures 2B and 2C). These data demonstrate that Ddx41 regulates R-loop levels *in vivo*.

We ascertained the effect of R-loop levels on hematopoiesis in *ddx41* mutants by measuring HSPC numbers in mutants and siblings following R-loop removal. As quantified by assessment of both absolute number of *runx1*:mcherry⁺ HSPCs per embryo and *runx1* *in situ* hybridization

mutants and siblings. We performed immunofluorescence with the S9.6 antibody, which is a monoclonal antibody that specifically binds RNA:DNA hybrids, and is a mainstay in the field for R-loop identification (Boguslawski et al., 1986). To confirm the S9.6 signal in zebrafish *ddx41* mutants was specific to RNA:DNA hybrids, we used Tg(*hsp:M27RNASEH1-GFP*) zebrafish that express human RNASEH1 fused to GFP under a heat shock-inducible promoter (Sorrells et al., 2018). RNase H1 is an enzyme which removes R-loops through the selective degradation of RNA in RNA:DNA hybrids and is the most rigorous confirmation to demonstrate R-loop dependency of a given phenotype (Suzuki et al., 2010; Paulsen et al., 2009). We induced RNASEH1-GFP expression by heat shocking *ddx41* mutants and siblings

staining at 40 hpf, HSPC levels were significantly reduced in *ddx41* mutants after RNASEH1-GFP expression (Figures 2D–2G). Next, we assessed if this effect was via a cell-intrinsic or cell-extrinsic mechanism. To address this, we isolated *cd41*:gfp⁺ HSPCs from 40 hpf sibling controls and *ddx41* mutants using fluorescent-activated cell sorting (FACS) and performed immunofluorescence with the S9.6 antibody to assess R-loop levels. Similar to the results in the whole embryo, R-loop levels were increased nearly 2-fold in *ddx41* mutant *cd41*:gfp⁺ HSPCs compared with siblings (Figure S2). To elucidate if the impact of excess R-loops on HSPC expansion was cell intrinsic, we injected *ddx41* mutants with either *ubi:gfp* (control) or *fli1:M27RNASEH1-GFP*, which would deplete R-loops only in *fli1*⁺

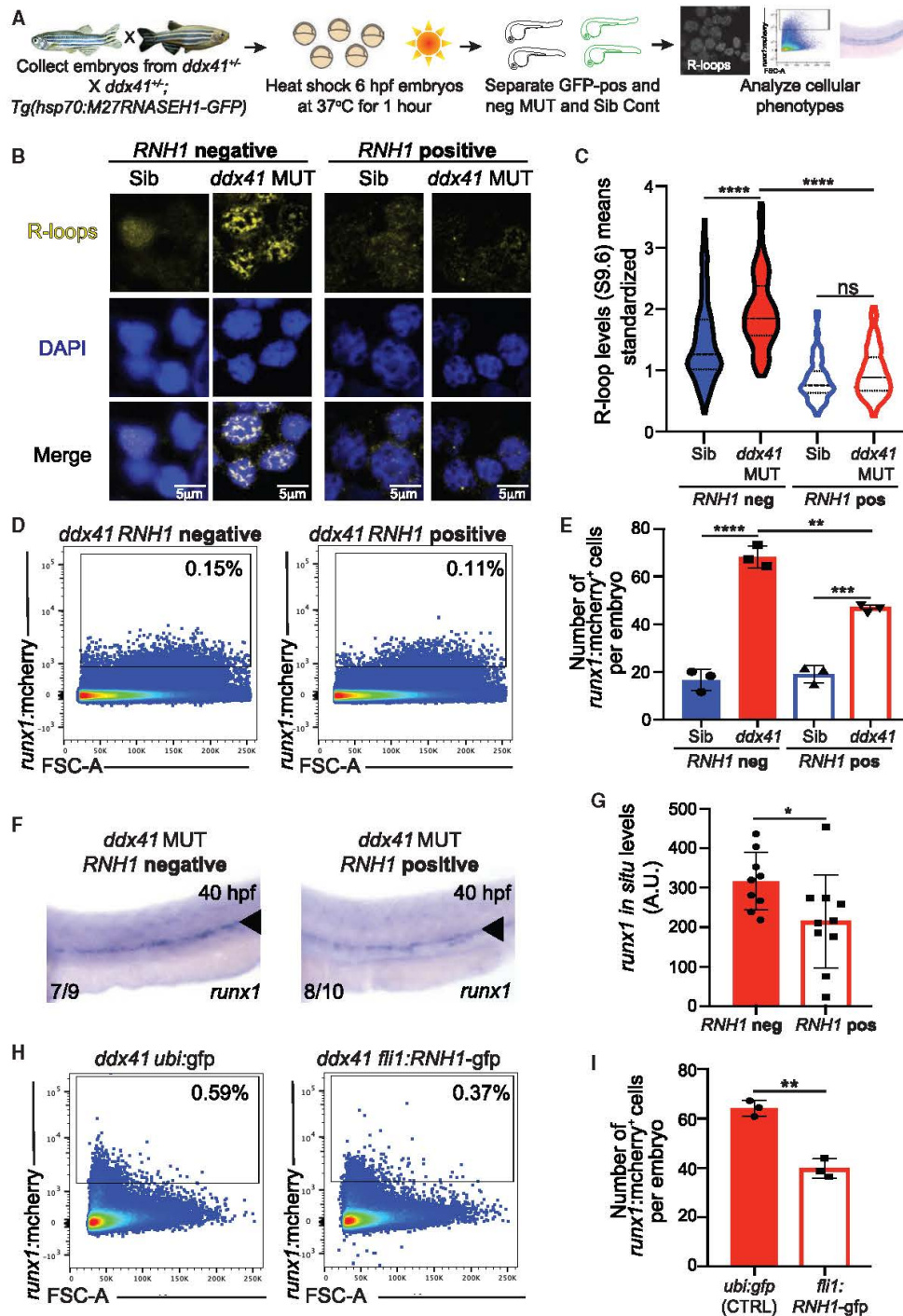


Figure 2. Ddx41 constraint of R-loop levels is critical for HSPC homeostasis

(A) Schematic of the RNASEH1 overexpression experiments.

(B) Confocal images showing immunofluorescence of R-loops and nuclei (DAPI) in cells isolated from 28 hpf siblings (left) and *ddx41* mutants (right) that are either *Tg(hsp70:M27RNASEH1-GFP)* negative (left) or *Tg(hsp70:M27RNASEH1-GFP)* positive (right). Scale bar, 5 μ m.

(legend continued on next page)

endothelial cells, including those that give rise to HSPCs (Lawson and Weinstein, 2002). As quantified by assessment of *runx1:mcherry*⁺ HSPCs per embryo at 40 hpf, HSPC levels were significantly reduced in *ddx41* mutants injected with *fli1:M27RNASEH1-GFP* compared with their control counterparts (Figures 2H and 2I). These data show that aberrant R-loop accumulation can intrinsically promote HSPC production from endothelial cells.

R-loops promote inflammatory gene expression in *ddx41* mutants

To delve into the mechanism underlying the HSPC defect in *ddx41* mutants, we conducted RNA-sequencing (RNA-seq) on *cd41:gfp*⁺ HSPCs isolated from *ddx41* mutants and siblings at 40 hpf. Of the nearly 19,000 genes analyzed, 1,173 were downregulated and 1,327 were upregulated in *ddx41* mutants compared with siblings (Figure 3A; Table S1).

To gain an insight into the affected pathways, we performed gene-set analysis on the upregulated and downregulated gene lists by comparing each to the molecular signature database (MSigDB), a platform that computes overlaps between experimentally derived gene lists and lists of genes in known pathways (Liberzon et al., 2015; Subramanian et al., 2005). In the downregulated list, genes associated with MTORC1 signaling, epithelial-mesenchymal transition, coagulation, and apical junctions were enriched (Figure 3B; Table S2). In the upregulated gene list, spliceosome was the top gene set with heme metabolism, DNA repair, and IFN- α response also enriched (Figure 3C; Table S3).

Ddx41 interacts with components of the spliceosome and is implicated in pre-mRNA splicing (Polprasert et al., 2015); thus, we also examined how *ddx41* loss affected mRNA splicing in HSPCs. A total of 2,009 alternative splicing events were observed between *ddx41* mutants and siblings, with exon skipping being the most frequently altered splicing event followed by intron retention (Figures S3A and S3B; Table S4). These splicing defects are similar to those found in *DDX41*-depleted and *DDX41*-mutated human cells (Polprasert et al., 2015). We were also able to detect other splicing defects not reported previously, including alternative 5'-splice site usage, alternative 3'-splice site usage, and changes in mutually exclusive exon usage in *ddx41* mutants as compared with siblings. To understand if particular pathways were enriched in the alternatively spliced gene list, we compared it with the MSigDB and determined that immune system pathways were among the top-enriched pathways (Figure S3C). Among the alternatively spliced factors were several NF- κ B pathway components, including *map3k7*,

nfkb2, *nfkbiab*, and *irak3*. These results depict that *Ddx41* influences inflammatory gene expression in HSPCs at multiple levels.

Type I interferons and their target genes were significantly elevated in *ddx41* mutant HSPCs (Figure 3C; Table S3). We posited that excess R-loops might contribute to inflammatory signaling. The cytosolic nucleic acid sensor cGAS binds to—and can be activated by—RNA:DNA hybrids (Mankan et al., 2014). cGAS activity can induce a STING signaling cascade resulting in increased type I IFN-responsive gene expression (Ablasser et al., 2013; Li et al., 2013). To determine if R-loops contributed to inflammatory gene expression, we measured the expression of *ifn-phi1*, which is a zebrafish type I IFN, and several type I IFN-responsive genes identified in our RNA-seq analysis using RT-qPCR in embryos \pm RNASEH1-GFP expression. Depletion of R-loops significantly reduced expression of many of these genes in *ddx41* mutants, demonstrating that excessive R-loops promote inflammatory signaling (Figure 3D).

Ddx41 regulates inflammatory signaling via the cGAS-STING pathway

Our model is that excess R-loops promote inflammation by activating the cGAS-STING pathway. We first assessed if cGAS and R-loops were in the same cellular compartment, and thus capable of activating cGAS-STING signaling as previously characterized (Mankan et al., 2014). Prior studies show that in addition to being in the cytoplasm, cGAS can also be found tightly tethered to chromatin in the nucleus, suggesting that it can bind to nuclear RNA:DNA hybrids (Gentili et al., 2019; Jiang et al., 2019; Volkman et al., 2019; Liu et al., 2018). Consistent with these prior reports, we found cGAS to be predominantly in the nucleus of zebrafish cells by immunofluorescence (Figures S4A–S4E). Additionally, R-loops were present in both cellular compartments of *ddx41* mutant embryos (Figures 2B, 2C, S4F, and S4G). In combination, these results demonstrate that interactions between R-loops and cGAS are possible in multiple cellular compartments.

Next, we ascertained if the loss of *ddx41* led to activation of the cGAS-STING pathway. Phosphorylation of Ser172 in Tank Binding Kinase 1 (TBK1) is induced downstream of cGAS-STING activation; thus, we measured phospho-TBK1 levels in sibling controls and *ddx41* mutant cells by immunofluorescence and western blots (Bai et al., 2017). Levels of phospho-TBK1 were significantly elevated in *ddx41* mutants and dependent on cGAS and elevated R-loop levels (Figures 4A–4C, S4H, and S4I). These data indicate that the cGAS-STING pathway is elevated when *ddx41* levels are diminished.

(C) Quantification of R-loop levels from (B).

(D) Flow cytometry plots of *runx1:mcherry*⁺ HSPCs from *Tg(hsp70:M27RNASEH1-GFP)*-negative (left) and *Tg(hsp70:M27RNASEH1-GFP)*-positive (right) *ddx41* mutants at 40 hpf.

(E) Graph depicting the number of *runx1:mcherry*⁺ HSPCs per embryo from (D).

(F) *In situ* hybridization of the HSPC marker *runx1* at 40 hpf in *Tg(hsp70:M27RNASEH1-GFP)*-negative *ddx41* mutants (left) and *Tg(hsp70:M27RNASEH1-GFP)*-positive *ddx41* mutants (right). Numbers on bottom left corner indicate the fraction of embryos with the same phenotype as the one depicted in the image. A higher magnification view of the AGM region is displayed. The aorta is marked with arrowheads.

(G) Quantification of *runx1 in situ* hybridization levels from (F). Quantification was done using Fiji. a.u., arbitrary unit.

(H) Flow cytometry plots of *runx1:mcherry*⁺ HSPCs *ddx41* mutants injected with *ubi:gfp* (left, control) and *fli1:M27RNASEH1-GFP* (right) at 40 hpf.

(I) Graph depicting the number of *runx1:mcherry*⁺ HSPCs per embryo from (H). Graphs display means \pm stds with p values calculated with a one-way ANOVA with Tukey's multiple testing correction (C and E) or unpaired Student's t test (G and I). *p < 0.05, **p < 0.01, ***p < 0.001, ****p < 0.0001, ns, not significant (p > 0.05). N = 3–6 replicates per experiment.

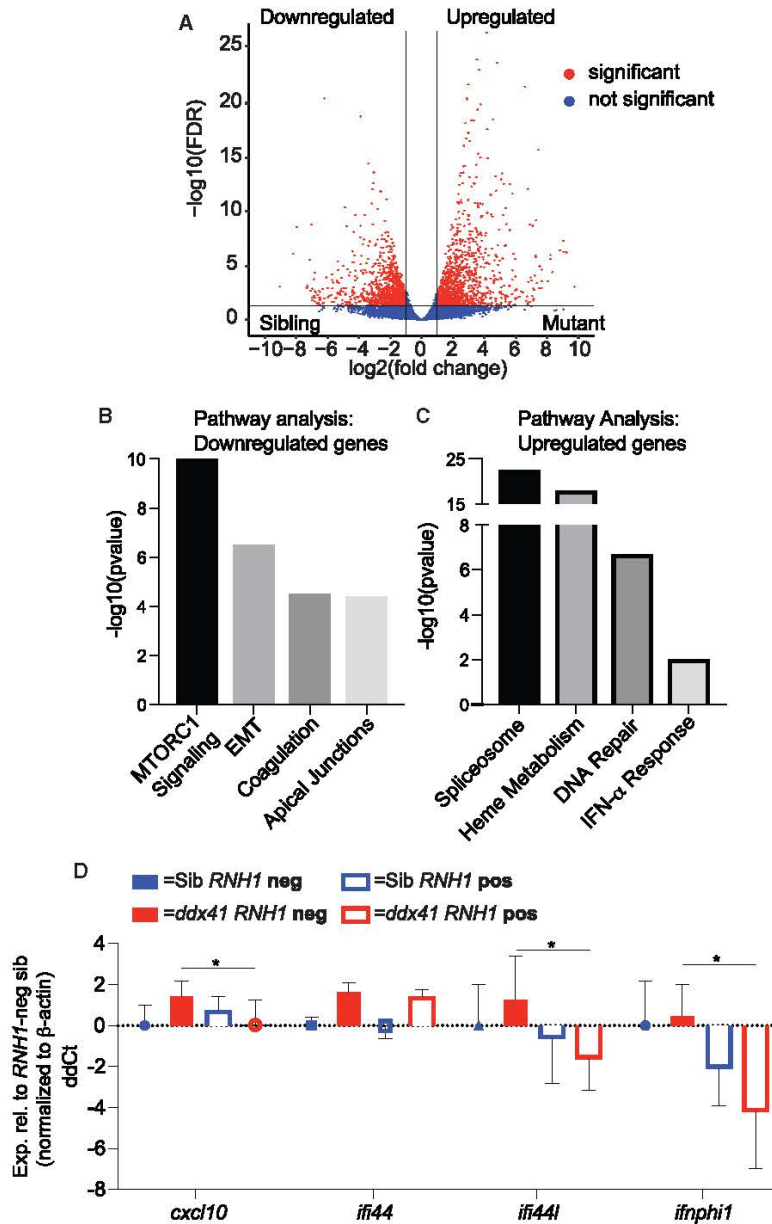


Figure 3. R-loops promote inflammatory gene expression in *ddx41* mutants

(A) Volcano plot displaying differentially expressed genes between *cd41:gfp*⁺ HSPCs from *ddx41* mutants and siblings. Significant differences are defined as FDR < 0.05 and \log_2 fold change > 1. Black vertical lines denote the fold-change threshold and the black horizontal line denotes the FDR threshold. Three biological replicates for both *ddx41* mutants and siblings were used to generate RNA-sequencing data.

(B and C) Representative charts of pathways significantly enriched in genes downregulated (B) or upregulated (C) in *ddx41* mutant HSPCs compared with sibling controls as determined by MSigDB analysis.

(D) Graph of RT-qPCR analysis of the expression of type I IFN-responsive genes between sibling controls and *ddx41* mutants that are *Tg(hsp70:M2TRNASEH1-GFP)*-negative versus *Tg(hsp70:M2TRNASEH1-GFP)*-positive. Expression levels were normalized to β -actin levels. All levels are relative to the RNASEH1-GFP (RNH1) negative sibling controls expressed as ddCt values, with positive values reflecting higher expression and negative values reflecting lower expression. Graph displays means \pm standard error mean with p values calculated with an unpaired t test, * $p < 0.05$. N = 4 replicates per experiment.

flow cytometry and demonstrated a significant increase in *ddx41* mutants (Figures 4D and 4E). We also determined that NF κ B activity was increased in *runx1:mcherry*⁺ HSPCs and *kdrl:dsred*⁺ endothelial cells in *ddx41* mutants (Figures S4J–S4M). These data support that Ddx41 regulates NF κ B signaling in numerous cell types, including HSPC and endothelial cells.

Next, we determined if inhibiting components of the cGAS-STING pathway would dampen inflammatory signaling in *ddx41* mutants by measuring *nfkb:gfp* reporter activity (Figure 4F). Morpholino knockdown of either STING or cGAS lowered *nfkb:gfp* reporter activity in *ddx41* mutants (Figures 4G, 4H, S4E, and S4N–S4P). Taken together, these data indicate that cGAS-STING pathway activation is functionally important for the inflammatory response in *ddx41* mutants.

Stimulation of the cGAS-STING pathway ultimately results in activation of the transcription factors IRF3/7 (interferon response factors 3 and 7) and NF κ B. As NF κ B is well established as a key inflammatory-stimulated transcription factor in regulating embryonic HSPC formation (Espin-Palazon et al., 2018), we examined the activation of this pathway. We measured activity using an NF κ B activity fluorescent reporter zebrafish that expresses GFP under the transcriptional control of a NF κ B-responsive promoter (*nfkb:gfp*) (Kanter et al., 2011). We quantified the absolute number of cells with high *nfkb:gfp* reporter activity using

Ddx41 regulates HSPC number via the cGAS-STING inflammatory pathway

Based on our finding that Ddx41 regulates NF κ B levels via the cGAS-STING axis, we tested the role of these signaling components on the HSPC expansion in *ddx41* mutants (Figure 5A). Lowering cGAS and STING levels using numerous genetic approaches significantly reduced HSPC numbers in *ddx41*

Stimulation of the cGAS-STING pathway ultimately results in activation of the transcription factors IRF3/7 (interferon response factors 3 and 7) and NF κ B. As NF κ B is well established as a key inflammatory-stimulated transcription factor in regulating embryonic HSPC formation (Espin-Palazon et al., 2018), we examined the activation of this pathway. We measured activity using an NF κ B activity fluorescent reporter zebrafish that expresses GFP under the transcriptional control of a NF κ B-responsive promoter (*nfkb:gfp*) (Kanter et al., 2011). We quantified the absolute number of cells with high *nfkb:gfp* reporter activity using

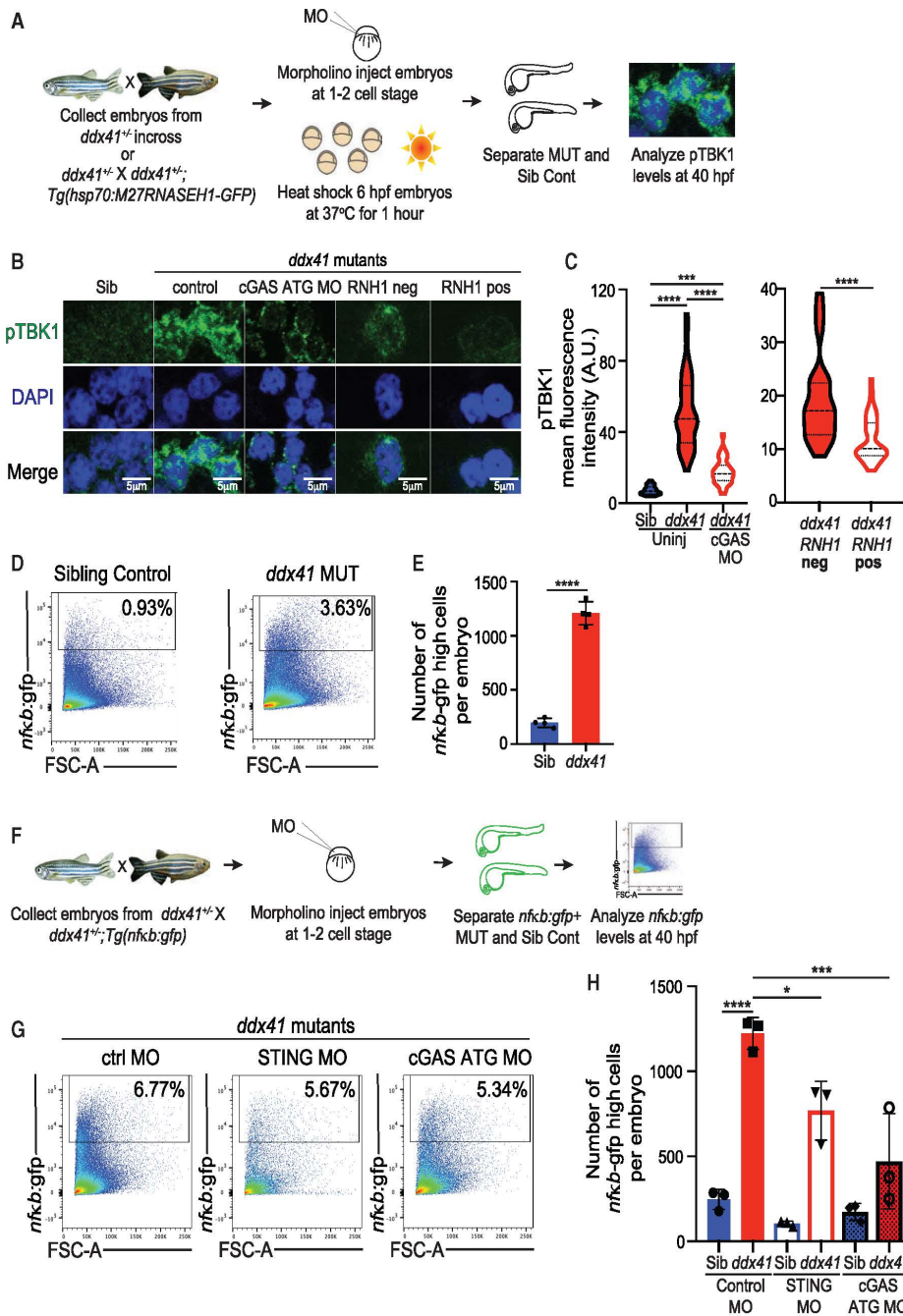


Figure 4. Ddx41 regulates inflammatory signaling via the cGAS-STING pathway

(A) Schematic of the Ser172-phosphorylated TBK1 (pTBK1) immunofluorescence experiments.
 (B) Confocal images showing immunofluorescence of pTBK1 and nuclei (DAPI) in cells isolated from 40 hpf siblings, *ddx41* mutants (control), *ddx41* mutants injected with cGAS translation-blocking (ATG) MO, RNH1-negative *ddx41* mutants and RNH1-positive *ddx41* mutants. Scale bar, 5 μ m.
 (C) Quantification of pTBK1 levels from (B).
 (D) Flow cytometry plots of *NFkB:gfp*⁺ cells from sibling controls (left) and *ddx41* mutants (right) at 40 hpf.
 (E) Graph depicting the absolute number of *NFkB:gfp*-high cells per embryo shown in (D).
 (F) Schematic of the cGAS-STING pathway knockdown experiments with *NFkB:gfp* quantification.
 (G) Flow cytometry plots of *NFkB:gfp*⁺ cells from *ddx41* mutants injected with control morpholino (left), splice-blocking *sting* morpholino (middle), or *cgas* ATG morpholino (right) at 40 hpf.
 (H) Graph depicting the absolute number of *NFkB:gfp*-high cells per embryo shown in (G). Graphs display means \pm stds with p values calculated with unpaired Student's t test (E) or a one-way ANOVA with Tukey's multiple testing correction (C and H), *p < 0.05, ***p < 0.001, ****p < 0.0001. N = 3–5 replicates per experiment.

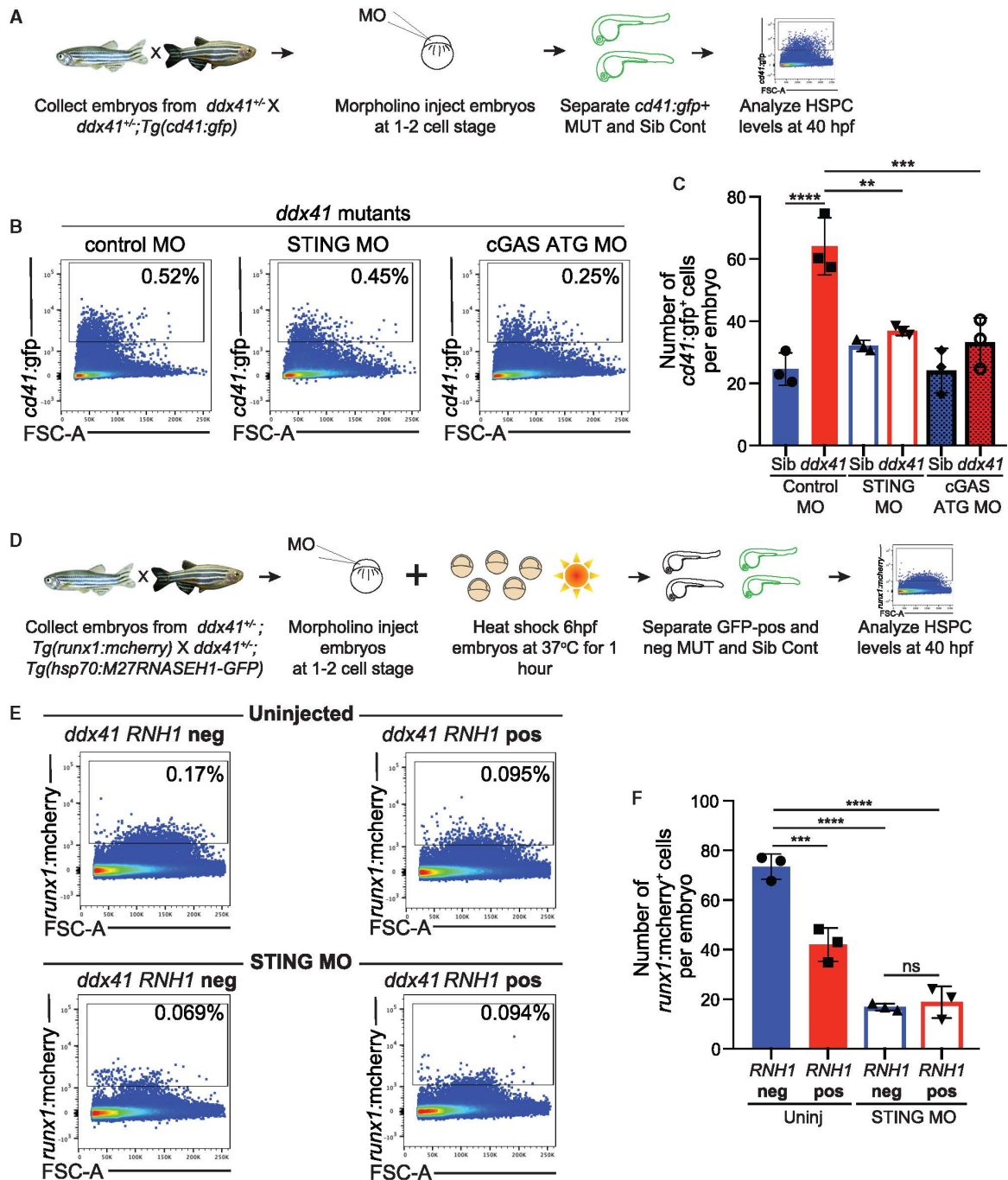


Figure 5. Ddx41 regulates HSPC number via the cGAS-STING inflammatory pathway

(A) Schematic of the cGAS-STING pathway knockdown experiments with HSPC quantification.

(B) Flow cytometry plots of *cd41:gfp⁺* HSPCs from *ddx41* mutants injected with control morpholino (left), splice-blocking *sting* morpholino (middle), or translation-blocking (ATG) *cgas* morpholino (right) at 40 hpf.

(C) Graph depicting the absolute number of *cd41:gfp⁺* cells per embryo shown in (B).

(D) Schematic of the STING knockdown and RNASEH1 overexpression experiment with HSPC quantification.

(legend continued on next page)

mutants, as measured by quantification of *cd41:gfp*⁺ HSPC numbers per embryo using flow cytometry and *runx1 in situ* hybridization (Figures 5B, 5C, and S5). These results indicate that the cGAS-STING inflammatory cascade promotes HSPC production in *ddx41* mutants.

Next, we determined if the increased HSPC formation from excessive R-loop levels was dependent or independent of the cGAS-STING signaling pathway. To do so, we assessed the impact of combined RNASEH1-GFP overexpression and STING knockdown on HSPC numbers in *ddx41* mutants (Figure 5D). If excess R-loops and STING are working via independent or parallel pathways, then we would expect an additive effect with further HSPC reduction compared with each manipulation alone. If they are working via a single pathway, then we would not see an additive suppression on HSPC expansion. We observed no difference between HSPC number in 40 hpf *ddx41* mutants with STING knockdown alone or in combination with RNASEH1-GFP overexpression (Figures 5E and 5F). These data support a single pathway with R-loops impacting HSPCs via a STING-mediated pathway.

Human cells with low *DDX41* have elevated inflammatory gene expression and R-loop levels

To test if the molecular features identified in zebrafish developmental HSPCs could be conserved in human cells, we examined clinical symptoms, gene expression, and R-loop levels in low versus high *DDX41* cells. We determined whether different *DDX41* expression levels were associated with different clinical outcomes. We compared blood counts and bone marrow blast levels in a cohort of 183 MDS patients (Pellagatti et al., 2010). The patients were stratified based on *DDX41* expression in their CD34⁺ HSPC bone marrow cells, comparing hematopoietic parameters in low- (bottom 20th percentile) versus high- (top 20th percentile) expressing patients (Figure S6A). Reduced white blood cell, neutrophil, and platelet counts were seen in MDS cases with lower levels of *DDX41* (Figures S6B–S6D). Significantly higher bone marrow blast counts were found in patients with lower *DDX41* levels (Figure 6A). Patients with low *DDX41* expression had inferior overall survival rates compared with patients with high levels of *DDX41* (Figure 6B). These data are suggestive that lower *DDX41* expression in HSPCs could contribute to hematologic changes in MDS.

Using this same patient dataset, we determined if lower *DDX41* levels in human CD34⁺ HSPCs are concordant with elevated inflammatory gene expression. We defined the genes with elevated expression in *DDX41* low versus high samples (Table S5), and then performed gene-set comparison with REACTOME pathways. Similar to our findings in *ddx41* mutant zebrafish, we observed that immune system pathways were also enriched (Figure 6C). We then took the genes that were highly expressed in *DDX41* low MDS samples and within the “Innate immune system” pathway and assessed how their expression correlated with blast counts in the cohort of 183 MDS patients

(Figure 6D). We observed a strong correlation between expression of these genes and high bone marrow blast counts (Figure 6E). These data support that low expression of *DDX41* in human CD34⁺ HSPCs leads to increased inflammatory signaling that correlates with increased blast levels.

Finally, we assessed if *DDX41* hypomorphic mutations could modulate R-loop levels. We focused on the *DDX41*^{R525H} mutant, which is a common hotspot somatic mutation that is thought to result in diminished helicase activity (Yoneyama-Hirozane et al., 2017; Polprasert et al., 2015). We analyzed R-loop levels in HEK-293 cells overexpressing wild-type *DDX41* (control) or mutant *DDX41*^{R525H}. We showed that R-loop levels were significantly increased in *DDX41*^{R525H}-overexpressing cells compared with *DDX41*^{wildtype}-overexpressing cells (Figures 6F and 6G). These data demonstrate that similar to our finding in zebrafish, human *DDX41* suppresses R-loop accumulation.

DISCUSSION

Here, we unveil a critical role for *Ddx41* as a key regulator of HSPC homeostasis via its role as a gatekeeper of inflammatory signaling. We demonstrated that R-loop dysregulation triggered by *ddx41* deficiency stimulates the cGAS-STING inflammatory cascade. This, in turn, increased the HSPC production during development by promoting EHT events. These results indicate that tight regulation of R-loop levels is critical for limiting HSPC numbers.

Inflammatory signaling, mainly via NFκB, is well established to play a critical role in HSPC emergence (Espin-Palazon et al., 2018). We determined that cGAS-STING is a new signaling pathway that feeds into NFκB to control HSPC production during embryonic hematopoiesis. Prior work showed that sterile inflammation drives NFκB-mediated inflammatory effects on HSPC formation (He et al., 2015; Espín-Palazón et al., 2014; Li et al., 2014; Sawamiphak et al., 2014). However, the upstream triggers of such signaling remain unclear. Our work shows that endogenous signals, such as excessive R-loops, can function as innate damage-associated molecular patterns (DAMPs) during development to alter HSPC formation. Repetitive elements and metabolic activity were recently identified as additional endogenous cues that regulate HSPC formation via sterile inflammatory signaling (Frame et al., 2020; Lefkopoulos et al., 2020). These findings open new avenues for considering the role for other naturally occurring internal inflammatory triggers as native constituents of the HSPC formation microenvironment.

Previous work demonstrated that *DDX41* can act as a sensor for cytoplasmic DNA and bacterial cyclic di-GMP/AMP activating a type I IFN immune response (Zhang et al., 2013; Parvatiyar et al., 2012; Zhang et al., 2011). Out of context, these data are in apparent contradiction to our findings that deficiency of *ddx41* results in increased type I IFN signaling. Previous studies were mainly performed in myeloid dendritic cells or monocytes, which may reflect how *DDX41* functions in immune effector cells.

(E) Flow cytometry plots of *runx1:mcherry*⁺ HSPCs from *Tg(hsp70:M27RNASEH1-GFP)*-negative (top left) and *Tg(hsp70:M27RNASEH1-GFP)*-positive (top right) uninjected *ddx41* mutants versus *Tg(hsp70:M27RNASEH1-GFP)*-negative (bottom left) and *Tg(hsp70:M27RNASEH1-GFP)*-positive (bottom right) STING morpholino-injected *ddx41* mutants at 40 hpf.

(F) Graph depicting the number of *runx1:mcherry*⁺ HSPCs per embryo from (E). Graphs display means ± stds with p values calculated with a one-way ANOVA with Tukey's multiple testing correction, **p < 0.01, ***p < 0.001, ****p < 0.0001, ns, not significant (p > 0.05). N = 3–6 replicates per experiment.

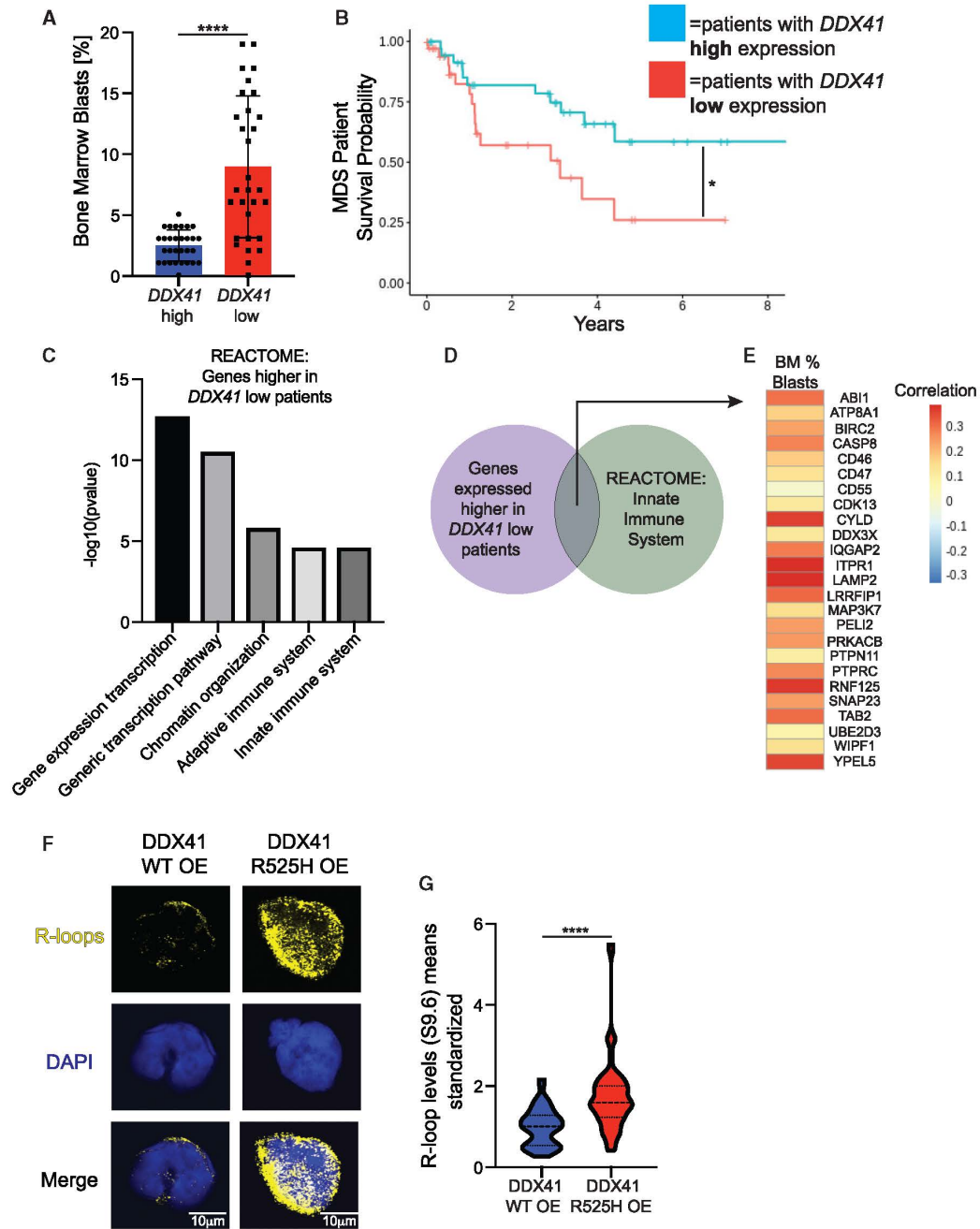


Figure 6. Conserved properties in *DDX41* low and mutated human cells

(A) Graph depicting bone marrow blast percentages of MDS patients with high (top 20%) or low (bottom 20%) *DDX41* expression.

(B) Kaplan-Meier survival curve comparing MDS patients with high or low *DDX41* expression.

(C) Representative charts of REACTOME pathways significantly enriched in *DDX41* low patients’ CD34⁺ HSPCs compared with *DDX41* high patients’ CD34⁺ HSPCs.

(D) Venn diagram showing overlap between genes that were highly expressed in *DDX41* low MDS samples and within the “Innate immune system” pathway and assessed for how their expression correlated with blast counts in the cohort of 183 MDS patients in (E).

(legend continued on next page)

DDX41 is ubiquitously expressed (Fagerberg et al., 2014). Zebrafish *ddx41* mutants have the loss-of-function mutation in all cells, opening the possibility of a different role for DDX41 in non-immune cell types, such as HSPCs. Another contributing factor to the differences between the prior immune signaling studies and our work is the pleiotropic functions of DDX41. Although numerous cellular roles of DDX41 are described, understanding how these processes interact and influence one another is still in its infancy. Our data indicate at least one example of how DDX41 regulation of R-loops and inflammatory signaling are intertwined.

Similarly, the function of cGAS-STING signaling has been studied mostly in immune effector cells where it induces anti-pathogen or anti-tumor immunity (Hoong et al., 2020; Devaux et al., 2018). More recently, activation of cGAS-STING has been associated with promoting stemness in CD8⁺ T cells, indicating the involvement of this pathway in cell-fate decisions (Li et al., 2020). In adult murine HSPCs, bacterial bis-(3'5')-cyclic dimeric guanosine monophosphate-stimulated STING activation can promote proliferation of multipotent progenitors, while transiently suppressing long-term HSC function (Kobayashi et al., 2015). Of note, stimulation with cGAMP, the second messenger generated by cGAS, led to a different response. Our data suggest a stemness-promoting effect of intrinsic cGAS activation during HSPC production. Taken together, these findings indicate that there are contextual and cell-type-specific responses to STING pathway activation, implying greater complexity in STING-mediated effects than was previously appreciated.

Several groups showed that excessive R-loops promote DNA damage (Crossley et al., 2019). Due to this effect, R-loop imbalance is often associated with genomic instability in cancers. Mutations in R-loop-regulating factors are also found in inherited autoimmune disorders (Günther et al., 2015; Lim et al., 2015). Though this clinical linkage suggests R-loop imbalance could derail normal inflammatory signaling, our work provides *in vivo* and mechanistic evidence of this occurring. That said, our findings do not preclude genomic instability as another contributor to the effects of R-loops on HSPC production. Further exploration of the connections of DNA damage and inflammatory signaling in HSPC biology is needed.

DDX41 also interacts with multiple components of the spliceosome (Polprasert et al., 2015). Our work aligns with prior studies showing that *DDX41* insufficiency is associated with numerous deleterious splicing outcomes. If, and how, these splicing events contribute to hematopoietic defects is uncertain. We show that immune signaling components are commonly mis-spliced in *ddx41* mutants. Therefore, although we demonstrated a clear impact of R-loops on inflammatory signaling in *ddx41* mutants, our data do not preclude the possibility that splicing alterations could also contribute to perturbed inflammatory signaling and HSPC expansion. Mutations or deficiency of splicing factors,

similar to our results with *ddx41* deficits, cause R-loop imbalance in addition to splicing alterations (Sollier and Cimprich, 2015). The crosstalk of pre-mRNA processing and R-loop regulation is a major outstanding question in the field that remains to be addressed.

In summary, our study uncovers an important link between R-loops, inflammation, and the developing hematopoietic system. We demonstrate that the loss of *ddx41* leads to elevated R-loop levels, which trigger an inflammatory response contributing to increased HSPC production. This mechanistic connection between R-loops and inflammation gives us a greater understanding of HSPC development. Additionally, the conservation of mechanism observed in human cells with diminished DDX41 suggests our findings could have potential implications for HSPC-driven hematologic malignancies, such as MDS.

STAR★METHODS

Detailed methods are provided in the online version of this paper and include the following:

- KEY RESOURCES TABLE
- RESOURCE AVAILABILITY
 - Lead contact
 - Materials availability
 - Data and code availability
- EXPERIMENTAL MODEL AND SUBJECT DETAILS
 - Zebrafish
 - Cell lines
- METHOD DETAILS
 - Zebrafish embryo morpholino and construct injections
 - Whole-mount *in situ* hybridization
 - Flow cytometry
 - Cell cycle analysis
 - Single-cell immunofluorescence
 - Human cells
 - Fluorescent microscopy and time-lapse imaging
 - Image acquisition and processing
 - RNA-sequencing and splicing analysis
 - Reverse transcription-PCR
 - Western analysis
 - Patient database and survival data
- QUANTIFICATION AND STATISTICAL ANALYSIS
 - Statistics

SUPPLEMENTAL INFORMATION

Supplemental Information can be found online at <https://doi.org/10.1016/j.devcel.2021.02.006>.

(E) Heatmap correlating clinical hematological variables with the genes in the REACTOME “innate immune signature” pathway from *DDX41* low patients' CD34⁺ HSPCs (D). Each cell represents the correlation between the 183 values of the clinical variable (column), and the 183 values of the gene probe (row) matched by patient.

(F) Confocal images showing immunofluorescence of R-loops and nuclei (DAPI) in HEK-293 cells that are overexpressing DDX41 wildtype (left) or a DDX41 R525H mutant (right). Scale bar, 10 μm.

(G) Quantification of R-loop levels from (F). Graphs display means ± stds with p values calculated with unpaired Student's t test, *p < 0.05, ****p < 0.0001.

ACKNOWLEDGMENTS

This work was funded by American Cancer Society RSG-129527-DDC, Kimmel Foundation, the Edward P. Evans Foundation, DOD BM180109, 1R56DK121738-01, 1R01DK121728-01A1 (to T.V.B.), MSTP training grant T32GM007288-45 and F30 fellowship 1F30HL142161 (to J.T.W.), T32 GM007491 (to N.G.), R01HL139487 and R01HL150832 (to A.V.), the American Australian Association Sir Rupert Murdoch Postdoctoral Fellowship (to K.S.P.), and R01-HL132071 and a grant from the Vera and Joseph Dresner Foundation (to R.A.P.).

We want to thank Eirini Trompouki, Charles Query, Andreas Jenny, and Sara Nik for helpful discussions regarding this work. We want to thank Mary Goll for sharing the *sting^{mk30}* mutant zebrafish. We also want to acknowledge the assistance of numerous Core Facilities at Albert Einstein College of Medicine including flow cytometry, Analytical Imaging, and Genomics Facilities (funded by NCI Cancer grant P30CA013330), as well as the Zebrafish Core Facility.

AUTHOR CONTRIBUTIONS

J.T.W., A.V., and T.V.B. designed the project experimental approach. J.T.W., N.G., K.S.P., B.T., and S.D.O. performed the experiments. K.P. and V.G. performed bioinformatics analysis. N.J.D. and R.A.P. shared critical reagents. J.T.W. and T.V.B. analyzed the data. J.T.W. and T.V.B. wrote the manuscript; all authors reviewed and approved the manuscript.

DECLARATION OF INTERESTS

The authors declare no competing interests.

Received: October 19, 2019

Revised: December 1, 2020

Accepted: February 3, 2021

Published: March 1, 2021

REFERENCES

Ablasser, A., Schmid-Burgk, J.L., Hemmerling, I., Horvath, G.L., Schmidt, T., Latz, E., and Homung, V. (2013). Cell intrinsic immunity spreads to bystander cells via the intercellular transfer of cGAMP. *Nature* **503**, 530–534.

Bai, J., Cervantes, C., Liu, J., He, S., Zhou, H., Zhang, B., Cai, H., Yin, D., Hu, D., Li, Z., et al. (2017). DsbA-L prevents obesity-induced inflammation and insulin resistance by suppressing the mtDNA release-activated cGAS-cGAMP-STING pathway. *Proc. Natl. Acad. Sci. USA* **114**, 12196–12201.

Bertrand, J.Y., Chi, N.C., Santoso, B., Teng, S., Stainer, D.Y., and Traver, D. (2010). Haematopoietic stem cells derive directly from aortic endothelium during development. *Nature* **464**, 108–111.

Boguslawski, S.J., Smith, D.E., Michalak, M.A., Mickelson, K.E., Yehle, C.O., Patterson, W.L., and Carrico, R.J. (1986). Characterization of monoclonal antibody to DNA:RNA and its application to immunodetection of hybrids. *J. Immunol. Methods* **89**, 123–130.

Boisset, J.C., van Cappellen, W., Andrieu-Soler, C., Galjart, N., Dzierzak, E., and Robin, C. (2010). In vivo imaging of haematopoietic cells emerging from the mouse aortic endothelium. *Nature* **464**, 116–120.

Burns, C.E., DeBlasio, T., Zhou, Y., Zhang, J., Zon, L., and Nimer, S.D. (2002). Isolation and characterization of *runx*a and *runx*b, zebrafish members of the runt family of transcriptional regulators. *Exp. Hematol.* **30**, 1381–1389.

Collins, T.J. (2007). ImageJ for microscopy. *BioTechniques* **43** (Supplement), 25–30.

Crossley, M.P., Bocek, M., and Cimprich, K.A. (2019). R-loops as cellular regulators and genomic threats. *Mol. Cell* **73**, 398–411.

Devaux, L., Kaminski, P.A., Trieu-Cuot, P., and Firon, A. (2018). Cyclic di-AMP in host-pathogen interactions. *Curr. Opin. Microbiol.* **47**, 21–28.

Dobin, A., Davis, C.A., Schlesinger, F., Drenkow, J., Zaleski, C., Jha, S., Batut, P., Chaisson, M., and Gingeras, T.R. (2013). STAR: ultrafast universal RNA-seq aligner. *Bioinformatics* **29**, 15–21.

Dobrzycki, T., Krecsmarik, M., Bonkhofer, F., Patient, R., and Monteiro, R. (2018). An optimised pipeline for parallel image-based quantification of gene expression and genotyping after in situ hybridisation. *Biol. Open* **7**, bio031096.

Espin-Palazon, R., Stachura, D.L., Campbell, C.A., Garcia-Moreno, D., Del Cid, N., Kim, A.D., Candel, S., Meseguer, J., Mulero, V., and Traver, D. (2014). Proinflammatory signaling regulates hematopoietic stem cell emergence. *Cell* **159**, 1070–1085.

Espin-Palazon, R., Weijts, B., Mulero, V., and Traver, D. (2018). Proinflammatory signals as fuel for the fire of hematopoietic stem cell emergence. *Trends Cell Biol.* **28**, 58–66.

Fagerberg, L., Hallström, B.M., Oksvold, P., Kampf, C., Djureinovic, D., Odeberg, J., Habuka, M., Tahmasebpoor, S., Danielsson, A., Edlund, K., et al. (2014). Analysis of the human tissue-specific expression by genome-wide integration of transcriptomics and antibody-based proteomics. *Mol. Cell. Proteomics* **13**, 397–406.

Fraint, E., Feliz Norberto, M., and Bowman, T.V. (2020). A novel conditioning-free hematopoietic stem cell transplantation model in zebrafish. *Blood Adv.* **4**, 6189–6198.

Frame, J.M., Kubaczka, C., Long, T.L., Esain, V., Soto, R.A., Hachimi, M., Jing, R., Shwartz, A., Goessling, W., Daley, G.Q., and North, T.E. (2020). Metabolic regulation of inflammasome activity controls embryonic hematopoietic stem and progenitor cell production. *Dev. Cell* **55**, 133–149.e6.

Ge, R., Zhou, Y., Peng, R., Wang, R., Li, M., Zhang, Y., Zheng, C., and Wang, C. (2015). Conservation of the STING-mediated cytosolic DNA sensing pathway in zebrafish. *J. Virol.* **89**, 7696–7706.

Gentili, M., Lahaye, X., Nadalín, F., Nader, G.P.F., Lombardi, E.P., Herve, S., De Silva, N.S., Rookhuizen, D.C., Zueva, E., Goudot, C., et al. (2019). The N-terminal domain of cGAS determines preferential association with centromeric DNA and innate immune activation in the nucleus. *Cell Rep* **26**, 3798.

Günther, C., Kind, B., Reijns, M.A., Berndt, N., Martinez-Bueno, M., Wolf, C., Tüngler, V., Chara, O., Lee, Y.A., Hübner, N., et al. (2015). Defective removal of ribonucleotides from DNA promotes systemic autoimmunity. *J. Clin. Invest.* **125**, 413–424.

He, Q., Zhang, C., Wang, L., Zhang, P., Ma, D., Lv, J., and Liu, F. (2015). Inflammatory signaling regulates hematopoietic stem and progenitor cell emergence in vertebrates. *Blood* **125**, 1098–1106.

Hess, I., Iwanami, N., Schorpp, M., and Boehm, T. (2013). Zebrafish model for allogeneic hematopoietic cell transplantation not requiring preconditioning. *Proc. Natl. Acad. Sci. USA* **110**, 4327–4332.

Hoong, B.Y.D., Gan, Y.H., Liu, H., and Chen, E.S. (2020). cGAS-STING pathway in oncogenesis and cancer therapeutics. *Oncotarget* **11**, 2930–2955.

Huemer, K., Squirrell, J.M., Swader, R., LeBert, D.C., Huttenlocher, A., and Eliceiri, K. W. (2017). zWEDGI: wounding and entrapment device for imaging live zebrafish larvae. *Zebrafish*. **14**, 42–50, <https://doi.org/10.1089/zeb.2016.1323>.

Jiang, H., Xue, X., Panda, S., Kawale, A., Hooy, R.M., Liang, F., Sohn, J., Sung, P., and Gekara, N.O. (2019). Chromatin-bound cGAS is an inhibitor of DNA repair and hence accelerates genome destabilization and cell death. *EMBO J.* **38**, e102718.

Kanther, M., Sun, X., Mühlbauer, M., Mackey, L.C., Flynn, E.J., 3rd, Bagnat, M., Jobin, C., and Rawls, J.F. (2011). Microbial colonization induces dynamic temporal and spatial patterns of NF- κ B activation in the zebrafish digestive tract. *Gastroenterology* **141**, 197–207.

Kettleborough, R.N., Busch-Nentwich, E.M., Harvey, S.A., Dooley, C.M., de Bruijn, E., van Eeden, F., Sealy, I., White, R.J., Herd, C., Nijman, I.J., et al. (2013). A systematic genome-wide analysis of zebrafish protein-coding gene function. *Nature* **496**, 494–497.

Kissa, K., and Herbomel, P. (2010). Blood stem cells emerge from aortic endothelium by a novel type of cell transition. *Nature* **464**, 112–115.

Kobayashi, H., Kobayashi, C.I., Nakamura-Ishizu, A., Karigane, D., Haeno, H., Yamamoto, K.N., Sato, T., Ohteki, T., Hayakawa, Y., Barber, G.N., et al. (2015). Bacterial c-di-GMP affects hematopoietic stem/progenitors and their niches through STING. *Cell Rep.* **11**, 71–84.

- Kurre, P. (2018). Hematopoietic development: a gap in our understanding of inherited bone marrow failure. *Exp. Hematol.* *59*, 1–8.
- Lawrence, C. (2011). Advances in zebrafish husbandry and management. *Methods Cell Biol.* *104*, 429–451.
- Lawson, N.D., Scheer, N., Pham, V.N., Kim, C.H., Chitnis, A.B., Campos-Ortega, J.A., and Weinstein, B.M. (2001). Notch signaling is required for arterial-venous differentiation during embryonic vascular development. *Development* *128*, 3675–3683.
- Lawson, N.D., and Weinstein, B.M. (2002). In vivo imaging of embryonic vascular development using transgenic zebrafish. *Dev. Biol.* *248*, 307–318.
- Lefkopoulos, S., Polyzoou, A., Derecka, M., Bergo, V., Clapes, T., Cauchy, P., Jerez-Longres, C., Onishi-Seebacher, M., Yin, N., Martagon-Calderson, N.A., et al. (2020). Repetitive elements trigger RIG-I-like receptor signaling that regulates the emergence of hematopoietic stem and progenitor cells. *Immunity* *53*, 934–951.e9.
- Li, W., Lu, L., Lu, J., Wang, X., Yang, C., Jin, J., Wu, L., Hong, X., Li, F., Cao, D., et al. (2020). cGAS-STING-mediated DNA sensing maintains CD8+ T cell stemness and promotes antitumor T cell therapy. *Sci. Transl. Med.* *12*, eaay9013.
- Li, X., Shu, C., Yi, G., Chaton, C.T., Shelton, C.L., Diao, J., Zuo, X., Kao, C.C., Herr, A.B., and Li, P. (2013). Cyclic GMP-AMP synthase is activated by double-stranded DNA-induced oligomerization. *Immunity* *39*, 1019–1031.
- Li, Y., and Andrade, J. (2017). DEApp: an interactive web interface for differential expression analysis of next generation sequence data. *Source Code Biol. Med.* *12*, 2.
- Li, Y., Esain, V., Teng, L., Xu, J., Kwan, W., Frost, I.M., Yzaguirre, A.D., Cai, X., Cortes, M., Majenberg, M.W., et al. (2014). Inflammatory signaling regulates embryonic hematopoietic stem and progenitor cell production. *Genes Dev.* *28*, 2597–2612.
- Liberzon, A., Birger, C., Thorvaldsdóttir, H., Ghandi, M., Mesirov, J.P., and Tamayo, P. (2015). The molecular signatures database (MSigDB) hallmark gene set collection. *Cell Syst.* *1*, 417–425.
- Lim, Y.W., Sanz, L.A., Xu, X., Hartono, S.R., and Chédin, F. (2015). Genome-wide DNA hypomethylation and RNA:DNA hybrid accumulation in Aicardi-Goutieres syndrome. *eLife* *4*, e08007.
- Lin, H.F., Traver, D., Zhu, H., Dooley, K., Paw, B.H., Zon, L.I., and Handin, R.I. (2005). Analysis of thrombocyte development in CD41-GFP transgenic zebrafish. *Blood* *106*, 3803–3810.
- Liu, H., Zhang, H., Wu, X., Ma, D., Wu, J., Wang, L., Jiang, Y., Fei, Y., Zhu, C., Tan, R., et al. (2018). Nuclear cGAS suppresses DNA repair and promotes tumorigenesis. *Nature* *563*, 131–136.
- Love, M.I., Huber, W., and Anders, S. (2014). Moderated estimation of fold change and dispersion for RNA-seq data with DESeq2. *Genome Biol.* *15*, 550.
- Mankan, A.K., Schmidt, T., Chauhan, D., Goldeck, M., Höning, K., Gaidt, M., Kubarenko, A.V., Andreeva, L., Hopfner, K.P., and Hornung, V. (2014). Cytosolic RNA:DNA hybrids activate the cGAS-STING axis. *EMBO J.* *33*, 2937–2946.
- Meeker, N.D., Hutchinson, S.A., Ho, L., and Trede, N.S. (2007). Method for isolation of PCR-ready genomic DNA from zebrafish tissues. *BioTechniques* *43*, 610–614.
- Nakayama, S., Ikenaga, T., Kawakami, K., Ono, F., and Hatta, K. (2012). Transgenic line with gal4 insertion useful to study morphogenesis of craniofacial perichondrium, vascular endothelium-associated cells, floor plate, and dorsal midline radial glia during zebrafish development. *Dev. Growth Differ.* *54*, 202–215.
- Nik, S., Weinreb, J.T., and Bowman, T.V. (2017). Developmental HSC microenvironments: lessons from zebrafish. *Adv. Exp. Med. Biol.* *1041*, 33–53.
- Ottersbach, K. (2019). Endothelial-to-hematopoietic transition: an update on the process of making blood. *Biochem. Soc. Trans.* *47*, 591–601.
- Parvatiyar, K., Zhang, Z., Teles, R.M., Ouyang, S., Jiang, Y., Iyer, S.S., Zaver, S.A., Schenk, M., Zeng, S., Zhong, W., et al. (2012). The helicase DDX41 recognizes the bacterial secondary messengers cyclic di-GMP and cyclic di-AMP to activate a type I interferon immune response. *Nat. Immunol.* *13*, 1155–1161.
- Paulsen, R.D., Soni, D.V., Wollman, R., Hahn, A.T., Yee, M.C., Guan, A., Hesley, J.A., Miller, S.C., Cromwell, E.F., Solow-Cordero, D.E., et al. (2009). A genome-wide siRNA screen reveals diverse cellular processes and pathways that mediate genome stability. *Mol. Cell* *35*, 228–239.
- Pellagatti, A., Cazzola, M., Giagounidis, A., Perry, J., Malcovati, L., Della Porta, M.G., Jädersten, M., Killick, S., Verma, A., Norbury, C.J., et al. (2010). Deregulated gene expression pathways in myelodysplastic syndrome hematopoietic stem cells. *Leukemia* *24*, 756–764.
- Pietras, E.M. (2017). Inflammation: a key regulator of hematopoietic stem cell fate in health and disease. *Blood* *130*, 1693–1698.
- Polprasert, C., Schulze, I., Sekeres, M.A., Makishima, H., Przychodzen, B., Hosono, N., Singh, J., Padgett, R.A., Gu, X., Phillips, J.G., et al. (2015). Inherited and somatic defects in DDX41 in myeloid neoplasms. *Cancer Cell* *27*, 658–670.
- Rajshekar, S., Yao, J., Arnold, P.K., Payne, S.G., Zhang, Y., Bowman, T.V., Schmitz, R.J., Edwards, J.R., and Goll, M. (2018). Pericentromeric hypomethylation elicits an interferon response in an animal model of ICF syndrome. *eLife* *7*, e39658.
- Sawamiphak, S., Kontarakis, Z., and Stainier, D.Y. (2014). Interferon gamma signaling positively regulates hematopoietic stem cell emergence. *Dev. Cell* *31*, 640–653.
- Schinke, C., Giricz, O., Li, W., Shastri, A., Gordon, S., Barreyro, L., Bhagat, T., Bhattacharya, S., Ramachandra, N., Bartenstein, M., et al. (2015). IL3-CXCR2 pathway inhibition as a therapeutic strategy against MDS and AML stem cells. *Blood* *125*, 3144–3152.
- Shen, S., Park, J.W., Lu, Z.X., Lin, L., Henry, M.D., Wu, Y.N., Zhou, Q., and Xing, Y. (2014). rMATS: robust and flexible detection of differential alternative splicing from replicate RNA-seq data. *Proc. Natl. Acad. Sci. USA* *111*, E5593–E5601.
- Sollier, J., and Cimprich, K.A. (2015). Breaking bad: R-loops and genome integrity. *Trends Cell Biol.* *25*, 514–522.
- Sorrells, S., Nik, S., Casey, M.J., Cameron, R.C., Truong, H., Toruno, C., Gulfo, M., Lowe, A., Jette, C., Stewart, R.A., and Bowman, T.V. (2018). Spliceosomal components protect embryonic neurons from R-loop-mediated DNA damage and apoptosis. *Dis. Models Mech.* *11*, dmm031583.
- Sperling, A.S., Gibson, C.J., and Ebert, B.L. (2017). The genetics of myelodysplastic syndrome: from clonal haematopoiesis to secondary leukaemia. *Nat. Rev. Cancer* *17*, 5–19.
- Stavrou, S., Aguilera, A.N., Blouch, K., and Ross, S.R. (2018). DDX41 recognizes RNA:DNA retroviral reverse transcripts and is critical for in vivo control of murine leukemia virus infection. *mBio* *9*, e00923-18.
- Subramanian, A., Tamayo, P., Mootha, V.K., Mukherjee, S., Ebert, B.L., Gillette, M.A., Paulovich, A., Pomeroy, S.L., Golub, T.R., Lander, E.S., et al. (2005). Gene set enrichment analysis: a knowledge-based approach for interpreting genome-wide expression profiles. *Proc. Natl. Acad. Sci. USA* *102*, 15545–15550.
- Suzuki, Y., Holmes, J.B., Cerritelli, S.M., Sakhuja, K., Minczuk, M., Holt, I.J., and Crouch, R.J. (2010). An upstream open reading frame and the context of the two AUG codons affect the abundance of mitochondrial and nuclear RNase H1. *Mol. Cell. Biol.* *30*, 5123–5134.
- Szilvassy, S.J., Ragland, P.L., Miller, C.L., and Eaves, C.J. (2003). The marrow homing efficiency of murine hematopoietic stem cells remains constant during ontogeny. *Exp. Hematol.* *31*, 331–338.
- Tamplin, O.J., Durand, E.M., Carr, L.A., Childs, S.J., Hagedorn, E.J., Li, P., Yzaguirre, A.D., Speck, N.A., and Zon, L.I. (2015). Hematopoietic stem cell arrival triggers dynamic remodeling of the perivascular niche. *Cell* *160*, 241–252.
- Thisse, C., and Thisse, B. (2008). High-resolution in situ hybridization to whole-mount zebrafish embryos. *Nat. Protoc.* *3*, 59–69.
- van der Vaart, M., Korbee, C.J., Lamers, G.E., Tengeler, A.C., Hosseini, R., Haks, M.C., Ottenhoff, T.H., Spaink, H.P., and Meijer, A.H. (2014). The DNA damage-regulated autophagy modulator DRAM1 links mycobacterial recognition via TLR-MYD88 to autophagic defense [corrected]. *Cell Host Microbe* *15*, 753–767.

- Volkman, H.E., Cambier, S., Gray, E.E., and Stetson, D.B. (2019). Tight nuclear tethering of cGAS is essential for preventing autoreactivity. *eLife* 8, e47491.
- Wang, I.X., Grunseich, C., Fox, J., Burdick, J., Zhu, Z., Ravazian, N., Hafner, M., and Cheung, V.G. (2018). Human proteins that interact with RNA/DNA hybrids. *Genome Res.* 28, 1405–1414.
- Yan, P., Liu, Z., Song, M., Wu, Z., Xu, W., Li, K., Ji, Q., Wang, S., Liu, X., Yan, K., et al. (2020). Genome-wide R-loop landscapes during cell differentiation and reprogramming. *Cell Rep.* 32, 107870.
- Yoneyama-Hirozane, M., Kondo, M., Matsumoto, S.I., Morikawa-Oki, A., Morishita, D., Nakanishi, A., Kawamoto, T., and Nakayama, M. (2017). High-throughput screening to identify inhibitors of DEAD box helicase DDX41. *SLAS Discov.* 22, 1084–1092.
- Zhang, Z., Bao, M., Lu, N., Weng, L., Yuan, B., and Liu, Y.J. (2013). The E3 ubiquitin ligase TRIM21 negatively regulates the innate immune response to intracellular double-stranded DNA. *Nat. Immunol.* 14, 172–178.
- Zhang, Z., Yuan, B., Bao, M., Lu, N., Kim, T., and Liu, Y.J. (2011). The helicase DDX41 senses intracellular DNA mediated by the adaptor STING in dendritic cells. *Nat. Immunol.* 12, 959–965.

STAR★METHODS

KEY RESOURCES TABLE

REAGENT or RESOURCE	SOURCE	IDENTIFIER
Antibodies		
Alexa Fluor® 488 Goat Anti-Mouse IgG (H+L) for IF	Fisher	Cat# A-10667; RRID: AB_2534057
goat anti-mouse AlexaFluor-488 IgG2a secondary antibody for IF	Thermo Fisher Scientific	Cat# A-21135, RRID: AB_2535774
monoclonal S9.6 primary antibody for IF	This paper	N/A
Phospho-TBK1/NAK (Ser172) (D52C2) XP®Rabbit mAb (Alexa Fluor®647Conjugate) for western and IF	Cell Signaling Technology	Cat# 14590, RRID: AB_2798527
TBK1/NAK (D1B4) Rabbit mAb for western	Cell Signaling Technology	Cat# 3504T
Anti-GAPDH antibody [6C5] (ab8245), 100ug for western	Abcam	Cat# ab8245, RRID: AB_2107448
goat anti-mouse IgG-HRP for western	santa-cruz	Cat# sc-2005, RRID: AB_631736
goat anti-rabbit IgG-HRP	santa-cruz	Cat# sc-2004, RRID: AB_631746
rabbit anti-cGAS for IF and western	abcam	Cat# 224144
Critical commercial assays		
Click-IT EdU Flow Cytometry Assay Kit	Life Technologies/ThermoFisher	C10424
Deposited data		
Raw and analyzed data RNA-seq	This paper	GEO: GSE146995
Experimental models: cell lines		
Human HEK-293 cells overexpressing DDX41 constructs	Gift from Richard Padgett	N/A
Experimental models: organisms/strains		
Zebrafish: <i>ddx41</i> sa14887	Zebrafish International Resource Center (ZIRC) as part of the Sanger Institute Zebrafish Mutation Project	ZFIN: ZDB-ALT-130411-3515
Zebrafish: <i>sting</i> mk30	Rajshekar et al., 2018	ZFIN: ZDB-ALT-190912-7
Zebrafish: <i>cd41:egfp</i>	Lin et al., 2005	ZFIN: ZDB-TGCONSTRUCT-190821-1
Zebrafish: <i>kdrt:dsred</i>	Nakayama et al., 2012	ZFIN: ZDB-ALT-130522-1
Zebrafish: <i>runx1:mcherry</i>	Tamplin et al., 2015	ZFIN: ZDB-TGCONSTRUCT-150512-2
Zebrafish: <i>nfxb:egfp</i>	Kanther et al., 2011	ZFIN: ZDB-TGCONSTRUCT-120409-6
Zebrafish: <i>Tg(hsp70:M27RNASEH1-GFP)</i>	Sorrells et al., 2018	ZFIN: ZDB-ALT-150518-2
Oligonucleotides		
Primer for genotyping zebrafish <i>ddx41</i> _WT_Forward: GAGGCCAAGATGGTTTAT	This paper	N/A
Primer for genotyping zebrafish <i>ddx41</i> _WT_Reverse: GCCTCCACACCTTTTAGCAG	This paper	N/A
Primer for genotyping zebrafish <i>ddx41</i> _MUT_Forward: GCCTCCACACCTTTTAGCAG	This paper	N/A
Primer for genotyping zebrafish <i>ddx41</i> _MUT_Reverse: GAGGCCAAGATGGTTTAA	This paper	N/A

(Continued on next page)

Continued

REAGENT or RESOURCE	SOURCE	IDENTIFIER
Primer for <i>cxcl10</i> _qPCR ^{F1} : TGCAGAAAGAGCAGCAGAAAA	This paper	N/A
Primer for <i>cxcl10</i> _qPCR ^{R1} : GGCTGGAAGAAGCTACAACG	This paper	N/A
Primer for <i>ifi44</i> _qPCR ^{F1} : TCTCTGAAGAAGCTGGCACA	This paper	N/A
Primer for <i>ifi44</i> _qPCR ^{R1} : ACTGGTCCTCCACCAGTTTG	This paper	N/A
Primer for <i>ifi44l</i> _qPCR ^{F1} : CGGCAGAAGGAAACAAAGTC	This paper	N/A
Primer for <i>ifi44l</i> _qPCR ^{R1} : GCGGATTTTACCGTCACACT	This paper	N/A
Primer for <i>ifn-phi1</i> -F: GTGGCAAGATACGCAAAGCC	This paper	N/A
Primer for <i>ifn-phi1</i> -R: ATTGACCCTTGCGTTGCTTG	This paper	N/A
Primer for <i>bactin</i> -F: GCTGTTTTCCCTCCATTGTT	Burns et al. G&D 2005	N/A
Primer for <i>bactin</i> -R: TCCCATGCCAACCATCACT	Burns et al. G&D 2005	N/A
Primer for <i>sting</i> _RTPCR_Ex1_F: TCTTACTCTGGCCGTTGCTT	This paper	N/A
Primer for <i>sting</i> _RTPCR_Ex3_R: ACCATGAGCCACGTTTCATCT	This paper	N/A
Primer for <i>cgas</i> _RTPCR_Ex2_F: TGCTGACTGTTCCCTGTGGAG	This paper	N/A
Primer for <i>cgas</i> _RTPCR_Ex4_R: GTGTGGCCATGTGATTTGAG	This paper	N/A
Primer for <i>tubulin</i> _RTPCR_F: ATGCCCTGCTGGGAACTGTAT	This paper	N/A
Primer for <i>tubulin</i> _RTPCR_R: GGTGAACAGCTGACGGTAT	This paper	N/A
Morpholino: splice-blocking <i>sting</i> GCCATGATACCTGGA	Gene tools	ZFIN: ZDB-MRPHLNO-140826-4
Morpholino: translation-blocking <i>cgas</i> CTGGTCTCCTGTGGCTGCTCATGAT	Gene tools	ZFIN: ZDB-MRPHLNO-171109-2
Morpholino: splicing-blocking <i>cgas</i> CAGATTGTGGGCATAGTATACCTCT	This paper	N/A
Morpholino: control CCTCTTACCTCAGTTACAATTATA	Gene tools	N/A
Recombinant DNA		
<i>ubi:gfp</i> plasmid	This paper	N/A
<i>fli1:M27RNASEH1-GFP</i> plasmid	This paper	N/A
Software and Algorithms		
Fiji/ImageJ	Dobrzycki et al., 2018	https://imagej.nih.gov/ij/
DE-App	Li and Andrade, 2017	https://yanli.shinyapps.io/DEApp/
MSigDB	Liberzon et al., 2015	https://www.gsea-msigdb.org/gsea/msigdb/index.jsp
rMATS	Shen et al., 2014	http://rnaseq-mats.sourceforge.net/

RESOURCE AVAILABILITY

Lead contact

Further information and requests for resources and reagents should be directed to and will be fulfilled by the Lead Contact, Teresa Bowman (teresa.bowman@einsteinmed.org).

Materials availability

The *fli1:rnaseh1-gfp* plasmid generated for this work is available by request.

Data and code availability

The accession numbers for the RNA-Seq data reported in this paper are under Gene Expression Omnibus (GEO) GSE146995.

EXPERIMENTAL MODEL AND SUBJECT DETAILS

Zebrafish

Zebrafish were maintained as described (Lawrence, 2011). All fish were maintained according to IACUC-approved protocols in accordance with Albert Einstein College of Medicine research guidelines. We utilized several established zebrafish lines. Genotyping and phenotyping to confirm their identity was performed for each new generation and for embryos. Mutants for *ddx41* (*ddx41^{sa14887}*) were acquired from the Zebrafish International Resource Center (ZIRC) as part of the Sanger Institute Zebrafish Mutation Project (Kettleborough et al., 2013). The mutation results in a premature stop codon at Tyrosine 410. As early as 24 hpf, there appears to be slight brain death and abnormal curvature of the tail in *ddx41* mutants, allowing for phenotypic identification of mutants compared to siblings based on morphology (Figure S1B). Homozygous mutants are embryonic lethal, dying between 2-3 dpf. This allows for the assessment of definitive hematopoietic development in zebrafish up to 3 dpf but precludes the assessment of hematopoiesis beyond this point of development. Mutants for *sting* (*sting^{nrk30}*) were acquired from Mary Goll (Rajshekar et al., 2018). The following strains were used: *cd41:gfp* (Lin et al., 2005), *runx1:mcherry* (Tamplin et al., 2015), *kdr1:dsred* (Nakayama et al., 2012), *nfkB:gfp* (Kanter et al., 2011), and *Tg(hsp70:M27RNASEH1-GFP)* (Sorrells et al., 2018). *ddx41* genotyping was determined by mutant-specific PCR, which was initially verified by Sanger sequencing. Additionally, the genotype of *ddx41^{sa14887/+}* carriers were validated by paired mating of heterozygous adult animals followed by examination of embryos for the expected homozygous recessive phenotype. All transgenic strains used in this study were scored for their distinctive fluorescence pattern during embryogenesis. Genomic DNA for genotyping was isolated by alkaline lysis (Meeker et al., 2007). The *ddx41^{sa14887}* mutant and wildtype-specific PCR products were analyzed by gel electrophoresis. Genotyping primers are in the Key resources table.

Cell lines

The parental human embryonic kidney 293 cells (HEK-293) cell line was acquired from ATCC (CRL-1573). HEK-293 cells were grown on 100 mm plates in Dulbecco's Modified Eagle's Medium with 4.5 g/L glucose, L-glutamine, and sodium pyruvate (DMEM, Corning Cellgro #10-013-CV) supplemented with 10% (v/v) fetal bovine serum (Atlanta Biologicals) and 100 U/mL penicillin–streptomycin (Gibco) at 37°C and 5% (v/v) CO₂. The DDX41-V5 lentiviral expression vector (pLX304, clone ID: HsCD00442077) was obtained from DNASU Plasmid Repository. The DDX41^{R525H}-V5 plasmid was generated by introducing a point mutation in the DDX41-V5 vector using QuikChange site directed mutagenesis kit with the following primers (DDX41-R525H-F: CGCACCGGGCACTCGGGAAC and DDX41-R525H-R: GCCAATCCGGTGACATAGTTCTC). DDX41-V5 and DDX41^{R525H}-V5 vectors were used to generate lentiviral supernatants in HEK-293T cells. HEK-293 cells were subjected to 8ug/ul polybrene and viral supernatants for 24hrs followed by antibiotic selection using 10ug/ml of blasticidin to generate stable HEK-293 wildtype DDX41-V5 or mutant DDX41^{R525H}-V5 overexpression cell lines. DDX41 protein levels were validated using V5 (A190-120A, Bethyl) and DDX41 (NB100-57488, Novus Biosciences) antibodies. These constructs are published in (Polprasert et al., 2015).

METHOD DETAILS

Zebrafish embryo morpholino and construct injections

Embryos derived from *ddx41* heterozygous incrosses were injected with 1.5 ng morpholino (MO) and compared with control morpholino injected sibling controls. Morpholino sequences used: control morpholino (5'- CCTCTTACCTCAGTTACAATTTATA-3'), splice-blocking *sting* (5'-GCCATGATACCTGGA-3') (van der Vaart et al., 2014), translation-blocking *cgas* (5'-CTGGTCTCCTGTGGCTGCTCATGAT-3') (Ge et al., 2015), and splice-blocking *cgas* (5'-CAGATTGTGGGCATAGTATACCTCT-3'). Translation-blocking morpholino was validated by western blot, and splice-blocking morpholinos were validated by RT-PCR. For construct injections, *tol2* RNA was injected with either 100µg of *ubi:gfp* or 200 µg of *fli1:M27RNASEH1-GFP*. Embryos were scored at ~40 hpf for presence of the transgene according to GFP expression using a Zeiss Stereo Discovery V8 fluorescent dissecting scope.

Whole-mount *in situ* hybridization

In situ hybridization steps were performed as described previously by Thisse et al. (Thisse and Thisse, 2008), with minor modifications: before proteinase K permeabilization, embryos older than 28 hpf were bleached after re-hydration to remove pigmentation.

The bleaching was done for 5–10 minutes using a bleaching solution of 0.8% KOH, 0.9% H₂O₂ and 0.1% Tween 20. Embryos were then scored manually, imaged and genotyped. The *runx1* (Burns et al., 2002), *flt4* (Lawson et al., 2001), and *notch1b* (Lawson et al., 2001) probes were used, and *runx1* levels were quantified using FIJI in a similar manner to previously described methods (Dobrzycki et al., 2018).

Flow cytometry

At 40 hpf, mutant and sibling embryos were binned based on morphological differences. For generation of single-cell suspensions, 10–20 embryos were first removed from their chorions using pronase (Roche), and then homogenized by manual dissociation using a sterile razor blade followed by digestion with Liberase (Roche). For the digestion, dissociated embryos were resuspended in 600 μl 1 × Dulbecco's-PBS (D-PBS) (Life Technologies) supplemented with a 1:65 dilution (9.23 μl) of 5 mg/ml Liberase and then incubated at 37°C for 7 minutes. The reaction was stopped with the addition of 5% (30 μl) fetal bovine serum (FBS) (Life Technologies). The cells were then filtered through a 40-μm cell strainer (Falcon) and pelleted by centrifugation at 3000 rpm for 5 minutes. Cell pellets were resuspended in 400–700 μl FACS buffer (0.9 × D-PBS, 5% FBS, 1% Penn/Strep (Life Technologies)). DAPI (4',6-diamidino-2-phenylindole) was added to a final concentration of 1 μg/ml to facilitate exclusion of dead cells from the analysis. Samples were analyzed with a LSRII flow cytometer (BD Biosciences) and FlowJo software. Cells from non-fluorescent embryos were used to set gates above background. Quantification for the absolute number of cells was performed by acquiring all events in a tube on the flow cytometer to determine the total number of target cells. This number was then divided by the total number of embryos analyzed to calculate the number of target cells per embryo.

Cell cycle analysis

For EdU incorporation experiments, 38 hpf embryos were binned into 6 well plates, with ~30 embryos per well. Embryos were incubated with 20 mM EdU for 2 hours using the Click-IT EdU Flow Cytometry Assay Kit according to the manufacturer's instructions (Invitrogen C10424). Generation of single-cell suspensions of 40 hpf embryos was accomplished as described above. Samples were analyzed with a LSRII flow cytometer (BD Biosciences) and FlowJo software.

Single-cell immunofluorescence

Zebrafish

Single-cell suspensions were prepared as described above, and cell staining was performed as described in Sorrells & Nik et al. (Sorrells et al., 2018). The mouse monoclonal S9.6 (Boguslawski et al., 1986) primary antibody was used at a dilution of 1:50, the pTBK1 primary antibody (Cell Signaling Technology) was used at a dilution of 1:100, and the cGAS antibody (Abcam) was used at 1:200. All antibodies were diluted in blocking buffer (5% bovine serum albumin (BSA)/0.2% milk/PBS) and incubated for 3 h at room temperature followed by 3 washes in 0.1% Tween 20/PBS. The goat anti-mouse AlexaFluor-488 IgG2a (Thermo Fisher Scientific) and goat anti-mouse AlexaFluor-488 IgG (Fisher) secondary antibody were used at a dilution of 1:1000, while the mouse anti-rabbit AlexaFluor-488 (Thermo Fisher Scientific) secondary antibody was used at a dilution of 1:500; all secondary antibodies were incubated for 1 h at room temperature followed by 3 washes in 0.1% Tween 20/PBS. After final washes, cells were mounted with DAPI-Fluoromount-G (Southern Biotech), covered with a 25 × 25 mm glass coverslip and sealed with clear nail polish. Fluorescence intensity measurements of S9.6 were performed using FIJI. To quantify nuclear R-loop and cGAS levels, DAPI staining was used to define the nuclear border, and only R-loops or cGAS within the nucleus were measured using Fiji. To quantify non-nuclear R-loop levels, we measured R-loop levels using Fiji that were adjacent to, but not within the DAPI stained regions.

Human cells

HEK-293 cells grown on 25 × 25 mm glass coverslips were fixed in 4% paraformaldehyde (PFA) for 10 minutes followed by two 5-minute washes in D-PBS. Cells were permeabilized with 0.1% Triton-X in D-PBS for 10 minutes followed by two 10-minute washes in D-PBS. Cells were then blocked in 1% FBS/D-PBS for 1 h. The mouse monoclonal S9.6 (Boguslawski et al., 1986) primary antibody was used at a dilution of 1:100 in blocking buffer for 2 h at room temperature followed by 5 washes in D-PBS for 5 minutes each. The goat anti-mouse AlexaFluor-488 IgG2a was used at a dilution of 1:500 and incubated for 1 h at room temperature followed by 5 washes in D-PBS for 5 minutes each. After final washes, cells were mounted with DAPI-Fluoromount-G, placed on a glass slide and sealed with clear nail polish. Fluorescence intensity measurements of S9.6 were performed using FIJI.

Fluorescent microscopy and time-lapse imaging

Embryos were imaged using a Leica SP5 inverted confocal microscope (Leica). For time-lapse imaging, embryos were anesthetized with tricaine and then embedded in agarose (1% in E3 medium) containing tricaine in a zWEDGI device (Huemer et al., 2017). z-stacks were taken every 20 minutes over a six-hour period. Movies were created using Fiji software.

Image acquisition and processing

Brightfield and fluorescent images were acquired using a Zeiss Stereo Discovery.V8 with an AxioCam HRc camera. Confocal images for zebrafish single-cell immunofluorescence were acquired using a Leica SP5 AOBs Inverted DMI6000 microscope with a 63X oil objective and zoomed in fields were taken at 6.5X zoom. FIJI/ImageJ was used for quantification of images (Collins, 2007). Flowjo,

GraphPad Prism 8, Adobe Photoshop and Adobe Illustrator were used to generate figures. Graphical abstract was created with BioRender.com.

RNA-sequencing and splicing analysis

cd41:gfp⁺ HSPCs from *ddx41* mutants and siblings at 40 hpf were isolated by FACS on a Mo-Flo cell sorter (Beckman Coulter). RNA from these cells was subsequently isolated using the Zymo Quick-RNA microprep kit (R2080) according to the manufacturer specification. The TURBO DNA-free kit (Life Technologies) was used for DNA removal following RNA extraction. RNA and library quality was assessed using a bioanalyzer Pico Chip (Agilent) by the Einstein Genomics core facility. Libraries for RNA samples with RIN \geq 9 were prepared by BGI using the Nugene low-input RNA sequencing kit. Three independent biological replicates were analyzed. On average, approximately 30 million paired-end 150 base pair sequencing reads were acquired per sample using the Illumina NovoSeq platform. Zebrafish RNA sequencing reads were first trimmed with TRIM GALORE software to check for quality of 150bp reads and then mapped to the *D. rerio* GRCz10 genome build using STAR Aligner (Dobin et al., 2013) (version 2.4.2a). The GRCz10.85 gtf annotation file was used. DE-Seq2 (Love et al., 2014) was used via DEApp (Li and Andrade, 2017) to determine differential gene expression (defined as 2-fold change, FDR $p < 0.05$) between *ddx41* mutant and sibling control HSPCs. Pathway analysis was analyzed using the Molecular Signatures Database (MSigDB) (Liberzon et al., 2015; Subramanian et al., 2005). Differential inclusion rates across 17,040 splicing events between *ddx41* mutants and siblings were calculated using rMATS (Shen et al., 2014) (replicate Multivariate Analysis of Transcript Splicing). Splicing events with inclusion differences \geq 10% and FDR \leq 0.01 were considered significantly altered. Pathway analysis for alternatively spliced genes was also performed using MSigDB. RNA-seq data have been deposited at Gene Expression Omnibus (GEO) under GSE146995.

Reverse transcription-PCR

Mutant and sibling embryos were pooled based on morphology. Zebrafish embryo RNA was isolated from pools of 20–40 embryos at the 40 hpf stage using the TRIzol reagent (Thermo Fisher; 15596026) according to the manufacturer's protocol. Embryos were dissociated in TRIzol using a pestle. The High Capacity cDNA reverse transcriptase kit (Thermo Fisher; 4368814) was used to generate cDNA from 300ng input RNA. The cDNA was diluted 1:50 in nuclease-free water. Data were averaged from at least three independent replicates per sample. qPCR primers are in Key resources table. For RT-PCR analysis for morpholino functionality, wild-type embryos were first injected with control, splice-blocking *sting*, or splice-blocking *cgas* morpholinos. At 24 hpf, zebrafish embryo RNA was isolated and used to generate cDNA similar to the method described above. The cDNA was diluted 1:5 in nuclease-free water. The cDNA was then amplified using the RT-PCR primers in Key resources table, and the amplicons examined on an agarose gel to confirm proper exon-skipping induced by the splice-blocking morpholinos.

Western analysis

Embryos were pooled for protein collection on the basis of phenotype. Cell lysates of deyolked embryos were prepared with RIPA buffer (Boston BioProducts). Proteins were resolved by SDS-PAGE and transferred to nitrocellulose membranes (Bio-Rad), followed by immunoblotting with primary and secondary antibodies. Primary antibodies were: mouse anti-TBK1 (Cell Signaling Technology, 1:1000), mouse anti-pTBK1 (Cell Signaling Technology, 1:1000), rabbit anti-cGAS (Abcam, 1:700) and rabbit anti-GAPDH (Abcam, 1:10000). Secondary antibodies were goat anti-mouse IgG-HRP (Santa Cruz, 1:2000) and mouse anti-rabbit IgG-HRP (Santa Cruz, 1:2000 for rabbit anti-cGAS, and 1:5000 for rabbit anti-GAPDH). Catalog numbers for all antibodies are listed in the Key resources table.

Patient database and survival data

Gene expression data from 183 MDS CD34⁺ samples and 17 controls were obtained from Gene Expression Omnibus (GEO) (GSE19429) (Pellagatti et al., 2010). Clinical annotations and overall survival were compared to gene expression as performed previously (Schinke et al., 2015). Pathway analysis between *DDX41* low and *DDX41* high patient CD34⁺ cells was performed using MSigDB, with clinical annotation being performed as described above. Each cell represents the correlation between the 183 values of the clinical variable (column), and the 183 values of the gene probe (row) matched by patient.

QUANTIFICATION AND STATISTICAL ANALYSIS

Statistics

Experiments were performed with a minimum of three replicates. Statistical analyses were performed as indicated in each figure using unpaired Student's t-test or a one-way ANOVA with Tukey's multiple testing correction as appropriate; error bars indicate the standard deviation of mean, unless otherwise indicated.

Ddx41 inhibition of DNA damage signaling permits erythroid progenitor expansion in zebrafish

by Joshua T. Weinreb, Varun Gupta, Elianna Sharvit, Rachel Weil, and Teresa V. Bowman

Haematologica 2021 [Epub ahead of print]

*Citation: Joshua T. Weinreb, Varun Gupta, Elianna Sharvit, Rachel Weil, and Teresa V. Bowman. Ddx41 inhibition of DNA damage signaling permits erythroid progenitor expansion in zebrafish. Haematologica. 2021; 106:xxxx
doi:10.3324/haematol.2020.257246*

Publisher's Disclaimer

E-publishing ahead of print is increasingly important for the rapid dissemination of science. Haematologica is, therefore, E-publishing PDF files of an early version of manuscripts that have completed a regular peer review and have been accepted for publication. E-publishing of this PDF file has been approved by the authors. After having E-published Ahead of Print manuscripts will then undergo technical and English editing, typographical proof correction and be presented for the authors' final approval. The final version of the manuscript will then appear in print on a regular issue of the journal. All legal disclaimers that apply to the journal also pertain to this production process.

Ddx41 inhibition of DNA damage signaling permits erythroid progenitor expansion in zebrafish

Joshua T. Weinreb^{1,2}, Varun Gupta³, Elianna Sharvit¹, Rachel Weil¹, Teresa V. Bowman^{#1,2,4}

1. Albert Einstein College of Medicine, Department of Developmental and Molecular Biology, Bronx, NY, USA
2. Albert Einstein College of Medicine, Gottesman Institute for Stem Cell Biology and Regenerative Medicine, Bronx, NY, USA
3. Albert Einstein College of Medicine, Department of Cell Biology, Bronx, NY, USA
4. Albert Einstein College of Medicine and Montefiore Medical Center, Department of Medicine (Oncology), Bronx, NY, USA

#To whom correspondence should be addressed:

Address: 1300 Morris Park Avenue, Bronx, NY 10461

Email: teresa.bowman@einsteinmed.org

Phone: (718) 430-4001

Fax: (718) 430-8567

ACKNOWLEDGMENTS

This work was funded by American Cancer Society RSG-129527-DDC, DOD BM180109, NIH 1R01DK121738-01A1 and the Edward P. Evans Foundation (to TVB), NIH MSTP training grant T32GM007288-45 and F30 fellowship 1F30HL142161 (to JTW), and NIH 1R01GM057829-23 to Charles Query for support of VG.

We also want to acknowledge the assistance of numerous core facilities at Albert Einstein College of Medicine including Flow Cytometry, Analytical Imaging, and Genomics Facilities (funded by NCI Cancer Grant P30CA013330), and the Zebrafish Core Facility.

AUTHORSHIP CONTRIBUTIONS

JTW and TVB designed the project experimental approach. JTW, ES, RW, and TVB performed the experiments. VG performed bioinformatics analysis. JTW and TVB analyzed the data. JTW and TVB wrote and edited the manuscript; all authors reviewed and approved the manuscript.

CONFLICT OF INTEREST DISCLOSURES

The authors declare no competing financial interests.

Text word count: 3471

Abstract word count: 142

Number of figures: 6 main + 1 supplemental

Number of tables: 7

Number of references: 34

ABSTRACT

DEAD-box Helicase 41 (DDX41) is a recently identified factor mutated in hematologic malignancies whose function in hematopoiesis is unknown. Using an *in vivo* model of Ddx41 deficiency, we unveiled a critical role for this helicase in regulating erythropoiesis. We demonstrated that loss of *ddx41* leads to anemia caused by diminished proliferation and defective differentiation of erythroid progenitors. Mis-expression and alternative splicing of cell cycle genes is rampant in *ddx41* mutant erythroid progenitors. We delineated that the DNA damage response is activated in mutant cells resulting in an Ataxia-telangiectasia mutated (ATM) and Ataxia-telangiectasia and Rad3-related (ATR)-triggered cell cycle arrest. Inhibition of these kinases partially suppressed *ddx41* mutant anemia. These findings establish a critical function for Ddx41 in promoting healthy erythropoiesis via protection from genomic stress and delineate a mechanistic framework to explore a role for ATM and ATR signaling in DDX41-mutant hematopoietic pathologies.

INTRODUCTION

Mutations in *DEAD-box Helicase 41 (DDX41)* were identified recently in hematologic malignancies including myelodysplastic syndrome (MDS), acute myeloid leukemia (AML), and acute erythroid leukemia (AEL) (1, 2). Germline *DDX41* frameshift mutations are loss-of-function and somatic missense mutations are thought to result in hypomorphic helicase activity (1, 3). The human genetics thus suggest that diminished function of this helicase is detrimental to hematopoiesis, but this has yet to be demonstrated in an animal model.

In particular, a significant number of *DDX41*-mutated MDS patients experience mild cytopenia in the years preceding diagnosis, indicating that anemia may be one of the first warning signs of disease (4). Anemia in MDS is attributed to numerous cellular mechanisms including erythroid precursor apoptosis, defective progenitor expansion, and ineffective erythrocytic maturation (5-7). The clinical findings suggest *DDX41* could be important in erythropoiesis, but the cellular and molecular underpinnings remain unclear. Roles for *DDX41* have been implicated in genomic stability, inflammation, and splicing, all processes linked to hematopoietic health, but the current lack of *DDX41* mutant animal models has slowed exploration of its function in the blood system (8-11).

To uncover the *in vivo* role of *DDX41* in erythropoiesis, we established a zebrafish *ddx41* loss-of-function mutant. We demonstrated that *ddx41* mutants develop anemia due to a decrease in erythroid progenitor expansion and defective differentiation. Mechanistically, the erythroid proliferative defect is due in part to ATM- and ATR-mediated cell cycle arrest induced by elevated DNA damage as well as mis-expression and alternative splicing of cell cycle regulators. Our data demonstrate that *Ddx41* plays a critical role in hematopoiesis and provide a possible mechanism by which anemia may arise in *DDX41*-mutated hematopoietic pathologies.

METHODS

Zebrafish

Zebrafish were maintained as described (12) and according to IACUC-approved protocols in accordance with Albert Einstein College of Medicine research guidelines. Genotyping was performed to confirm animal identity. Mutants for *ddx41* (*ddx41^{sa14887}*) were acquired from the Zebrafish International Resource Center (13). The mutation results in a premature stop codon at Tyrosine 410. For all experiments, sibling controls are a mix of heterozygotes and wild types. Tg(*gata1:dsred*) (14) transgenics were used. Genotyping details are in the online supplement and Table S7.

Drug treatments

All drugs were dissolved in DMSO. Dilutions were made in E3 embryo water. KU60019 (ATM inhibitor) and AZ20 (ATR inhibitor) were used with DMSO as the vehicle control.

Whole-mount *in situ* hybridization and o-dianisidine staining

In situ hybridization was performed as described previously (15, 16). After *in situ*, embryos were scored manually, imaged and genotyped. The *βe3-globin* (17), *cmyb* (18), and *gata1* (19) probes were used, and *in situ* levels were quantified using FIJI (20). O-dianisidine staining was performed as described previously (21).

Flow cytometry

Mutant and sibling embryos were binned based on morphological differences. For generation of single-cell suspensions, 10-20 embryos were processed as previously described (15) (also see online supplement). Quantification for the absolute number of cells was performed by acquiring all events in a tube on the flow cytometer to determine the total number of target cells. This number was then divided by the total number of embryos analyzed to calculate the number of target cells per embryo.

Cell cycle and apoptosis analyses

For 5-ethynyl-2'-deoxyuridine (EdU) incorporation experiments, embryos were incubated with 20mM EdU for 2 hours. Single-cell suspensions of embryos were

generated. Click-IT EdU Flow Cytometry Assay Kit was used according to the manufacturer's instructions. Flow cytometry analysis for active caspase-3 was performed as previously described (22). Samples were analyzed with a LSRII flow cytometer (BD Biosciences) and FlowJo software.

RNA-sequencing and splicing analysis

Erythroid progenitors from *ddx41* mutants and siblings were isolated by fluorescently-activated cell sorting (FACS). RNA from these cells was subsequently isolated, DNase-digested and library prepared for sequencing. Details on library preparation, sequencing and bioinformatic analyses can be found in the online supplement. All data are deposited under GEO accession number GSE160979.

RT-qPCR

To validate the RNA-sequencing data, we performed reverse transcription (RT) quantitative PCR. RNA was isolated from 40 hpf embryos. Details are listed in the online supplement and Table S7.

Single-cell immunofluorescence of zebrafish embryonic cells

Single-cell suspensions were prepared, and cell staining was performed as described in Sorrells & Nik *et al.* (22) and detailed in the online supplement. Fluorescence intensity measurements of γ H2AX were performed using FIJI.

May-Grunwald Giemsa staining of primitive erythroid cells

May-Grunwald Giemsa staining was performed as previously described (15) and as detailed in the online supplement.

Statistics

Experiments were performed with a minimum of three replicates. Statistical analyses were performed as indicated in each figure using unpaired Student's t-test or a one-way ANOVA with Tukey's multiple testing correction as appropriate; error bars indicate the standard deviation of mean, unless otherwise indicated.

RESULTS

Ddx41 regulates erythroid development

To explore a function for Ddx41 in hematopoiesis, we examined erythrocyte formation and differentiation in zebrafish *ddx41* homozygous loss-of-function mutants (*ddx41^{sa14887}*). Maternally-deposited Ddx41 (data not shown) helps the mutants develop and survive until 3 days post fertilization (dpf) (Figure S1A-B). Based on this, we consider the mutants to be functionally hypomorphic with greatly diminished but not completely absent Ddx41 levels. DDX41 is highly conserved between humans and zebrafish suggesting that lessons learned about the *in vivo* role of zebrafish Ddx41 function in hematopoiesis will be relevant to human DDX41. In zebrafish, primitive hematopoiesis begins ~12-24 hours post fertilization (hpf), producing embryonic erythrocytes and myeloid cells that constitute the hematopoietic system early on in development (23, 24). Cells of the erythrocytic lineage first arise from the intermediate cell mass (ICM) within the posterior lateral mesoderm (PLM) (Figure 1A). These erythrocytes express factors such as the progenitor transcription factor *c-myb* and the erythroid-specific transcription factor *gata1* starting during somitogenesis (19, 25). Using *in situ* hybridization, we determined that these erythroid progenitor markers were expressed similarly in *ddx41* mutants compared to siblings (mix of *ddx41* heterozygotes + wild types) at 22hpf, indicating initial erythroid specification is unaffected (Figures 1B-E). Oxygenated hemoglobinized erythrocytes are detectable beginning around 36 hpf using o-dianisidine staining (26). In *ddx41* mutants, we observed little o-dianisidine-positive erythroid cells at 40 hpf (Figure 1F). We sorted *gata1:dsRed⁺* erythrocytes at 40 hpf and found that the *ddx41* mutant cells were larger than those from sibling controls (Figure 1G). This size difference could be indicative of delayed erythroid differentiation. As mutants display some developmental delay that becomes more severe as the embryos get older, it is possible that the erythroid delay is a side effect of the general developmental delay. To distinguish between these possibilities, we examined erythrocytes in *ddx41* mutants and siblings at 48 hpf. Oxygenated hemoglobin levels remained low in mutants at 48 hpf (Figures 1H-I). To assess maturation, we also bled *ddx41* mutants and sibling control embryos at 48 hpf and analyzed the morphology of

isolated erythrocytes using May-Grunwald-Giemsa staining (Figure 1J). The *ddx41* mutant erythrocytes displayed a megaloblastoid-like phenotype, suggesting some abnormalities in erythrocyte maturation.

To acquire enough erythrocytes to perform the morphological assessment, we needed to bleed four times as many *ddx41* mutant embryos as compared to sibling control embryos, suggesting mutants had fewer erythrocytes than siblings. To test this hypothesis, we assessed the number of *gata1:dsred*⁺ erythroid progenitors in *ddx41* mutants and siblings using flow cytometry quantification. We determined that the absolute number of *gata1:dsred*⁺ erythrocytes per embryo was significantly reduced in *ddx41* mutants compared to siblings at both 28 and 40 hpf (Figures 2A-D). These data indicate that decreased erythrocyte number contributes to the development of anemia in *ddx41* mutants.

Erythroid progenitors arising from both primitive and definitive erythroid-myeloid progenitor (EMP)-derived waves are present during the developmental time points analyzed. The gene programs for the specification and differentiation of primitive and EMP-derived erythropoiesis are highly similar, but the developmental timings are distinct (Figure 2E). EMP specification begins around 26 hpf (27). To determine whether there were defects in EMP-derived erythropoiesis, we performed *in situ* hybridization for the progenitor marker *c-myb* at 26 and 36 hpf and *gata1* at 26 hpf in siblings and *ddx41* mutants (Figures 2F-G and S1C-F). Expression of both *c-myb* and *gata1* within the posterior blood island (PBI) region where EMPs form were not decreased and in fact were increased in *ddx41* mutants as compared to siblings. As the gene programs are highly similar between these two waves of erythroid development, these data indicate that the reduction in erythrocytes in *ddx41* mutants is occurring at an erythroid progenitor stage after *c-myb* and *gata1* are both expressed, which is shortly after erythroid lineage specification.

To further characterize the maturation state of the erythrocytes at 40 hpf in *ddx41* mutants and siblings, we performed RT-qPCR for embryonic and larval globins.

Expression of the embryonic globins $\alpha\epsilon 1$, $\alpha\epsilon 3$, $\beta\epsilon 1$, and $\beta\epsilon 3$ begins during somitogenesis with expression of all of these globins except $\beta\epsilon 3$ persisting in primitive and EMP-derived erythrocytes throughout larval development (28). In contrast, levels of $\beta\epsilon 3$ globin diminish dramatically from 24-48 hpf, somewhat concomitant with the increasing expression of the larval $\beta\epsilon 2$ globin. The other larval globin $\alpha\epsilon 5$ is not expressed significantly until 14 dpf. In *ddx41* mutants, we determined that while the levels of the embryonic/larval globins $\alpha\epsilon 1$ and $\beta\epsilon 1$ were diminished, the levels of the embryonic-restricted $\beta\epsilon 3$ globin remained high, consistent with a maturational defect in primitive erythrocytes. Additionally, expression of the larval $\beta\epsilon 2$ globin was lower in mutants compared to sibling controls. Although *ddx41* mutants die before there are expansive numbers of maturing erythrocytes derived from EMPs, these data indicate that mutants have fewer definitive erythrocytes compared to siblings. This finding suggests that similar to primitive erythroid progenitors, EMPs are specified normally, but there is a later stage defect, although the underlying cause (e.g. diminished expansion, maturation or differentiation) cannot be deciphered. Together, our findings establish that Ddx41 is critical for erythrocyte expansion and maturation.

Cell cycle genes are mis-expressed and alternatively spliced in *ddx41* mutant erythroid progenitors

To mechanistically assess the underlying cause of the erythrocytic defect in *ddx41* mutants, we conducted RNA-sequencing (RNA-seq) on *gata1:dsred⁺* erythrocytes isolated from *ddx41* mutants and siblings at 40 hpf. Over 1,800 genes were downregulated and more than 1,900 were upregulated in *ddx41* mutants compared to siblings (Figure 3A, Table S1, log₂ fold change \geq |1|, adj. p-value < 0.05). To understand if particular pathways were enriched in the differentially expressed genes, we performed gene set level analysis on the upregulated and downregulated gene lists by comparing each to the Molecular Signature Database (MSigDb), a platform that computes overlaps between classes of genes that are over- or under-represented in lists of genes in known pathways (29, 30). In the downregulated gene list, mRNA splicing was the top gene set with DNA replication, cell cycle, and DNA repair also enriched (Figure 3B, Table S2). In the upregulated gene list, genes associated with

adaptive immunity, post-translational modifications, innate immune system, and cell cycle were enriched (Figure 3C, Table S3). We validated the expression changes in several cell cycle and DNA-damage-associated genes using RT-qPCR (Figure 3D).

Ddx41 interacts with components of the spliceosome (1). Additionally, the top downregulated pathway in our gene set was pre-mRNA splicing, thus we examined how *ddx41* loss affected mRNA splicing in erythrocytes. When comparing splicing between *ddx41* mutants and siblings, a total of 370 alternative splicing events were observed (Figures 3E, Table S4). The specific splicing defects detected included exon skipping (SE), which was the most frequently altered splicing event, intron retention (RI), alternative 5'-splice site usage, alternative 3'-splice site usage, and changes in mutually exclusive exon usage. Alternative splicing within protein-coding regions of a transcript can result in the introduction of premature termination codon (PTC) or generation of a novel peptide. For all SE and RI events (comprising nearly 85% of all splicing changes), we determined how the alternative splicing event might alter the protein sequence (Figure 3F and Table S5). More than 50% of SE events altered the protein sequence and are predicted to generate novel peptides. Approximately 43% of SE and 90% of RI events are predicted to target the alternatively spliced transcript for nonsense-mediated decay (NMD) due to the introduction of a PTC. For example, the retained intron variant for homologous repair-associated factor *structural maintenance of chromosome 5 (smc5)* identified in *ddx41* mutants is predicted to result in NMD that could result in elevated DNA damage (Figure 3G). Another example of an NMD isoform expressed in *ddx41* mutant is the exon 3 skipped isoform of *signal transducer and activator of transcription 1a (stat1a)* that would diminish signaling by numerous cytokine pathways. Pathway analysis of these alternatively spliced factors revealed that those resulting in novel peptide sequences are enriched in mRNA metabolism, morphogenesis, and cell cycle, and those predicted to result in NMD are enriched for mRNA processing, DNA replication, and gene expression (Figure 3H and Table S6). These results depict that Ddx41 influences the expression and splicing of cell cycle, DNA repair, and mRNA processing genes in erythrocytes.

Ddx41 deficiency triggers cell cycle arrest in erythroid progenitors

The diminished number of erythroid progenitors and dysregulated expression of cell cycle genes suggest that defects in erythrocyte proliferation could contribute to the anemia in *ddx41* mutants. To examine proliferation, we analyzed cell cycle status of 30 hpf *gata1:dsred*⁺ erythroid progenitors by flow cytometry quantification of DNA synthesis via 5-Ethynyl-2'-deoxyuridine (EdU) incorporation and DNA content via DAPI incorporation. The *ddx41* mutant *gata1:dsred*⁺ progenitors showed a reduction of cells in S phase and an accumulation of cells in the G0/G1 and G2/M phases compared to sibling controls (Figures 4A-B). These results are in-line with a decrease in proliferation in *ddx41* mutant erythrocytes caused by cell cycle arrests at the G0/G1-to-S phase and G2-to-M transitions. Prolonged cell cycle arrest can lead to apoptosis (31), thus we also assessed apoptosis in *ddx41* mutants. We measured levels of active caspase-3, an essential executor of apoptosis, in *ddx41* mutant and sibling *gata1:dsred*⁺ erythrocytes by flow cytometry. We observed a significant increase in active caspase-3 in *ddx41* mutant *gata1:dsred*⁺ erythrocytes at 30 hpf (Figures 4C-D). These data indicate that both cell cycle arrest and elevated apoptosis in *ddx41* mutant erythrocytes may drive anemia.

Ddx41 regulation of ATM and ATR signaling contributes to proper erythropoiesis

These molecular and cellular phenotypes in *ddx41* mutants imply that loss of *ddx41* could promote DNA damage. To address this question, we analyzed the DNA damage response (DDR) by performing immunofluorescence (IF) for γ H2AX in *ddx41* mutants and siblings. We showed that γ H2AX levels were increased nearly two-fold in *ddx41* mutants compared to sibling cells (Figures 4E-F). These data demonstrate that *ddx41* deficiency triggers DDR *in vivo*.

Our model is that loss of Ddx41 contributes to excessive DDR signaling and subsequent cell cycle arrest in erythrocytes, leading to anemia in *ddx41* mutants. If correct, then inhibiting components of the DDR pathway would 1) reverse cell cycle defects and 2) increase erythrocyte levels. To test this model, we examined how the two primary mediators of DDR, Ataxia-telangiectasia-mutated (ATM) and Ataxia-telangiectasia and

Rad3-related (ATR), affected erythrocytic cell cycle kinetics in *ddx41* mutants. We assessed cell cycle status of 30 hpf *ddx41*-mutant *gata1:dsred*⁺ erythroid progenitors in embryos treated with DMSO vehicle control, the ATM inhibitor KU60019, or the ATR inhibitor AZ20. There was a significant increase of *gata1:dsred*⁺ *ddx41*-mutant cells in S phase when treated with either ATM or ATR inhibitors as compared to DMSO vehicle control (Figures 5A-B). Additionally, pharmacological inhibition of ATM or ATR increased erythropoietic output in *ddx41* mutants, as measured by quantification of *gata1:dsred*⁺ erythrocyte numbers per embryo using flow cytometry (Figures 5C-F). Although there was a trend towards an increase in erythrocyte numbers in control siblings treated with ATM or ATR inhibitors these changes were not statistically significant. Taken together, these data indicate that DDR signaling triggers a G0/G1 cell cycle arrest in *ddx41*-mutant erythrocytes that results in a reduction of erythroid progenitor cell number.

Finally, we wanted to assess if increasing the number of erythroid progenitors via ATM or ATR inhibition would increase the number of oxygenated erythrocytes in *ddx41* mutants. Surprisingly, we only observed a significant increase in o-dianisidine-positive erythrocytes in *ddx41* mutants treated with ATM inhibitor, but not ATR inhibitor (Figures 6A-B). These data indicate that Ddx41 regulation of ATM might have a broader impact on erythropoiesis than ATR signaling.

DISCUSSION

Although *DDX41* mutations are found in numerous human hematologic diseases, its function in hematopoiesis is unknown. Our work is the first to establish Ddx41 as a critical mediator of erythropoiesis with *ddx41* loss suppressing the expansion and maturation of erythrocytes. We showed a profound effect on the expression of cell cycle and DNA damage-associated genes in *ddx41* mutant erythroid progenitors consistent with the observed cell cycle arrest. The DNA damage response is elevated in *ddx41* mutant cells and triggers an ATM and ATR-triggered cell cycle arrest. Inhibition of ATM and ATR partially suppressed anemia in *ddx41* mutants. These findings establish

Ddx41 as a positive regulator of erythropoiesis in part by preventing genomic stress and promoting proper erythroid progenitor expansion.

Patients with germline mutations in *DDX41* do not develop hematologic symptoms until later in life (1), yet zebrafish *ddx41* mutants show anemia within 40 hpf. We posit that the difference has to do with the extent of Ddx41 deficiency. Zebrafish homozygous mutants have maternally deposited Ddx41 that is naturally depleted over the first few days of life. When the levels reach below a certain threshold, the mutants die, demonstrating it is an essential factor. In contrast, zebrafish *ddx41* heterozygous animals are phenotypically indistinguishable from wild-type animals during embryogenesis and in adulthood, suggesting a 50% decrease of Ddx41 alone is insufficient to alter hematopoiesis. This is in agreement with the clinical observation that patients with germline *DDX41* mutations that develop hematologic malignancies often acquire somatic missense mutations in the second allele that are thought to diminish *DDX41* ATPase activity (1). Combined, the data indicate that when *DDX41* levels decrease to less than 50%, this leads to hematologic defects, but when critically too low, it leads to lethality.

DDX41 was previously identified as a mediator of genomic stability in a cell line-based genome-wide siRNA screen (11). However, a role for *DDX41* in genomic integrity as well as the downstream consequences of its loss were never demonstrated *in vivo*. Our current work revealed that Ddx41 regulates genomic integrity *in vivo*, and that loss of *ddx41* leads to both cell cycle arrest and apoptosis in erythrocytes that contributes to anemia in *ddx41* mutants. We established that ATM and ATR signaling contribute to these attributes, but only ATM inhibition significantly increased o-dianisidine-positive erythrocytes in *ddx41* mutants. The differential impact on oxygenated erythrocyte output by inhibition of ATM and ATR might indicate that Ddx41-regulated ATM signaling is more critical for proper erythropoiesis. ATM has an additional role in apoptosis, especially during development that might explain some of the phenotypic differences when comparing ATM and ATR inhibition effects on erythropoiesis. However, it should be noted that although the ATM and ATR kinases respond uniquely, there exists an

extensive 'cross-talk' between them, which can make determining which precise pathway is involved in a phenotype confusing (32). Further dissection of the role of DDX41 in ATM and ATR pathway regulation will need to be investigated.

Splicing mutations are commonly found in hematologic malignancies (33, 34). DDX41 interacts with multiple components of the spliceosome (1). Our work aligns with prior studies showing *DDX41* insufficiency associates with numerous deleterious splicing outcomes. If and how these splicing events contribute to hematopoietic pathogenesis is unclear. We showed that components related to cell cycle and DNA repair are commonly mis-spliced in *ddx41* mutants. Therefore, it is possible that loss of *ddx41* may be mediating cell cycle arrest and activation of DDR via mis-splicing of crucial regulators of these pathways. The contribution of DDR pathway component mis-splicing in human cytopenias remains to be addressed.

In addition to the effect on cell cycle, we delineated maturation defects in *ddx41* erythrocytes marked by aberrant globin expression and a megaloblastoid-like morphology of mutant erythrocytes. Although we could not perform a complete analysis of definitive erythropoiesis as *ddx41* mutants die before EMP-derived or HSC-derived erythrocytes fully mature, the diminished expression of the larval $\beta e2$ globin suggests a decrease in EMP-derived definitive erythrocytes. This finding combined with the elevated *cmyb* and *gata1* levels in EMP cells suggests that this defect could be caused in part by maturation defects. As the treatment with the ATM inhibitor KU60019 only partially increased hemoglobinized erythrocytes in *ddx41* mutants, it suggests that deregulation of another pathway underlies additional maturational defects in *ddx41* mutants.

In sum, our study unveils a critical role for Ddx41 as a key gatekeeper to maintain cell cycle progression, a necessary component for erythrocytic development. We demonstrated that deficiency of *ddx41* triggers cell cycle arrest via activation of ATM and ATR, which ultimately mediates a decrease in proliferation and maturation of erythrocytic progenitors in *ddx41* mutants. These findings establish a critical function for

Ddx41 in promoting healthy erythropoiesis by suppressing genomic stress and present a potential role for ATM and ATR signaling in *DDX41*-mutant pathologies.

REFERENCES

1. Polprasert C, Schulze I, Sekeres MA, et al. Inherited and Somatic Defects in DDX41 in Myeloid Neoplasms. *Cancer Cell*. 2015;27(5):658-670.
2. Iacobucci I, Wen J, Meggendorfer M, et al. Genomic subtyping and therapeutic targeting of acute erythroleukemia. *Nat Genet*. 2019;51(4):694-704.
3. Yoneyama-Hirozane M, Kondo M, Matsumoto SI, et al. High-Throughput Screening to Identify Inhibitors of DEAD Box Helicase DDX41. *SLAS Discov*. 2017;22(9):1084-1092.
4. Sebert M, Passet M, Raimbault A, et al. Germline DDX41 mutations define a significant entity within adult MDS/AML patients. *Blood*. 2019;134(17):1441-1444.
5. Schneider RK, Schenone M, Ferreira MV, et al. Rps14 haploinsufficiency causes a block in erythroid differentiation mediated by S100A8 and S100A9. *Nat Med*. 2016;22(3):288-297.
6. Danilova N, Sakamoto KM, Lin S. Ribosomal protein L11 mutation in zebrafish leads to haematopoietic and metabolic defects. *Br J Haematol*. 2011;152(2):217-228.
7. Payne EM, Virgilio M, Narla A, et al. L-Leucine improves the anemia and developmental defects associated with Diamond-Blackfan anemia and del(5q) MDS by activating the mTOR pathway. *Blood*. 2012;120(11):2214-2224.
8. Parvatiyar K, Zhang Z, Teles RM, et al. The helicase DDX41 recognizes the bacterial secondary messengers cyclic di-GMP and cyclic di-AMP to activate a type I interferon immune response. *Nat Immunol*. 2012;13(12):1155-1161.

9. Zhang Z, Yuan B, Bao M, et al. The helicase DDX41 senses intracellular DNA mediated by the adaptor STING in dendritic cells. *Nat Immunol.* 2011;12(10):959-965.
10. Zhang Z, Bao M, Lu N, et al. The E3 ubiquitin ligase TRIM21 negatively regulates the innate immune response to intracellular double-stranded DNA. *Nat Immunol.* 2013;14(2):172-178.
11. Paulsen RD, Soni DV, Wollman R, et al. A genome-wide siRNA screen reveals diverse cellular processes and pathways that mediate genome stability. *Mol Cell.* 2009;35(2):228-239.
12. Lawrence C. Advances in zebrafish husbandry and management. *Methods Cell Biol.* 2011;104:429-451.
13. Kettleborough RN, Busch-Nentwich EM, Harvey SA, et al. A systematic genome-wide analysis of zebrafish protein-coding gene function. *Nature.* 2013;496(7446):494-497.
14. Traver D, Paw BH, Poss KD, et al. Transplantation and in vivo imaging of multilineage engraftment in zebrafish bloodless mutants. *Nat Immunol.* 2003;4(12):1238-1246.
15. De La Garza A, Cameron RC, Nik S, Payne SG, Bowman TV. Spliceosomal component Sf3b1 is essential for hematopoietic differentiation in zebrafish. *Exp Hematol.* 2016;44(9):826-837.
16. Thisse C, Thisse B. High-resolution in situ hybridization to whole-mount zebrafish embryos. *Nat Protoc.* 2008;3(1):59-69.
17. Brownlie A, Hersey C, Oates AC, et al. Characterization of embryonic globin genes of the zebrafish. *Dev Biol.* 2003;255(1):48-61.

18. Liao EC, Paw BH, Oates AC, et al. SCL/Tal-1 transcription factor acts downstream of cloche to specify hematopoietic and vascular progenitors in zebrafish. *Genes Dev.* 1998;12(5):621-626.
19. Detrich HW 3rd, Kieran MW, Chan FY, et al. Intraembryonic hematopoietic cell migration during vertebrate development. *Proc Natl Acad Sci U S A.* 1995;92(23):10713-10717.
20. Dobrzycki T, Krecsmarik M, Bonkhofer F, Patient R, Monteiro R. An optimised pipeline for parallel image-based quantification of gene expression and genotyping after in situ hybridisation. *Biol Open.* 2018;7(4):bio031096.
21. Lieschke GJ, Oates AC, Crowhurst MO, Ward AC, Layton JE. Morphologic and functional characterization of granulocytes and macrophages in embryonic and adult zebrafish. *Blood.* 2001;98(10):3087-3096.
22. Sorrells S, Nik S, Casey M, et al. Spliceosomal components protect embryonic neurons from R-loop-mediated DNA damage and apoptosis. *Dis Model Mech.* 2018;11(2):dmm031583.
23. Carroll KJ, North TE. Oceans of opportunity: exploring vertebrate hematopoiesis in zebrafish. *Exp Hematol.* 2014;42(8):684-696.
24. Clements WK, Traver D. Signalling pathways that control vertebrate haematopoietic stem cell specification. *Nat Rev Immunol.* 2013;13(5):336-348.
25. Lyons SE, Lawson ND, Lei L, et al. A nonsense mutation in zebrafish gata1 causes the bloodless phenotype in vlad tepes. *Proc Natl Acad Sci U S A.* 2002;99(8):5454-5459.

26. Paffett-Lugassy NN, Zon LI. Analysis of hematopoietic development in the zebrafish. *Methods Mol Med.* 2005;105:171-198.
27. Bertrand JY, Kim AD, Violette EP, et al. Definitive hematopoiesis initiates through a committed erythromyeloid progenitor in the zebrafish embryo. *Development.* 2007;134(23):4147-4156.
28. Ganis JJ, Hsia N, Trompouki E, et al. Zebrafish globin switching occurs in two developmental stages and is controlled by the LCR. *Dev Biol.* 2012;366(2):185-194.
29. Liberzon A, Birger C, Thorvaldsdottir H, et al. The Molecular Signatures Database (MSigDB) hallmark gene set collection. *Cell Syst.* 2015;1(6):417-425.
30. Subramanian A, Tamayo P, Mootha VK, et al. Gene set enrichment analysis: a knowledge-based approach for interpreting genome-wide expression profiles. *Proc Natl Acad Sci U S A.* 2005;102(43):15545-15550.
31. Orth JD, Loewer A, Lahav G, Mitchison TJ. Prolonged mitotic arrest triggers partial activation of apoptosis, resulting in DNA damage and p53 induction. *Mol Biol Cell.* 2012;23(4):567-576.
32. Cimprich KA, Cortez D. ATR: an essential regulator of genome integrity. *Nat Rev Mol Cell Biol.* 2008;9(8):616-627.
33. Yoshida K, Sanada M, Shiraishi Y, et al. Frequent pathway mutations of splicing machinery in myelodysplasia [Research Support, Non-U.S. Gov't]. *Nature.* 2011;478(7367):64-69.
34. Haferlach T, Nagata Y, Grossmann V, et al. Landscape of genetic lesions in 944 patients with myelodysplastic syndromes. *Leukemia.* 2014;28(2):241-247.

FIGURE LEGENDS

Figure 1. Loss of *ddx41* causes anemia. **A.** Schema of primitive erythroid development, PLM=posterior lateral mesoderm, ProE=proerythroblasts, BasoE=basophilic erythroblasts, OrthoE=orthochromatophilic erythroblasts, func. ery=functional erythrocytes. **B,D.** *In situ* hybridization of the erythroid markers *cmyb* (**B**) [Scale bars=200 μ m] and *gata1* (**D**) [Scale bars=250 μ m] at 22 hours post fertilization (hpf) in sibling controls (top) and *ddx41* mutants (bottom). Arrowheads highlight the intermediate cell mass (ICM) region in the embryos. **C,E.** Quantification of *c-myb* (**C**) and *gata1* (**E**) *in situ* hybridization levels from (**B**) and (**D**), respectively. Quantification was done using Fiji. **F,H.** Staining for o-dianisidine, marking functional hemoglobin in mature primitive erythrocytes, in sibling controls (left) and *ddx41* mutants (right) at 40 hpf (**F**) [Scale bars=350 μ m] and 48 hpf (**H**) [Scale bars=400 μ m]. Numbers on bottom left corner indicate the fraction of embryos with the same phenotype as the one depicted in the image. **G.** Graph depicting size of erythrocytes in sibling controls and *ddx41* mutants at 40 hpf. **I.** Graph depicting frequency of designated o-dianisidine staining levels in sibling controls and *ddx41* mutants at 48 hpf. **J.** Representative images of orthochromatophilic erythroblasts stained with May–Grunwald–Giemsa from sibling controls (left) and *ddx41* mutants (right) at 48 hpf. Scale bars=5 μ m. Graphs display means \pm standard deviations (stds) with p-values calculated with unpaired Student's t-test, ns=not significant ($p>0.05$), **** $p\leq 0.0001$. For *in situs* and o-dianisidine staining n=6-72 embryos per experiment.

Figure 2. Ddx41 regulates erythroid progenitor numbers. **A,C.** Flow cytometry plots of *gata1:dsred*⁺ erythroid cells from sibling controls (left) and *ddx41* mutants (right) at 28 hpf (**A**) and 40 hpf (**C**). **B,D.** Graphs depicting the absolute number of *gata1:dsred*⁺ erythroid cells per embryo from (**A**) and (**C**), respectively. n=5 pools of ~5-20 embryos per pool. **E.** Schema of erythroid-myeloid progenitor (EMP) development. ProE=proerythroblasts, BasoE=basophilic erythroblasts, OrthoE=orthochromatophilic erythroblasts, func. ery=functional erythrocytes. **F.** *In situ* hybridization of *cmyb* at 26 hpf in sibling controls (left) and *ddx41* mutants (right) [Scale bars=150 μ m]. **G.** Quantification of *cmyb* PBI *in situ* hybridization levels from (**F**). Quantification was done using Fiji.

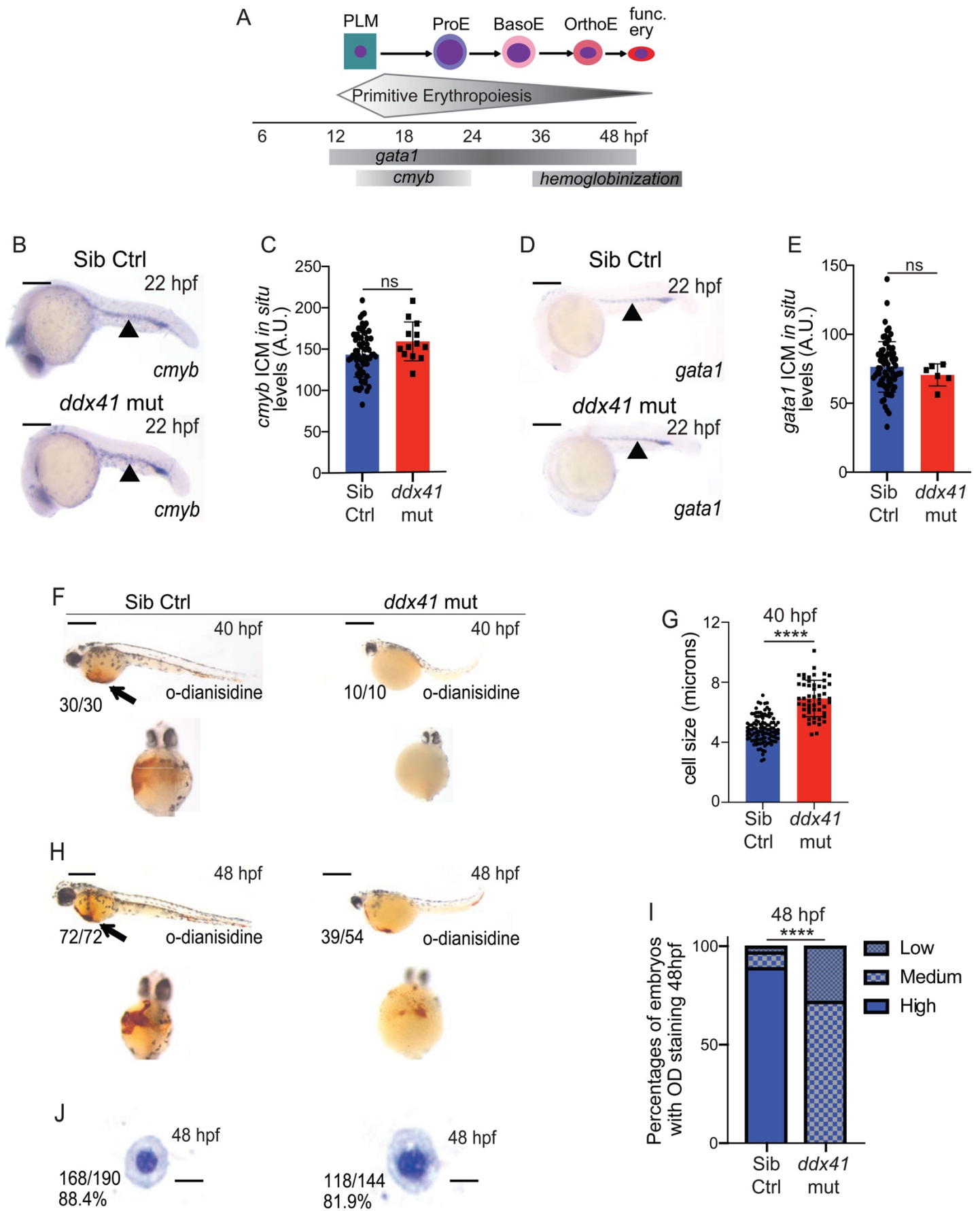
n=10-12 embryos. Graphs display means \pm standard deviations (stds). **H.** Graph of RT-qPCR analysis of the expression of globin genes between sibling controls and *ddx41* mutants. Expression levels were normalized to *slc4a1* levels. Graph displays means \pm standard error mean. The p-values were calculated with an unpaired t-test, *p<0.05, **p \leq 0.01, ***p \leq 0.001. N=3 replicates per genotype.

Figure 3. Cell cycle genes are mis-expressed and alternatively spliced in *ddx41* mutant erythroid progenitors. **A.** Volcano plot displaying differentially expressed genes between *gata1*.dsred⁺ erythrocytes from *ddx41* mutants and siblings. Significant differences are defined as FDR <0.05 and log₂ fold change \geq |1|. Black vertical lines denote the fold-change threshold and the black horizontal line denotes the FDR threshold. Five biological replicates for both *ddx41* mutants and siblings were used to generate RNA-sequencing data. **B-C.** Representative charts of pathways significantly enriched in genes downregulated (B) or upregulated (C) in *ddx41* mutant erythroid progenitors compared to sibling controls as determined by MSigDB analysis. **D.** Graph of RT-qPCR analysis of the expression of cell cycle and DNA damage-associated genes between sibling controls and *ddx41* mutants. Expression levels were normalized to *β -actin* levels. Graph displays means \pm standard error mean. The p-values were calculated with an unpaired t-test, *p<0.05, ****p \leq 0.0001. N=3 replicates per experiment. **E.** Graph depicting the $\Delta \psi$ of individual splicing events between sibling controls and *ddx41* mutants as detected by analysis with rMATS. Significant differences are defined as FDR \leq 0.01 and $\Delta \psi \geq$ 0.1. SE- skipped exons, RI- retained introns, A5SS- alternative 5' splice site, A3SS- alternative 3' splice site, and MXE- mutually exclusive exons. **F.** Graph depicting the frequency of alternatively spliced isoforms in *ddx41* mutants that are predicted to result in nonsense-mediated (NMD) decay, protein sequence alterations (non-NMD), or changes in untranslated regions (UTR). **G.** Sashimi plot for *smc5* (exons 18-19) and *stat1a* (exons 2-4) in *ddx41* mutant erythrocytes compared to sibling controls. RPKM, reads per kilobase of transcript per million mapped reads; Inc, inclusion. **H.** Representative charts of pathways significantly enriched in alternatively spliced genes in *ddx41* mutant erythrocytes compared to sibling controls as determined by pathway analysis.

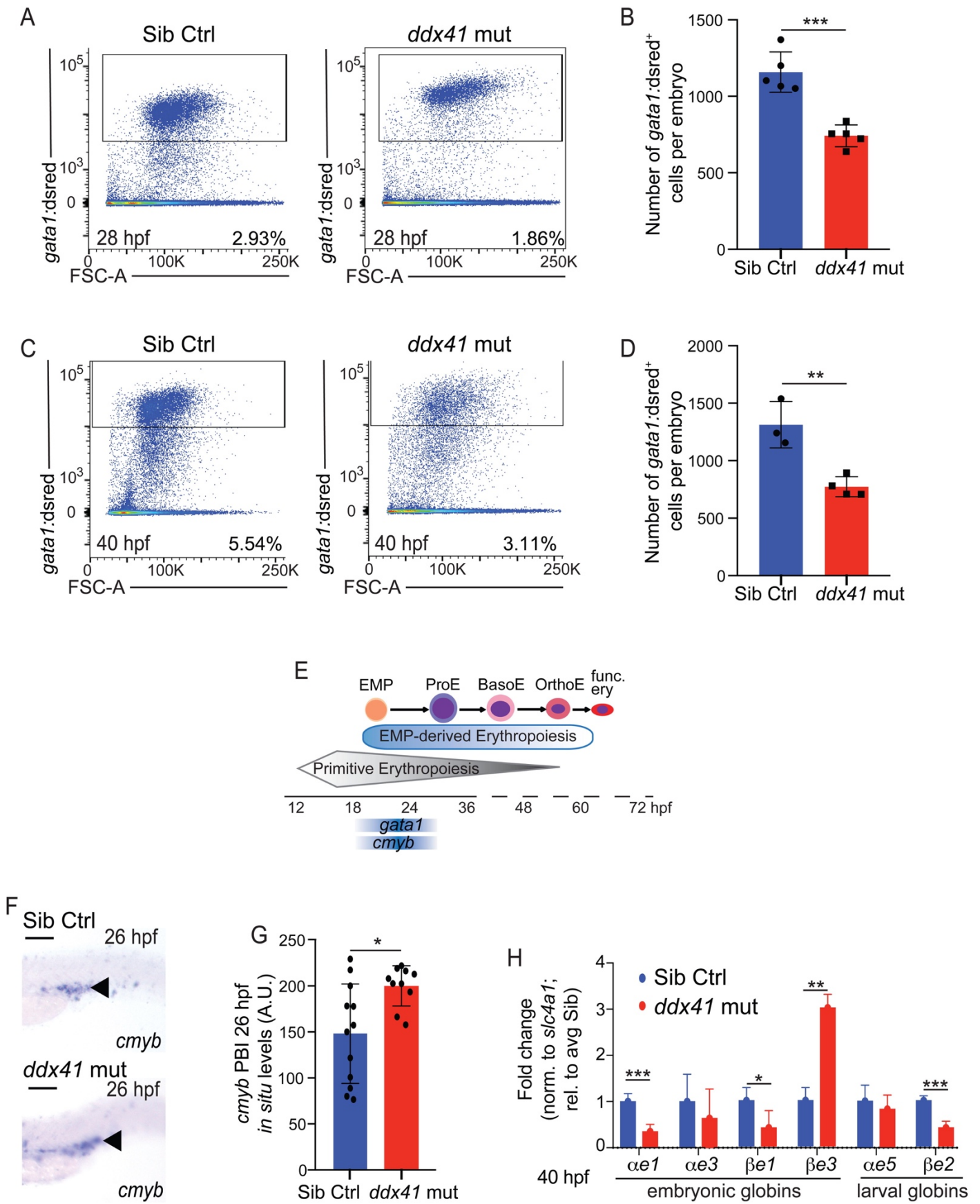
Figure 4. Ddx41 deficiency triggers cell cycle arrest and DNA damage response in erythroid progenitors. **A.** Cell cycle analysis of *gata1:dsred*⁺ erythroid cells from sibling controls (left) and *ddx41* mutants (right) after a 2-hour pulse of EdU at 28 hpf. EdU incorporation (y-axis) and DAPI content (x-axis) were measured by flow cytometry at 30 hpf. **B.** Quantification of the percentage of cells in each cell cycle phase from (A). **C.** Flow cytometry analysis of active-caspase 3 in *gata1:dsred*⁺ erythroid cells from sibling controls (left) and *ddx41* mutants (right). **D.** Quantification of the percentage of *gata1:dsred*⁺ erythroid cells that are active caspase-3-positive from (C). **E.** Confocal images showing immunofluorescence of nuclei (DAPI) and γ H2AX in cells isolated from 28 hpf siblings (top) and *ddx41* mutants (bottom). Scale bars=5 μ m. **F.** Quantification of γ H2AX levels from (E). Graphs display means \pm standard deviations (stds) with p-values calculated with unpaired Student's t-test, *p<0.05, **p<0.01, ***p<0.001, ****p<0.0001. For flow cytometry, n=3-5 pools of ~5-20 embryos per pool. For immunofluorescence imaging, n=100-300 cells per genotype.

Figure 5. Ddx41 regulation of ATM/ATR signaling contributes to proper erythroid progenitor proliferation. **A.** Cell cycle analysis of *gata1:dsred*⁺ erythroid cells from sibling controls (top) and *ddx41* mutants (bottom) treated with DMSO (left), 30nM KU60019 (ATM inhibitor, middle), and 30nM AZ20 (ATR inhibitor, right) after a 2-hour pulse of EdU at 28 hpf. EdU incorporation (y-axis) and DAPI content (x-axis) were measured by flow cytometry at 30 hpf. **B.** Quantification of the percentage of cells in each cell cycle phase from (A). **C,E.** Flow cytometry plots of *gata1:dsred*⁺ erythroid cells from sibling controls (C) and *ddx41* mutants (E) treated with DMSO (left), 30nM KU60019 (ATM inhibitor, middle), and 30nM AZ20 (ATR inhibitor, right). **D,F.** Graphs depicting the absolute number of *gata1:dsred*⁺ erythroid cells per embryo from (C) and (E). Graphs display means \pm standard deviations (stds) with p-values calculated with a one-way ANOVA with Tukey's multiple testing correction, *p<0.05, ***p<0.001, ****p<0.0001. For flow cytometry, n=3-5 pools of ~5-20 embryos per pool.

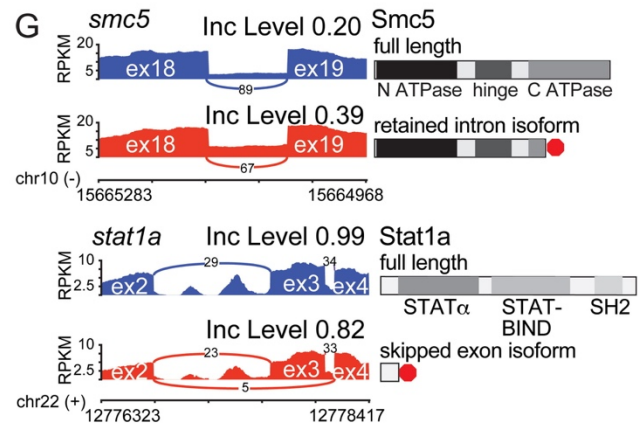
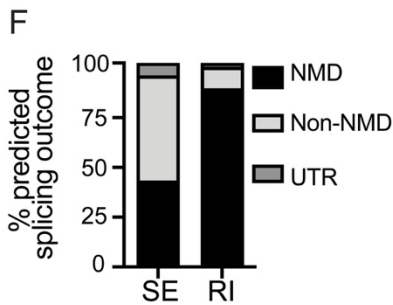
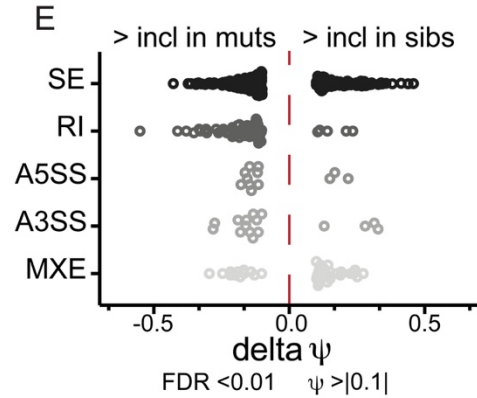
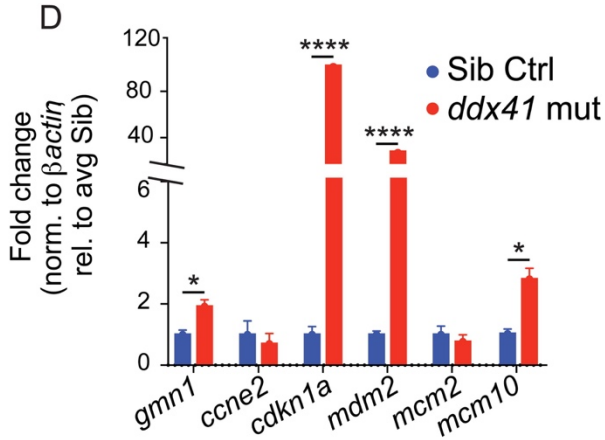
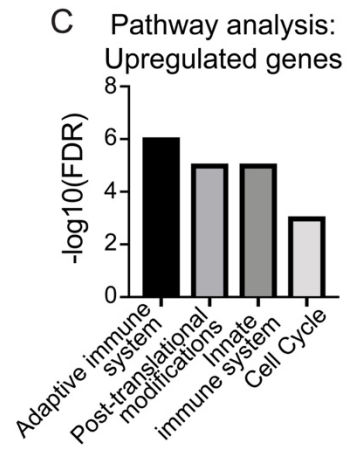
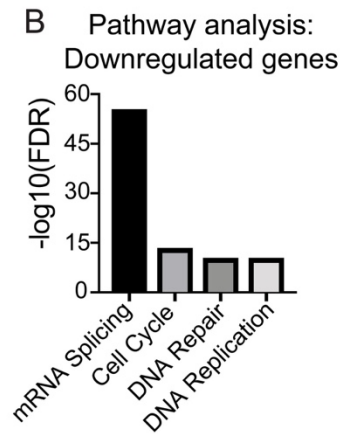
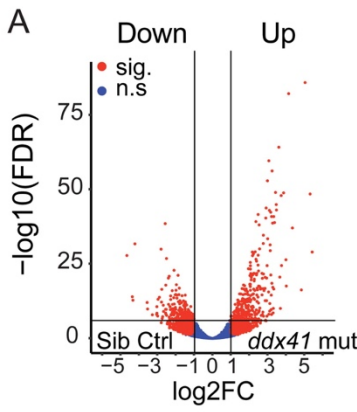
Figure 6. ATM inhibition partially suppresses *ddx41* mutant anemia. A. Representative images of o-dianisidine staining and corresponding levels of staining from sibling controls (left) and *ddx41* mutants (right) treated with DMSO (top), 30nM KU60019 (ATMi, middle), and 30nM AZ20 (ATRi, bottom). Numbers on bottom left corner indicate the fraction of embryos with the same phenotype as the one depicted in the image. Scale bars=100 μ m. **B.** Graph depicting frequency of designated o-dianisidine staining levels in sibling controls and *ddx41* mutants at 40 hpf treated with DMSO vehicle control, 30nM KU60019 (ATMi), and 30nM AZ20 (ATRi). Graphs display means \pm standard deviations (stds) with p-values calculated with a one-way ANOVA with Tukey's multiple testing correction, *p<0.05, ****p \leq 0.0001. For o-dianisidine staining, n=36-67 embryos per experiment.



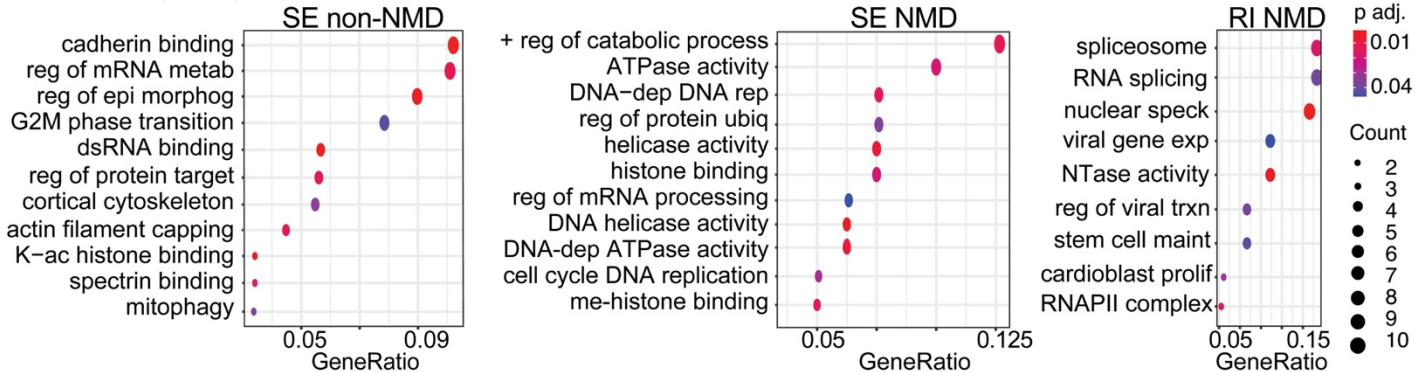
Weinreb et al. Figure 1



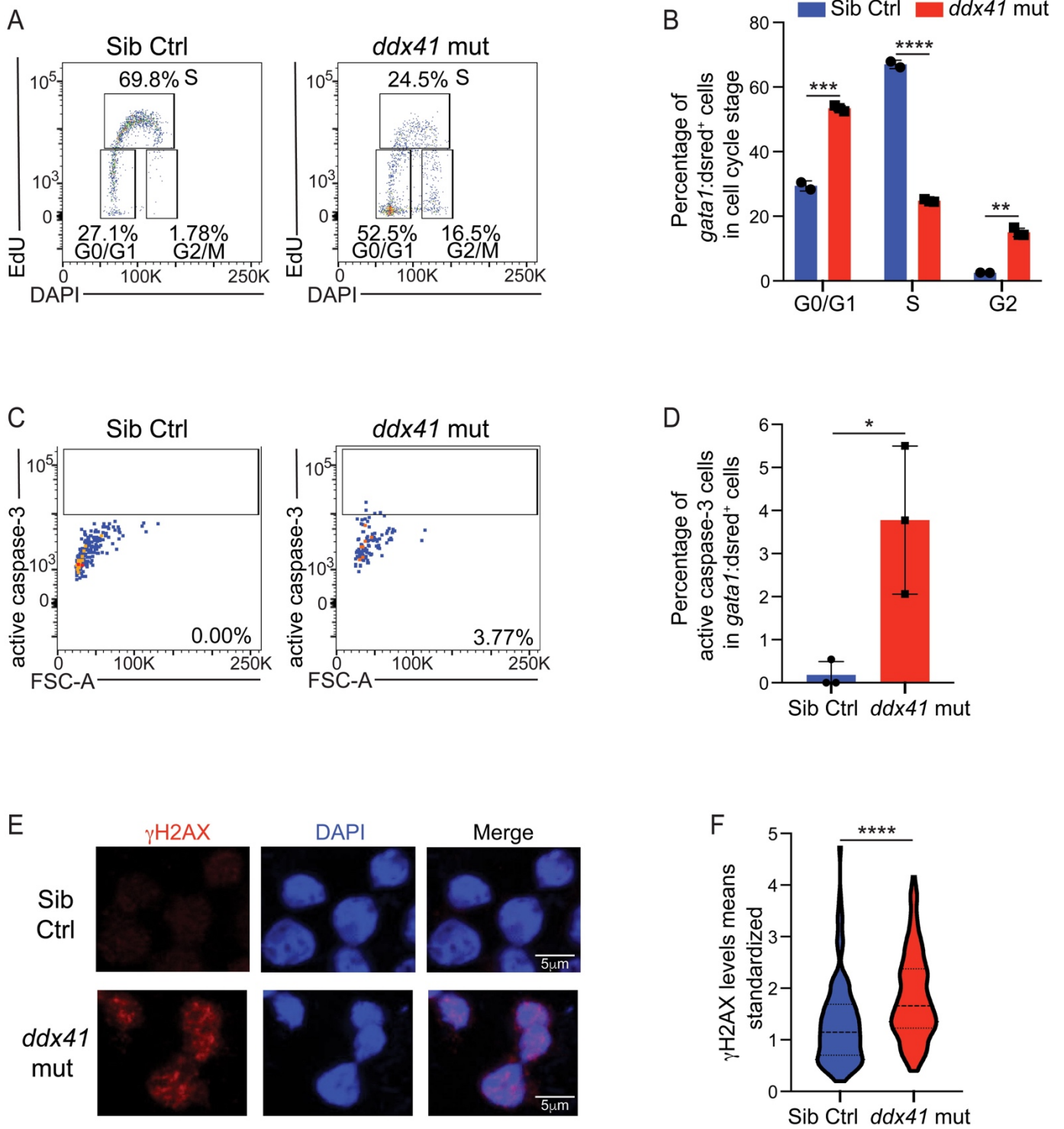
Weinreb et al. Figure 2



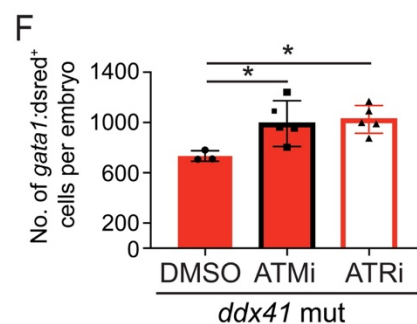
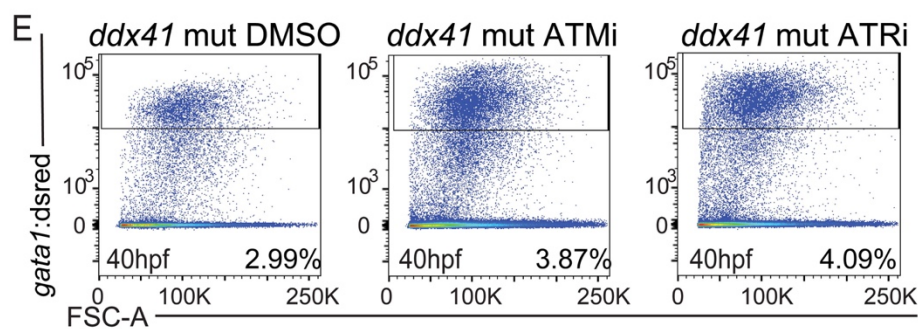
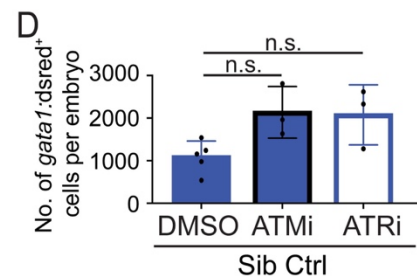
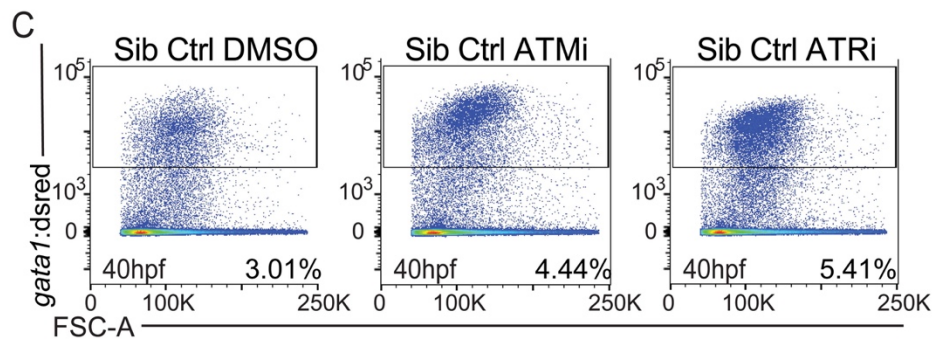
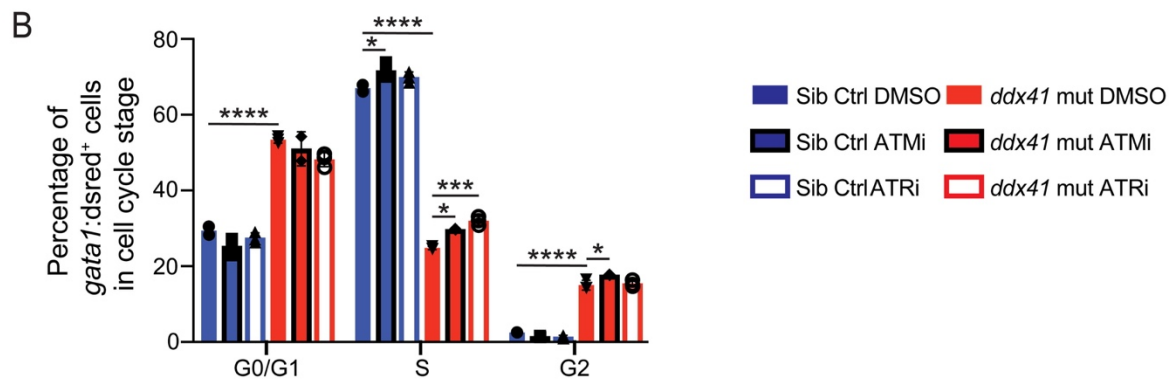
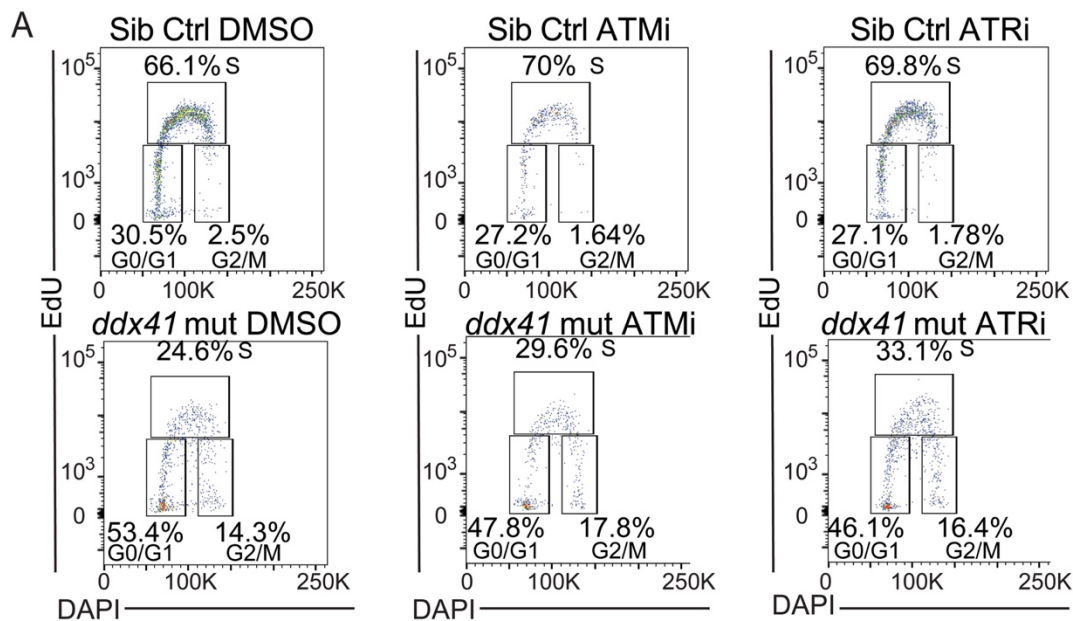
H Pathway analysis:



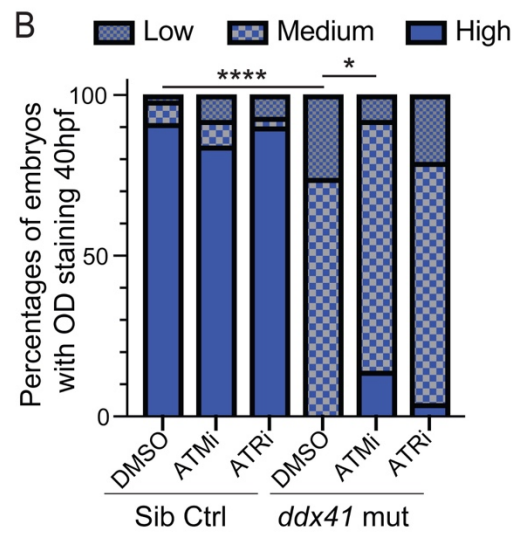
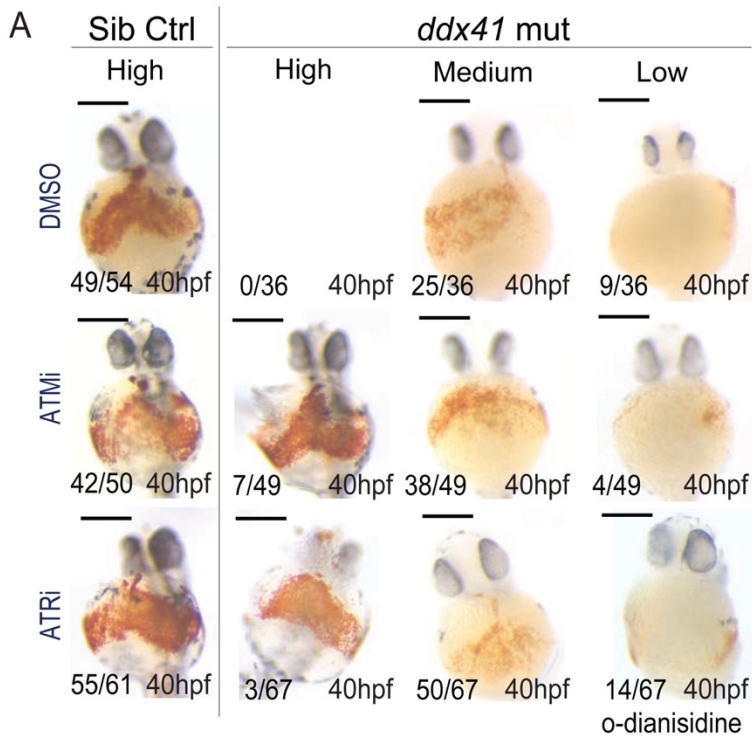
Weinreb et al. Figure 3



Weinreb et al. Figure 4



Weinreb et al. Figure 5



Weinreb et al. Figure 6

Ddx41 inhibition of DNA damage signaling permits erythroid progenitor expansion in zebrafish

Joshua T. Weinreb^{1,2}, Varun Gupta³, Elianna Sharvit¹, Rachel Weil¹, Teresa V. Bowman^{#1,2,4}

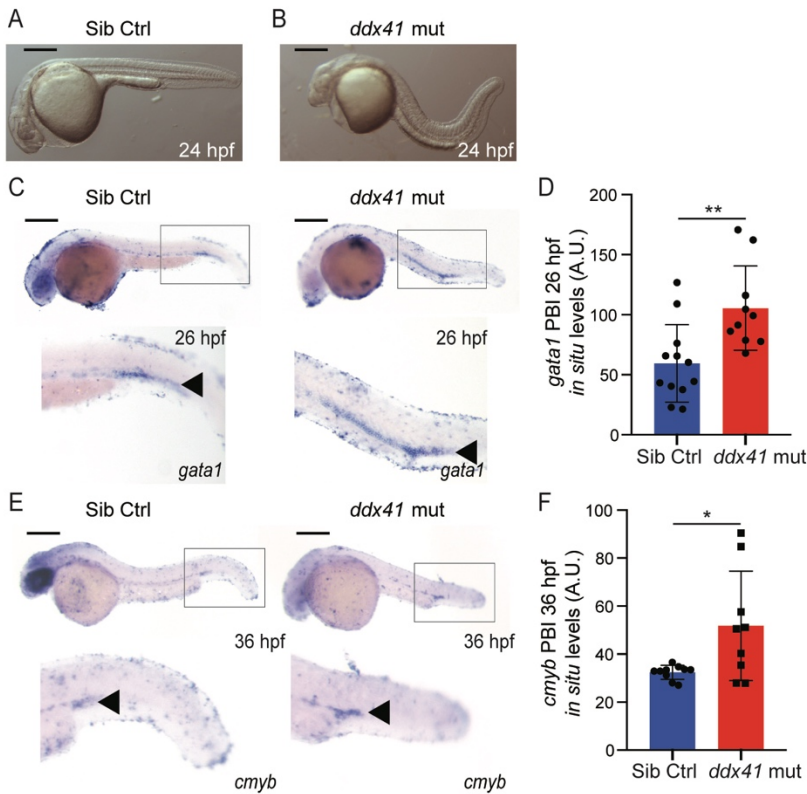
1. Albert Einstein College of Medicine, Department of Developmental and Molecular Biology, Bronx, NY, USA

2. Albert Einstein College of Medicine, Gottesman Institute for Stem Cell Biology and Regenerative Medicine, Bronx, NY, USA

3. Albert Einstein College of Medicine, Department of Cell Biology, Bronx, NY, USA

4. Albert Einstein College of Medicine and Montefiore Medical Center, Department of Medicine (Oncology), Bronx, NY, USA

SUPPLEMENTARY FIGURE



Supplemental Figure S1. Ddx41 regulates erythroid-myeloid progenitor levels *in vivo*.

A,B. Brightfield images of sibling controls (A) and *ddx41* mutants (B) at 24 hpf showing morphological differences, such as body curvature and mild brain death. Scale bars=250 μ m. **C,E.** *In situ hybridization* of *gata1* at 26 hpf (C) [Scale bars=250 μ m] and *cmyb* at 36 hpf (E) [Scale bars=350 μ m] in sibling controls (left) and *ddx41* mutants (right). **D,F.** Quantification of PBI *gata1* (D) and *cmyb* (F) *in situ hybridization* levels from (C) and (E), respectively. Quantification was done using Fiji. Graphs display means \pm standard deviations (stds) with p-values calculated with unpaired Student's t-test, * $p < 0.05$, ** $p \leq 0.01$. For *in situ hybridization*, $n \geq 10$ embryos per experiment.

SUPPLEMENTARY TABLE LEGENDS ON EXCEL FILE

Table S1. Differential gene expression.

DE-Seq2 differentially expressed genes in *gata1:dsred+* erythrocytes in *ddx41* mutants vs. siblings

Table S2. Pathway analysis on downregulated genes.

Reactome Pathways - downregulated genes in *ddx41* mutant vs. sibling *gata1:dsred+* erythrocytes

Table S3. Pathway analysis on upregulated genes.

Reactome Pathways - upregulated genes in *ddx41* mutant vs. sibling *gata1:dsred+* erythrocytes

Table S4. Differentially spliced genes.

Splicing analysis in sibling vs. *ddx41* mutant *gata1:dsred+* erythrocytes

Table S5. Changes to protein sequence from alternative splicing.

Prediction of splicing outcome on protein coding regions

Table S6. Pathway analysis of alternatively spliced genes.

Pathways enriched in alternatively spliced factors with NMD vs. protein sequence changes (non-NMD)

Table S7. Primer sequences.

Primers used in this study for genotyping and RT-qPCR.

METHODS

EXPERIMENTAL MODEL AND SUBJECT DETAILS

Zebrafish

Zebrafish were maintained as described (1). All fish were maintained according to IACUC-approved protocols in accordance with Albert Einstein College of Medicine research guidelines. We utilized several established zebrafish lines. Genotyping and phenotyping to confirm their identity was performed for each new generation and for embryos. Mutants for *ddx41* (*ddx41^{sa14887}*) were acquired from the Zebrafish International Resource Center as part of the Sanger Institute Zebrafish Mutation Project (2). The mutation results in a premature stop codon at Tyrosine 410. There is maternally-derived Ddx41 protein as detected by immunofluorescence that decreases in the mutants as the animals develop, suggesting the mutants are zygotic nulls. As early as 24 hpf, there appears to be slight brain death and abnormal curvature of the tail in *ddx41* homozygous mutants, allowing for phenotypic identification of mutants compared to siblings based on morphology (Figure S1A-B). Homozygous mutants are embryonic lethal dying by 3 dpf due to the depletion of maternal Ddx41 stores. This suggests that *ddx41* mutants should be considered functional hypomorphs. This allows for the assessment of primitive and definitive hematopoietic development in zebrafish up to 3 dpf, but precludes the assessment of hematopoiesis beyond this point. For all experiments, *ddx41* homozygous mutants are compared to

sibling controls, which are a mix of heterozygotes and wild types. In addition to *ddx41* mutants, *gata1:dsred* (3) transgenics were used and scored for dsRED fluorescence within erythrocytes. The genotyping for *ddx41* was determined by mutant-specific PCR, which was initially verified by Sanger sequencing. Additionally, the genotype of *ddx41^{sa14887/+}* carriers were validated by paired mating of heterozygous adult animals followed by examination of embryos for the expected homozygous recessive phenotype. Genomic DNA for genotyping was isolated by alkaline lysis (4). The *ddx41^{sa14887}* mutant and wild-type-specific PCR products were analyzed by gel electrophoresis. Genotyping primers are provided in Table S7.

Drug treatments

All drugs were dissolved in DMSO. Dilutions were made in E3 embryo water. Concentrations used for experiments were 30nM for KU60019 (ATM inhibitor; Fisher Scientific) and 30nM for AZ20 (ATR inhibitor; Fisher Scientific). DMSO in E3 embryo water was used as the vehicle control.

Whole-mount *in situ* hybridization and o-dianisidine staining

In situ hybridization steps were performed as described previously by Thisse *et al.* (5) with minor modifications: before proteinase K permeabilization, embryos older than 28 hpf were bleached after re-hydration to remove pigmentation. The bleaching was done for 5-10 minutes using a bleaching solution of 0.8% KOH, 0.9% H₂O₂ and 0.1% Tween 20. Embryos were then scored manually, imaged and genotyped. The *βe3-globin* (6), *cmyb* (7), and *gata1* (8) probes were used, and *in situ* levels were quantified using FIJI in a similar manner to previously described methods (9).

O-dianisidine staining was performed as described previously (10). Briefly, dechorionated live embryos were soaked in o-dianisidine staining solution (0.62 mg/mL o-dianisidine [Sigma-Aldrich], 10.9 μM sodium acetate, and 0.65% H₂O₂) for 10 minutes in the dark, then rinsed in phosphate-buffered solution plus 0.1% Tween 20 (PBT) twice and observed under the microscope. Afterward, embryos were preserved in a 4% paraformaldehyde (PFA) solution.

Flow cytometry

At 28 or 40 hpf, mutant and sibling embryos were binned based on morphological differences. For generation of single-cell suspensions, 10-20 embryos were first removed from their chorions using pronase (Roche), and then homogenized by manual dissociation using a sterile razor blade followed by digestion with Liberase (Roche). For the digestion, dissociated embryos were resuspended in 600 μl 1× Dulbeccos-PBS (D-PBS) (Life Technologies) supplemented with a 1:65 dilution (9.23 μl) of 5

mg/ml Liberase and then incubated at 37°C for 7 minutes. The reaction was stopped with the addition of 5% (30 μ l) fetal bovine serum (FBS) (Life Technologies). The cells were then filtered through a 40- μ m cell strainer (Falcon) and pelleted by centrifugation at 3000 rpm for 5 minutes. Cell pellets were resuspended in 400-700 μ l FACS buffer (0.9 \times D-PBS, 5% FBS, 1% Penn/Strep (Life Technologies)). DAPI (4',6-diamidino-2-phenylindole) was added to a final concentration of 1 μ g/ml to facilitate exclusion of dead cells from the analysis. Samples were analyzed with a LSRII flow cytometer (BD Biosciences) and FlowJo software. Cells from non-fluorescent embryos were used to set gates above background. Quantification for the absolute number of cells was performed by acquiring all events in a tube on the flow cytometer to determine the total number of target cells. This number was then divided by the total number of embryos analyzed to calculate the number of target cells per embryo.

Cell cycle and apoptosis analysis

For 5-ethynyl-2'-deoxyuridine (EdU) incorporation experiments, 28 hpf embryos were binned into 6 well plates, with ~30 embryos per well. Embryos were incubated with 20 mM EdU for 2 hours. Generation of single-cell suspensions of 40 hpf embryos was accomplished as described above. EdU was detected using the Click-IT EdU Flow Cytometry Assay Kit according to the manufacturer's instructions (Invitrogen C10424). Flow cytometry analysis for active caspase-3 at 30 hpf was performed as previously described (11). Samples were analyzed with a LSRII flow cytometer (BD Biosciences) and FlowJo software.

RNA-sequencing and splicing analysis

Erythrocytic progenitors from *ddx41* mutants and siblings at 40 hpf were isolated by fluorescently-activated cell sorting (FACS) on a Mo-Flo cell sorter (Beckman Coulter). RNA from these cells was subsequently isolated using the Zymo Quick-RNA microprep kit (R2080) according to the manufacturer specification. The TURBO DNA-free kit (Life Technologies) was used for DNA removal following RNA extraction. RNA and library quality was assessed using a bioanalyzer Pico Chip (Agilent) by the Einstein Genomics core facility. Libraries for RNA samples with RIN \geq 9 were prepared by BGI using the Nugene low-input RNA sequencing kit. Five independent biological replicates were analyzed. On average, approximately 30 million paired-end 150 base pair sequencing reads were acquired per sample using the Illumina NovoSeq platform. All data are deposited under GEO accession number GSE160979. DE-Seq2 (12) was used to determine differential gene expression (defined as log₂ fold change \geq |1|, FDR p <0.05) between *ddx41* mutant and sibling control erythrocytes. Differential inclusion rates of splicing events between *ddx41* mutants and siblings were calculated using rMATS (13) (replicate Multivariate Analysis of Transcript Splicing, version 4.0.2). Splicing events with inclusion differences \geq 10% and

FDR \leq 0.01 were considered significantly altered. After obtaining alternatively spliced events from rMATS, we calculated whether any of these spliced events would lead to protein sequence alterations or promote nonsense-mediated decay (NMD) of the splice variant. First, a refFlat file was downloaded from UCSC (for appropriate zebrafish version 10). It contains the information of the coding frames for all the annotated exons. Custom-based PERL scripts were used along with refFlat and rMATS output files for skipped exon (SE) and retained intron (RI) spliced events to obtain sequences for both the wild-type and alternative splice variant transcripts. These sequences were then converted to protein sequences with stop codon positions and altered protein sequences calculated for all variants. Pathway analysis was analyzed using the Molecular Signatures Database (MSigDB) or PANTHER (14-17).

RT-qPCR

To validate the RNA-sequencing data, we performed reverse transcription (RT) quantitative PCR. RNA was isolated from 40 hpf embryos using TRIzol (ThermoFisher) followed by DNA removal with TurboDNase (ThermoFisher). High-capacity cDNA synthesis kit (ThermoFisher) was used to generate cDNA. Real-time quantitative PCR was performed with PowerSYBR (ThermoFisher) on a QuantStudio 5 384-well instrument (ThermoFisher). Analysis was performed with Design Analysis 2 software with fold-change calculated via the $\Delta\Delta C_t$ method. Primer sequences are listed in Table S7. For quantification of embryonic and larval globins, values were normalized to the erythrocyte-specific gene *slc4a1*, which encodes Band3, as previously described (18). For quantifying cell cycle-related genes, values were normalized to β -actin.

Single-cell immunofluorescence of zebrafish embryonic cells

Single-cell suspensions were prepared as described above, and cell staining was performed as described in Sorrells & Nik *et al.* (19). The rabbit polyclonal anti-zebrafish γ H2AX primary antibody (GeneTex GTX127342) was used at a dilution of 1:500. All antibodies were diluted in blocking buffer (5% bovine serum albumin (BSA)/0.2% milk/PBS) and incubated for 3 h at room temperature followed by 3 washes in PBT. The goat anti-rabbit AlexaFluor-594 (Thermo Fisher Scientific) was used at a dilution 1:1000 and incubated for 1 h at room temperature followed by 3 washes in PBT. After final washes, cells were mounted with DAPI-Fluoromount-G (Southern Biotech), covered with a 25 \times 25 mm glass coverslip and sealed with clear nail polish. Fluorescence intensity measurements of γ H2AX were performed using FIJI.

May-Grunwald Giemsa staining of primitive erythroid cells

This protocol was performed as described by (20). Erythrocytes were isolated via two methods. At 40 hpf, *gata1:dsred*⁺ cells were isolated by FACS. Alternatively, two-day old embryos were placed on poly-L-lysine coated slides in a drop of 1× D-PBS + 1% bovine serum albumin (Sigma). Blood cells were released from the embryo by puncturing the pericardial sac and upper yolk sac with fine forceps. The slides were air-dried at room temperature prior to staining. For staining, slides were immersed in undiluted May-Grunwald stain (Eng Scientific May-Grunwald stain solution 1, Fisher Scientific) for 2 minutes and briefly rinsed in ddH₂O. Slides were then immersed in diluted Giemsa stain (diluted 1:4 with milliQ water) for 20 minutes (Eng Scientific May-Grunwald stain solution II, Fisher Scientific) and briefly rinsed in ddH₂O. Once slides were dry, a drop of Permount solution (Fisher Scientific) was added and slides were covered with a 25×25 mm glass cover slip and left overnight to dry. Once slides were dry, the cells were visualized with a 63× oil-immersion lens.

Image acquisition and processing

Brightfield and fluorescent images were acquired using a Zeiss Axio Discovery.V8 with an AxioCam HRc camera. Confocal images for zebrafish single-cell immunofluorescence were acquired using a Leica SP5 AOBS Inverted DMI6000 microscope with a 63X oil objective and zoomed in fields were taken at 6.5X zoom. FIJI/ImageJ was used for quantification of images (21). Flowjo, GraphPad Prism 8, Adobe Photoshop and Adobe Illustrator were used to generate figures.

Statistics

Experiments were performed with a minimum of three replicates. Statistical analyses were performed as indicated in each figure using unpaired Student's t-test or a one-way ANOVA with Tukey's multiple testing correction as appropriate; error bars indicate the standard deviation of mean, unless otherwise indicated.

REFERENCES

1. Lawrence C. Advances in zebrafish husbandry and management. *Methods Cell Biol.* 2011;104:429-451.
2. Kettleborough RN, Busch-Nentwich EM, Harvey SA, et al. A systematic genome-wide analysis of zebrafish protein-coding gene function. *Nature.* 2013;496(7446):494-497.

3. Traver D, Paw BH, Poss KD, et al. Transplantation and in vivo imaging of multilineage engraftment in zebrafish bloodless mutants. *Nat Immunol.* 2003;4(12):1238-1246.
4. Meeker ND, Hutchinson SA, Ho L, Trede NS. Method for isolation of PCR-ready genomic DNA from zebrafish tissues. *Biotechniques.* 2007;43(5):610, 612, 614.
5. Thisse C, Thisse B. High-resolution in situ hybridization to whole-mount zebrafish embryos. *Nat Protoc.* 2008;3(1):59-69.
6. Brownlie A, Hersey C, Oates AC, et al. Characterization of embryonic globin genes of the zebrafish. *Dev Biol.* 2003;255(1):48-61.
7. Liao EC, Paw BH, Oates AC, et al. SCL/Tal-1 transcription factor acts downstream of cloche to specify hematopoietic and vascular progenitors in zebrafish. *Genes Dev.* 1998;12(5):621-626.
8. Detrich HW, 3rd, Kieran MW, Chan FY, et al. Intraembryonic hematopoietic cell migration during vertebrate development. *Proc Natl Acad Sci U S A.* 1995;92(23):10713-10717.
9. Dobrzycki T, Krecsmarik M, Bonkhofer F, Patient R, Monteiro R. An optimised pipeline for parallel image-based quantification of gene expression and genotyping after in situ hybridisation. *Biol Open.* 2018;7(4).
10. Lieschke GJ, Oates AC, Crowhurst MO, Ward AC, Layton JE. Morphologic and functional characterization of granulocytes and macrophages in embryonic and adult zebrafish. *Blood.* 2001;98(10):3087-3096.
11. Sorrells S, Nik S, Casey M, et al. Spliceosomal components protect embryonic neurons from R-loop-mediated DNA damage and apoptosis. *Dis Model Mech.* 2018;11(2).
12. Love MI, Huber W, Anders S. Moderated estimation of fold change and dispersion for RNA-seq data with DESeq2. *Genome Biol.* 2014;15(12):550.
13. Shen S, Park JW, Lu ZX, et al. rMATS: robust and flexible detection of differential alternative splicing from replicate RNA-Seq data. *Proc Natl Acad Sci U S A.* 2014;111(51):5593-5601.

14. Subramanian A, Tamayo P, Mootha VK, et al. Gene set enrichment analysis: a knowledge-based approach for interpreting genome-wide expression profiles. *Proc Natl Acad Sci U S A*. 2005;102(43):15545-15550.
15. Liberzon A, Birger C, Thorvaldsdottir H, et al. The Molecular Signatures Database (MSigDB) hallmark gene set collection. *Cell Syst*. 2015;1(6):417-425.
16. Mi H, Muruganujan A, Thomas PD. PANTHER in 2013: modeling the evolution of gene function, and other gene attributes, in the context of phylogenetic trees. *Nucleic Acids Res*. 2013;41(Database issue):D377-86.
17. Thomas PD, Campbell MJ, Kejariwal A, et al. PANTHER: a library of protein families and subfamilies indexed by function. *Genome Res*. 2003;13(9):2129-2141.
18. Ganis JJ, Hsia N, Trompouki E, et al. Zebrafish globin switching occurs in two developmental stages and is controlled by the LCR. *Dev Biol*. 2012;366(2):185-194.
19. Sorrells S, Nik S, Casey M, et al. Spliceosomal components protect embryonic neurons from R-loop-mediated DNA damage and apoptosis. *Dis Model Mech*. 2018.
20. De La Garza A, Cameron RC, Nik S, Payne SG, Bowman TV. Spliceosomal component Sf3b1 is essential for hematopoietic differentiation in zebrafish. *Exp Hematol*. 2016;44(9):826-837.
21. Collins TJ. ImageJ for microscopy. *Biotechniques*. 2007;43(1 Suppl):25-30.